

**APPROXIMATE MULTIPHASE FLOW MODELING BY CHARACTERISTIC
METHODS**

by

**James W. Weaver
Processes and Systems Research Division
Robert S. Kerr Environmental Research Laboratory
United States Environmental Protection Agency
Ada, Oklahoma 74820**

**ROBERT S. KERR ENVIRONMENTAL RESEARCH LABORATORY
OFFICE OF RESEARCH AND DEVELOPMENT
UNITED STATES ENVIRONMENTAL PROTECTION AGENCY
ADA, OKLAHOMA 74820**

TECHNICAL REPORT DATA
(Please read Instructions on the reverse before completion)

1. REPORT NO. EPA/600/2-91/015		3. PB91-190959	
4. TITLE AND SUBTITLE APPROXIMATE MULTIPHASE FLOW MODELING BY CHARACTERISTIC METHODS		5. REPORT DATE May 1991	
7. AUTHOR(S) James W. Weaver		6. PERFORMING ORGANIZATION CODE	
9. PERFORMING ORGANIZATION NAME AND ADDRESS Robert S. Kerr Environmental Research Laboratory U.S. Environmental Protection Agency P.O. Box 1198 Ada, Oklahoma 78420		8. PERFORMING ORGANIZATION REPORT NO.	
12. SPONSORING AGENCY NAME AND ADDRESS Robert S. Kerr Environmental Research Laboratory U.S. Environmental Protection Agency P.O. Box 1198 Ada, Oklahoma 78420		10. PROGRAM ELEMENT NO. ABWD1A	
		11. CONTRACT/GRANT NO. In-House	
		13. TYPE OF REPORT AND PERIOD COVERED Project Report/Summary	
		14. SPONSORING AGENCY CODE EPA/600/15	
15. SUPPLEMENTARY NOTES Project Officer: James W. Weaver FTS: 743-2420			
16. ABSTRACT The flow of petroleum hydrocarbons, organic solvents and other liquids that are immiscible with water presents the nation with some of the most difficult subsurface remediation problems. One aspect of contaminant transport associated releases of such liquids, is the transport as a water-immiscible liquid phase. In this document approximate models of immiscible flow are presented for two- and three-phase flow. The approximations are constructed by representing the flow by hyperbolic equations which have method of characteristics solutions. This approximation has the additional benefit of being based on the fundamental wave behavior of the flow, which is revealed by the solutions of the models. An important result is that for three-phase flow, two flow regimes exist. The first is characterized by the displacement of one of the liquids into a bank which moves ahead of the other liquid. The second is characterized by almost complete bypassing of a liquid by the other. The occurrence of the flow regimes is dependent on the organic liquid properties, soil type and the initial amounts of the fluids present.			
17. KEY WORDS AND DOCUMENT ANALYSIS			
a. DESCRIPTORS		b. IDENTIFIERS/OPEN ENDED TERMS	c. COSATI Field, Group
18. DISTRIBUTION STATEMENT RELEASE TO THE PUBLIC		19. SECURITY CLASS (This Report) UNCLASSIFIED	21. NO OF PAGES 128
		20. SECURITY CLASS (This page) UNCLASSIFIED	22. PRICE

DISCLAIMER

The information in this document has been funded wholly or in part by the United States Environmental Protection Agency. It has been subjected to the Agency's peer and administrative review, and it has been approved for publication as an EPA document. Mention of trade names or commercial products does not constitute endorsement or recommendation for use.

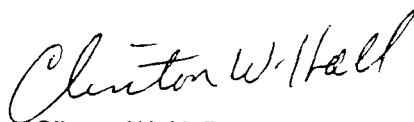
All research projects making conclusions or recommendations based on environmentally related measurements and funded by the United States Environmental Protection Agency are required to participate in the Agency Quality Assurance Program. This project did not involve environmentally related measurements and did not involve a Quality Assurance Plan.

FOREWORD

EPA is charged by Congress to protect the Nation's land, air and water systems. Under a mandate of national environmental laws focused on air and water quality, solid waste management and the control of toxic substances, pesticides, noise and radiation, the Agency strives to formulate and implement actions which lead to a compatible balance between human activities and the ability of natural systems to support and nurture life.

The Robert S. Kerr Environmental Research Laboratory is the Agency's center of expertise for investigation of the soil and subsurface environment. Personnel at the Laboratory are responsible for management of research programs to: (a) determine the fate, transport and transformation rates of pollutants in the soil, the unsaturated and the saturated zones of the subsurface environment; (b) define the processes to be used in characterizing the soil and subsurface environment as a receptor of pollutants; (c) develop techniques for predicting the effect of pollutants on ground water, soil, and indigenous organisms; and (d) define and demonstrate the applicability and limitations of using natural processes, indigenous to the soil and subsurface environment, for the protection of this resource.

This report describes a mathematical technique for simulating the flow of water, organic liquids and air in the unsaturated zone. A suite of assumptions are made in order to reduce the governing equations to simple forms. From the solutions of the latter, the fundamental behavior of such systems is revealed. Critical insight into the flow of fluids in the subsurface is gained from this work.



Clinton W. Hall

Director

Robert S. Kerr Environmental Research Laboratory

ABSTRACT

The flow of petroleum hydrocarbons, organic solvents and other liquids that are immiscible with water presents the nation with some of the most difficult subsurface remediation problems. One aspect of contaminant transport associated with releases of such liquids is transport as a water-immiscible liquid phase. Conventional finite element and finite difference models of multiphase flow may have extreme data and computational requirements. Sites with insufficient data or modeling for screening purposes may warrant using a simplified approach. In this document approximate models of immiscible flow are presented for two- and three-phase flow. The approximations are constructed by representing the flow by hyperbolic equations which have method of characteristics solutions. This approximation has the additional benefit of being based on the fundamental wave behavior of the flow, which is revealed by the solutions of the models. An important result is that for three-phase flow, two flow regimes exist. The first is characterized by the displacement of one of the liquids into a bank which moves ahead of another liquid. The second is characterized by almost complete bypassing of a liquid by the other. The occurrence of the flow regimes is dependent on the organic liquid properties, soil type and the initial amounts of the fluids present. Two-phase flows consisting of pulse applications of water result in overlapping simple waves and contact discontinuities. These models form the basis for future extension of the three-phase model to include pulse boundary conditions.

This report covers a period from October 1988 to September 1990, and work was completed as of September 1990.

TABLE OF CONTENTS

Foreword	iii
Abstract	iv
Figures	vi
Tables	vii
1. Introduction	1
2. Conclusions and Recommendations	3
3. Research Scope and Background Literature	6
Review of Related Literature	7
Sharp Front Approximation for Infiltration	7
Method of Characteristics Solutions for Multiphase Flow	7
4. Physical Principles Governing Flow in Porous Media	9
5. Model Formulation	18
Classical Method of Characteristics Solutions for Systems of Hyperbolic Equations	23
Generalized Method of Characteristics Solutions for Discontinuities	26
Riemann Problem Definition and Solution	28
On the Occurrence of Continuous and Discontinuous Waves	33
Summary of Approximate Governing Equations	41
Numerical Solution Methods	43
Construction of the Saturation Composition Space for Three-Phase Flow	44
Qualitative Nature of Three-Phase Flow	47
Construction of Saturation Profiles	48
Two-Phase Injections	50
Example 1 Oleic Liquid Bank Formation	50
Example 2 Oleic Liquid Bypassing	56
Example 3 Oleic Liquid Bank Formation, Second Type	56
Example 4 Flow of TCE	66
Example 5 Horizontal Flow	66
Example 6 Oleic Liquid/Air Injection	71
Parameter Variability	73
Single-Phase Water Injection	79
6. Generalization of Riemann Problem Solutions	82
Model Equations for the Infiltration of Water Subject to Air Phase Resistance	82
Generalized Total Flux	83
Overlapping Characteristic Patterns	85
7. Discussion of Results	92
References	95
Appendices	98
1 Derivation of the Three-Phase Fractional Flow Equations	98
2 Kinematic Model Solution	105
3 Horizontal Flow	109
4 Derivation of the Two-Phase Fractional Flow Equations	111
5 Input Data Sets	114

FIGURES

1	Typical Capillary Pressure Curve	12
2	Typical Two-Phase Relative Permeability Curve	14
3	Sharp Front Approximation to True Spreading Front	22
4	General Boundary Transition Effects in Two-Wave Systems	34
5	Multiple Boundary Transitions in Two-Wave Systems	35
6	Abrupt Transition in Two-Wave Systems	36
7	Monotonically Increasing Wave Generating Function	37
8	Monotonically Decreasing Wave Generating Function	39
9	Composite Wave Generating Function	40
10	Example 1 λ_1 Eigenvalues	42
11	Example 1 λ_2 Eigenvalues	42
12	Example 1 Saturation Composition Space	45
13	Example 1 Saturation Routes	49
14	Example 1 Base Characteristic Plane	51
15	Example 1 Saturation Profile at 24 Hours	53
16	Example 1 Saturation Profile at 48 Hours	54
17	Example 2 Bypassing Profile	57
18	Example 2 Base Characteristic Plane	58
19	Example 3 Bank Profile	59
20	Example 3 Saturation Routes	60
21	Profile Transition from Bypassing to Bank Forming	61
22	Example 4 TCE Saturation Composition Space	67
23	Example 5 Horizontal Flow Saturation Composition Space	68
24	Example 5 Comparison of Horizontal and Vertical Bank Profiles at 1 Day	69
25	Example 5 Comparison of Horizontal and Vertical Bank Profiles at 2 Days	70
26	Example 6 Oleic Fluid Injection	72
27	Saturation Composition Space for Hydraulic Conductivity of $3.35\text{e-}3 \text{ cm/s}$	74
28	Effect of Saturated Hydraulic Conductivity on Bank Profiles	75
29	Effect of Saturated Hydraulic Conductivity on Bypassing Profiles	76
30	Saturation Composition Space for Brooks and Corey's $\Lambda = 0.30$	77
31	Effect of Brooks and Corey's Λ on Bank Profiles	78
32	Effect of Brooks and Corey's Λ on Bypassing Profiles	80
33	Water-Air Infiltration Base Characteristic Plane	87
34	Water-Air Infiltration Profile at 0.2 Days	88
35	Water-Air Infiltration Profile at 0.3 Days	90
36	Water-Air Infiltration Profile After Overtaking	91

TABLES

1	Mass Balance Errors for Examples 1 to 3	62
2	Shock Inequalities Satisfied by Examples 1 to 3	63

SECTION 1

INTRODUCTION

The focus of the research described in this report is the transport of oily liquids within the subsurface. Subsurface contamination by oily wastes is recognized as a ubiquitous problem which presents some of the most challenging remediation difficulties. The three-phase flow of oily liquids in the unsaturated zone comprises one aspect of this problem. These fluids act as carriers for, or are themselves, hazardous organic chemicals. Motion of the organic liquid phase can enhance transport of hydrophobic organics, by orders of magnitude over that occurring when water is the only mobile liquid.

Transport in the unsaturated zone is characterized by transient water flow caused by discrete rainfall events of varying intensity, duration, and inter-storm arrival time. Varying water fluxes play a central role in multiphase subsurface flow, as the rainfalls provide a driving force for the hydrologic inputs to the system. A focus of the research discussed in this report is the effect of transient flows in the water, organic, and air phases.

Since the governing equations for this problem are a system of coupled non-linear partial differential equations, numerical methods must be used for their solution. Existing complex models of multiphase flow can be CPU time intensive and their proper application is data intensive. Numerical solution techniques sometimes introduce difficulties, since they are not approximation-error free. During the initial phase of site investigation, or for alternatives screening, a simplified approach is warranted, because data from typical RCRA and CERCLA sites is usually inadequate to justify a complex model. The approach that is taken in this report is to represent the flow by a system of hyperbolic equations, which describe the wave behavior of the flow system. These equations can be solved by the method of characteristics. As will be shown, this technique results in models which have semi-analytic solutions. The latter are important because their analytic character allows rapid computation of many alternative scenarios. The models also have intrinsic value for checking

numerical simulators. Most important, however, is the insight they provide into the fundamental character of the flow.

As stated above, the phases modeled in this report are water, a water-immiscible organic liquid and air. The term oleic liquid is used to indicate the organic liquid. The commonly used acronym NAPL (Non Aqueous Phase Liquid) is avoided, because some nonaqueous liquids are completely miscible with water (i.e. alcohols) and as such are not considered here. The word oleic is used because it means "oily," and carries the connotation of immiscibility with water. The terminology and the models presented herein are not restricted to petroleum based oleic liquids, but also include organic solvents and other liquids.

The remainder of the report is organized as follows. Section 2 contains a summary of the conclusions and recommendations. Section 3 describes the background and motivation for the work. Related models are briefly discussed. Section 4 reviews the multiphase, porous media, flow theory upon which the models are based. In section 5 the classical and generalized method of characteristics solutions of hyperbolic equations are presented. The solution of a "Riemann problem" of mathematical physics is presented. The solution methodology is applied to one-dimensional, three-phase flow in soils. The fundamental character of the flow is shown through a series of illustrative examples. Since Riemann problems have restrictive boundary and initial conditions, the generalization to pulse boundary conditions is discussed in section 6. Application of this theory is made to the infiltration of water subject to air phase resistance. A discussion of the results is presented in section 7.

SECTION 2

CONCLUSIONS AND RECOMMENDATIONS

The application of characteristic methods to one-dimensional flow problems reveals the fundamental behavior of three-phase systems. Although the full governing equations are parabolic, the approximate hyperbolic equations which are solved in this report describe a fundamental portion of the flow phenomena. The following conclusions are drawn from the work.

- 1) For three-phase systems with constant injection conditions and uniform initial conditions, flow occurs in two regimes. When the injection consists mostly of water, mobile oleic liquids (organic liquids or so-called NAPLs) are displaced into "banks" or are bypassed. The banks are regions in the profile where the oleic liquid fills a higher fraction of the pore space. The banks move ahead of, and are driven by, the incoming water. The bypassing profile is characterized by the injected water moving past the oleic liquid, without causing it to be displaced deeper into the profile. The occurrence of the regimes is determined by the oleic liquid properties, media properties, and the initial amount of all fluids present. Numerical solution of the model quantifies these phenomena.
- 2) That the character of the results depends on the initial condition suggests that for cases where the oleic liquid has drained to a low saturation in the upper part of the soil profile, incoming rainfall will likely bypass the oleic liquid. This conclusion holds even for oleic liquids with relatively high mobilities in the subsurface. Conversely, water injections with relatively high initial oleic liquid saturations are dominated by the bank forming regime.
- 3) For systems with injections of oleic liquid, the dominant flow regime is water bypassing. This conclusion confirms the intuition that the oleic liquid, which occupies a mid-range of the pore space due to its wetting behavior, does not displace water from the small pores. Preferential wetting causes the water to be too tightly held to the media to be easily displaced by a non-wetting liquid.

4) In all cases, the behavior of the oleic liquid is dependent on its transport properties (density and viscosity) relative to water. As the oleic liquid becomes more mobile, water injections favor the bank formation regime, because the oleic liquid is of high enough mobility to match the speed of the incoming water. The character of the results, however, always reflects preferential wetting as indicated in conclusion number three.

The following recommendations are derived from this work.

1) The three-phase solutions should be extended to simulate conditions with more general boundary and initial conditions. The methodology presented for two-phase flow simulation in section 6 appears to be adaptable for this purpose.

2) Laboratory validation of the existence of sharp fronts would be valuable for demonstrating the usefulness of the model. Absolutely sharp fronts are not necessary, for the model, because the sharp fronts can be shown theoretically to move at the same speed as the true fronts. Experimental verification of the bypassing and bank forming regimes is needed as this work proposes their existence from purely theoretical considerations. A non-destructive imaging technique, such as dual gamma ray attenuation, is necessary for tracking the time dependent fluid saturations. Also, experimental work would indicate the importance of hysteresis in the constitutive relations governing the flow.

3) The laboratory work should include investigation of the saturation conditions at the ground surface. Somewhat arbitrary conditions are used in the work discussed in this report. A related issue is that the injections used here force flow to be unidirectional. Experimental work indicates countercurrent flow is common, so the model should also be adapted for this condition.

4) Useful models for field problems should be constructed from the immiscible transport model developed herein and the extension proposed in item 1. Such models must include interphase partitioning phenomena. Previous work on kinematic models demonstrates that such phenomena are amenable for inclusion into this type of model.

5) Multi-dimensional extension of the models should be considered, since one-dimensional flow is a restrictive condition which doesn't apply to heterogeneous field sites. The one-dimensional models can be useful, however, for spills occurring over large areas.

SECTION 3

RESEARCH SCOPE AND BACKGROUND LITERATURE

The specific motivation for this work is that previous attempts to model multiphase flow of contaminants by simplified methods are limited to plug flow or to kinematic conditions. Plug flow models require the assumption that the fluids occupy a fixed portion of the pore space. Kinematic models allow more realistic fluid distributions, but are limited to gravity driven flows. As a result, an intense rainfall, high viscosity oleic phase, and/or low permeability soil may cause the model to break down (Charbeneau et al., 1989). In the present work, the general approximate framework of the kinematic approach is retained and extensions to overcome the model's limitations are sought. The models that are presented allow some dynamic phenomena to be included along with the kinematic or gravity phenomena.

In this report two types of solutions are presented. First is the solution to a classical problem of mathematical physics, called a Riemann problem. Mathematically, a Riemann problem is defined as a hyperbolic system of equations with constant injection and uniform initial conditions. Although this is of limited direct applicability to field problems, the solution of the Riemann problem is important for several reasons: Mathematically, there has been a great deal of work done on these solutions for systems other than those presented here. In this report, the application of this work to multiphase flow is explored. Second, the solutions of the Riemann problem reveal some of the fundamental character of the flow. Results will be presented which illustrate several typical flow regimes for three-phase flows. Third, one-dimensional solutions of the Riemann problem form the basis for multi-dimensional front tracking models of petroleum reservoirs (e.g., Glimm et al., 1983) which may be adaptable for subsurface contaminant transport.

The second type of solution presented in the report is for systems which can be represented by injection conditions which consist of discrete pulses. The model system for this application is the infiltration of water, subject to air phase resistance. The solution of this problem consists of an extension and generalization of the Riemann problem solution techniques. The solution which is

presented is the first step in developing a model for a surface spill of an oleic contaminant, followed or preceded by a sequence of rainfall events.

REVIEW OF RELATED LITERATURE

Models which are related to method of characteristics solutions presented in this report are reviewed below. These include sharp front approximations and method of characteristics solutions for one and two phases.

Sharp Front Approximation for Infiltration

Green and Ampt (1911) used a sharp front at the leading edge of infiltrating water, and the assumption of constant moisture content above the front to develop an analytical solution for constant head infiltration. Mull (1970) developed a sharp front model of oleic liquid profiles to simulate non-uniform redistribution of the oleic liquid after the release ends. Each profile in Mull's model consisted of oil filling a fixed amount of the pore space from the surface to the front. A series of such uniform profiles constituted the model's result. Reible et al. (1990) used a sharp front at the leading and trailing edges of an infiltrating oleic liquid to develop a similar simple model. The water saturation was assumed to be residual so that the oleic liquid displaces air only. Parameters from the model were fitted to laboratory column data.

Method of Characteristics Solutions

Smith (1983) and Charbeneau (1984) developed similar models for approximate solution of Richards' (1931) equation. These models assumed that the flow is kinematic (or equivalently driven by gravity), so the governing equation can be approximated by a hyperbolic equation which allows solution by the method of characteristics. Weaver and Charbeneau (1989) extended this methodology

for infiltration of an oleic liquid with a constant water saturation. The last three models have an advantage over the previous models, because they do not require a uniform moisture or oleic liquid profile. All of the models mentioned above share the characteristic that they are essentially single phase flow models. The presence of the other phase(s) is included implicitly, but their flow is not modeled. Charbeneau et al. (1989) developed a kinematic model which included the simultaneous unsteady flow of water and oleic liquid; the presence of air in the unsaturated zone was included, but its flow not explicitly considered. The scenario modeled was a surface release of an oleic liquid, followed by a series of discrete rainfall events. The model, being limited to gravity flow, breaks down when fluxes exceed the gravity flux. An advantage of the approach, and also that of Weaver and Charbeneau (1989), is that the model executes rapidly on small computers.

The simplest solution of a Riemann problem for multiphase flow is the two-phase Buckley-Leverett (1942) solution, which consists of a simple wave and a contact discontinuity. The work presented here is essentially a generalization of the Buckley-Leverett model to three-phase flow including the effects of gravity. Helfferich (1981) presented the theory of "coherence" for multiphase, multicomponent porous media flows. For systems of hyperbolic equations, the method of coherence is equivalent to the method of characteristics solution of the Riemann problem. Helfferich (1986) believed that the method of coherence contains the solutions of systems of hyperbolic equations as a special case, but applies in general to other systems also. Pope et al. (1978) presented solutions with straight paths across the saturation composition space, which is an essential difference with the work presented here. Dougherty and Sheldon (1964) presented a similar Riemann problem solution, but restricted their work to only one of the dominant flow regimes presented in the present report, and to horizontal flow.

SECTION 4

PHYSICAL PRINCIPLES GOVERNING FLOW IN POROUS MEDIA

The equations that govern multiphase flow in porous media are coupled, nonlinear, partial differential equations (PDEs). There is a mass conservation equation for each fluid, auxiliary relationships which incorporate various physical phenomena into the PDEs. By nature, these relations are empirical, since the phenomena are highly complex and thus are not suited to exact mathematical expression. Taken together these equations form a mathematical model of the flow (e.g., Peaceman, 1977).

A typical mass conservation equation may be written in one dimension as

$$\frac{\partial m}{\partial t} + \frac{\partial J_m}{\partial z} = \beta_m \quad 1$$

where m [M/L^3] is the mass per bulk volume of porous media, J_m [M/T] is the mass flux, and β_m [M/TL^3] is the source strength per unit volume. Throughout the rest of this work, the liquids will be assumed incompressible and the medium non-deformable. The resulting continuity (or phase conservation) equation is

$$\eta \frac{\partial S_i}{\partial t} + \frac{\partial q_i}{\partial z} = \beta_i^* \quad 2$$

where q_i [L^3/L^2T] is the volume flux of fluid i per unit area, η [L^3/L^3] is the porosity, β_i^* [$1/T$] is the source strength of fluid i divided by the fluid density of i , and S_i [L^3/L^3] is the fraction of the pore space filled by fluid i . S_i is called the degree of saturation of fluid i , or simply the saturation. In a multiphase flow system,

$$\sum S_i = 1$$

3

where i represents each fluid present. For water, an oleic liquid and air, equation 3 becomes $S_w + S_o + S_a = 1$. In order to model the fluids with the phase conservation equation (2), the composition of each phase is assumed to have no effect upon any fluid's transport properties. Fluids for which partitioning phenomena can significantly alter the saturation during the period of simulation are not suited to this approach.

The flux term of equation 2 can be related to fundamental properties of the system through use of Darcy type equations. Specifically,

$$q_i = \frac{k k_{ri}(S)}{\mu_i} \left(\rho_i g - \frac{\partial P_i}{\partial z} \right) \quad 4$$

where z is directed positive downward, $k [L^2]$ is the intrinsic permeability of the media, k_{ri} is the relative permeability of the medium to fluid i , $\mu_i [M/LT]$ is the dynamic viscosity, $\rho_i [M/L^3]$ the density, $g [L/T^2]$ is the acceleration due to gravity, and $P_i [M/LT^2]$ is the fluid pressure. The quantity $K_{ei}(S) [L/T]$ is called the effective hydraulic conductivity of the media to fluid i and is defined by

$$K_{ei}(S) = \frac{k k_{ri}(S) \rho_i g}{\mu_i} = K_{si} k_{ri}(S) \quad 5$$

where $K_{si} [L/T]$ is the fully saturated hydraulic conductivity to fluid i . The last equation underscores that the intrinsic permeability, density, and viscosity play an important role in determining the conductivity, and thus the fluxes, in multiphase flow systems. The relative permeability is the ratio of conductivity at any saturation to the fully saturated conductivity and thus is dimensionless. In these

last two equations no subscript appears on the saturation, because $k_n(S)$ may or may not depend on the amounts of the other fluids present.

Equation 4 is an extended form of Darcy's law. It incorporates the physical phenomena occurring in a porous medium containing immiscible fluids into a form that can be used in the continuity equations. Thus, knowledge of the geometry of each individual pore and of the fluid interactions within the matrix is not needed. As outlined below, this information is contained in an integrated sense in the relative permeability and capillary pressure functions. The dependence of these functions on saturations of two or more fluids results in coupling of the conservation equations.

In multiphase systems the fluid pressures are related by the capillary pressure, P_c . This fundamental relationship is defined for each pair of fluids present by

$$P_c = P_{nw} - P_w \quad 6$$

where the pressure, P_w , is the pressure in the wetting phase – the fluid most strongly attracted to the solid. P_{nw} is the pressure in the nonwetting fluid. For simple geometries (i.e., single circular tubes), there are analytic expressions for the capillary pressure (e.g., Bear, 1972, pg. 446). Soils, however, are composed of a variety of irregular, tortuous pores. The relationship expressed by equation 6 still holds, but must be expanded to represent the variation in P_c which can occur over a representative elementary volume. In contrast to media composed of uniform geometries, certain sized pores are filled by certain fluids, leading to varying contributions to the overall pressure difference.

A typical capillary pressure function for a strongly wetted system is shown in figure 1. This curve shows that the capillary pressure is infinite when the wetting phase is at the residual saturation. In three-phase systems, there are three possible capillary pressure curves, one for each pair of fluids. Only two of the capillary pressures are independent, however, as the third can be obtained from the other two.

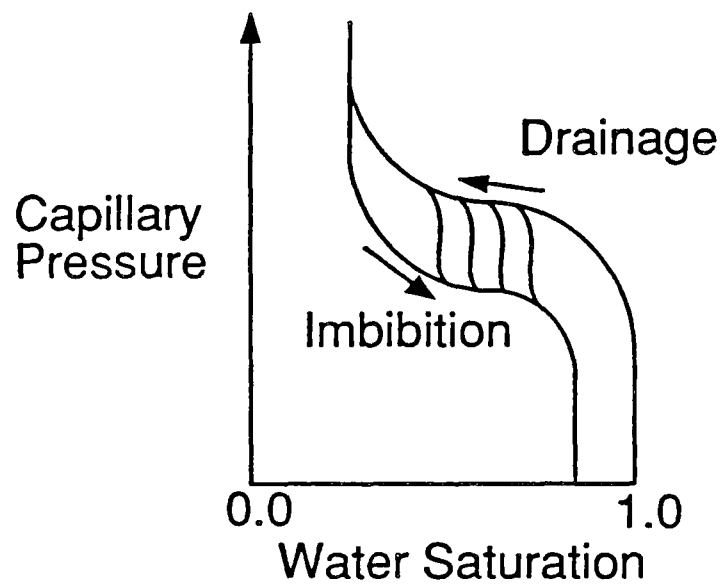


Figure 1 Typical two-phase capillary pressure curve showing hysteresis.

Numerous characteristics of both the capillary pressure and relative permeability functions can be related to the underlying physical phenomena (Weaver, 1984, pp. 57-60, 62-76). Interpretation of directly measured capillary curves reveals information concerning these phenomena. Notably, capillary pressure (and relative permeability) are subject to hysteresis. That is, the capillary pressure depends on the displacement direction. As indicated by the arrows in figure 1, it is higher during drainage (displacement of a wetting fluid by a nonwetting fluid) than during imbibition (the opposite displacement).

The relative permeability function, $k_{ri}(S)$ is the fraction of the fully saturated hydraulic conductivity existing at any saturation. Numerically, it is a number from 0 to 1. It quantifies the notion that the presence of other fluids reduces the hydraulic conductivity of the medium to a given fluid. Physically, this occurs due to reduction in the numbers of pores available to the fluid and due to the increased tortuosity of those remaining. These effects are illustrated by the typical two-phase relative permeability curves in figure 2. The permeabilities drop off rapidly in a characteristic manner, when the saturation is reduced. At the trapped or residual saturations, S_{ir} , the relative permeability is zero, implying that all of the fluid exists as a discontinuous phase. Residual wetting fluid is held in the smallest pores, while residual nonwetting fluids are found in larger pores as isolated droplets.

Due to the considerable difficulties of measurement, three-phase relative permeability is rarely measured (Stone, 1970). Alternatively, various models of relative permeability are used. One way to develop these is to begin with conceptual models of the porous medium, presumed distributions of fluids within the medium, and a solution of laminar flow through the medium (Bear, 1972, pg. 463). The Burdine equations form one such model (Burdine, 1953, Wyllie and Gardner, 1958); for the water, oleic liquid, and air phases, the relative permeability equations are:

$$k_{rw} = \left(\frac{S_w - S_{wr}}{1 - S_{wr}} \right)^2 \int_0^{S_w} \frac{dS}{dP_c^2} \bigg/ \int_0^1 \frac{dS}{dP_c^2} \quad 7a$$

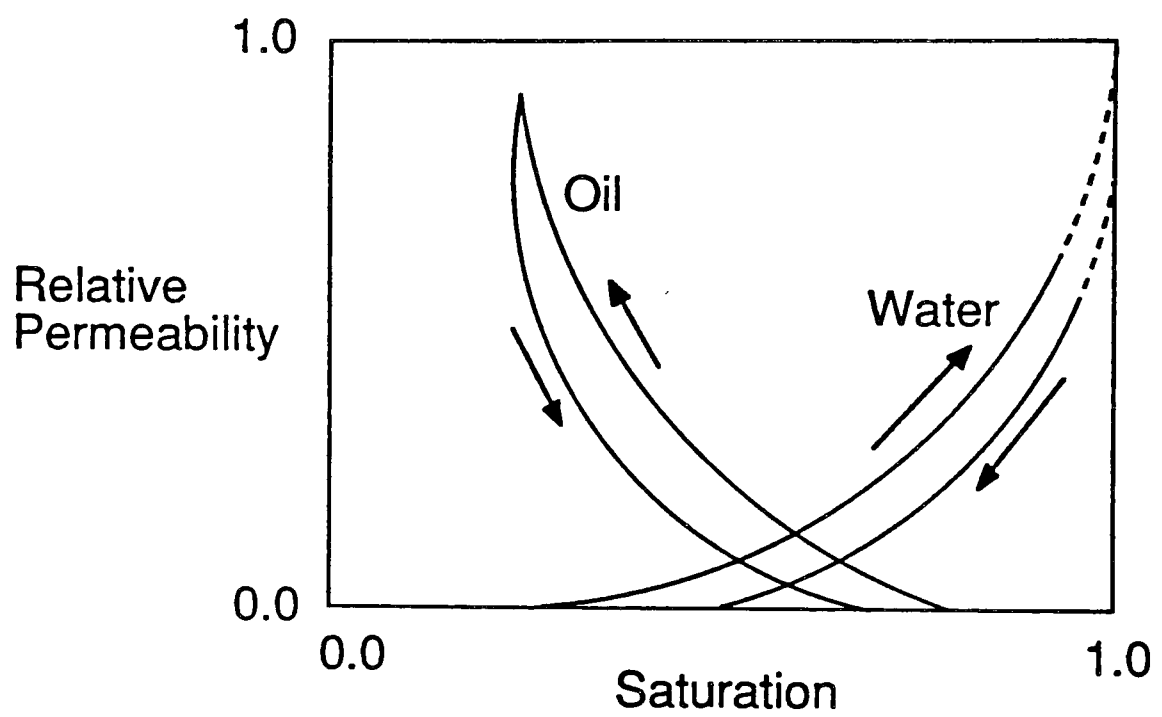


Figure 2 Typical two-phase water/oil relative permeability curve showing hysteresis.

$$k_{ro} = \left(\frac{S_o - S_{or}}{1 - S_{or}} \right)^2 \int_{S_w}^{S_o + S_w} \frac{dS}{dP_c^2} \Bigg/ \int_0^1 \frac{dS}{dP_c^2} \quad 7b$$

$$k_{ra} = \left(\frac{S_a - S_{ar}}{1 - S_{ar}} \right)^2 \int_{S_o + S_w}^1 \frac{dS}{dP_c^2} \Bigg/ \int_0^1 \frac{dS}{dP_c^2} \quad 7c$$

Originally, the three-phase integration of the Burdine equations contained no provision for a residual oleic liquid saturation (Wyllie and Gardner, 1958). Equation 7b has been modified to fit the requirements of the definition of relative permeability: that k_{ro} equals one only when the pore space is completely filled with oleic liquid, and when the oleic liquid is at its residual saturation the relative permeability is zero. The modification is to the squared term of 7b, which represents the ratio of the tortuosities at full saturation to that at any saturation, S_o (Brooks and Corey, 1964). At $S_o = S_{or}$ the tortuosity is infinite, since the oleic liquid is found as disconnected blobs in the pore space. This condition gives zero relative permeability. When the oleic liquid fills the pore space (meaning that there is no residual water or air saturations), the tortuosity is equal to the saturated tortuosity. A similar modification is made in the air phase equation.

The capillary pressure as a function of saturation is needed to evaluate the integrals in equation 7. The capillary pressure per se is not needed in the equation, but rather the distribution of pore sizes, which is conveniently given by the capillary pressure. Brooks and Corey (1964) proposed a model for drainage capillary pressure,

$$S_e = \left(\frac{S_w - S_{wr}}{1 - S_{wr}} \right) = \left(\frac{P_{ce}}{P_c} \right)^\lambda \quad 8$$

where S_e is the effective water saturation, P_{ce} is the minimum capillary pressure required to force a non-wetting fluid into a fully saturated medium, and λ is a dimensionless parameter that is indicative of the pore size distribution. Using equation 8 in equation 7 results in the following model of drainage relative permeability for water, the oleic phase and air:

$$k_{rw} = \left(\frac{S_w - S_{wr}}{1 - S_{wr}} \right)^\epsilon \quad 9$$

$$\text{where } \epsilon = \frac{(2 + 3\lambda)}{\lambda}$$

$$k_{ro} = \left(\frac{S_o - S_{or}}{1 - S_{or}} \right)^2 \left[\left(\frac{S_o + S_w - S_{wr}}{1 - S_{wr}} \right)^{\epsilon-2} - \left(\frac{S_w - S_{wr}}{1 - S_{wr}} \right)^{\epsilon-2} \right] \quad 10$$

$$k_{ra} = \left(\frac{S_a - S_{ar}}{1 - S_{ar}} \right)^2 \left[1 - \left(\frac{S_o + S_w - S_{wr}}{1 - S_{wr}} \right)^{\epsilon-2} \right] \quad 11$$

Despite its apparent analytic nature, certain parameters must always be measured to fit the model to a specific situation. For equations 9, 10, and 11 the parameters are the residual water, oleic liquid, and air saturations, and the Brooks and Corey exponent. The values of S_{wr} , λ , and P_{ce} are obtainable through a procedure outlined by Brooks and Corey (1964). They are essentially the result of a capillary pressure curve measurement. An extensive tabulation of these parameters for many different soil types has been developed, making this an attractive model (Brakensiek et al., 1981, and Rawls et al., 1983).

The wetting fluid relative permeability (equation 9), is the same as would result from a two-phase integration of the Burdine equations. This is because in a strongly wetted system, the strongest wetting phase (say water) is most strongly attracted to the solid. Thus, water is assumed always to be found in the smallest pores and grain contacts, independent of the non-wetting fluid(s)

composition. The most nonwetting fluid (air) is repelled by the surfaces so it is found in the largest pores. The attraction of the oleic liquid to the surfaces is intermediate between that of water and air, the amounts present of which determine the size of the pores occupied by the oleic liquid. Visual studies confirm this distribution for some systems (e.g., Schwille, 1988).

SECTION 5

MODEL FORMULATION

The three-phase flow model is based on the assumption that the medium is uniform and the flow is one dimensional. Each phase has a residual or trapped saturation which remains constant. The relative permeabilities are described by equations 9 through 11. All phase transport properties are assumed to remain constant. The model describes immiscible transport without interphase partitioning phenomena, or any sources/sinks in the domain of interest. Assuming incompressible flow in non-deforming uniform media, the phase conservation equations (2) for the water, oleic liquid, and air are

$$\eta \frac{\partial S_w}{\partial t} + \frac{\partial q_w}{\partial z} = 0 \quad 12$$

$$\eta \frac{\partial S_o}{\partial t} + \frac{\partial q_o}{\partial z} = 0 \quad 13$$

and

$$\eta \frac{\partial S_a}{\partial t} + \frac{\partial q_a}{\partial z} = 0 \quad 14$$

Mass is conserved in all three phases, since the source terms are set to zero. Summing gives,

$$\eta \frac{\partial}{\partial t} \left(S_a + S_o + S_w \right) + \frac{\partial}{\partial z} \left(q_a + q_o + q_w \right) = 0 \quad 15$$

By defining the total flux, q_t as, $q_t = q_a + q_o + q_w$, and recalling that the three fluids fill the pore space, i.e., $S_a + S_o + S_w = 1$, equation 15 reduces to

$$\frac{\partial q_t}{\partial z} = 0 \quad 16$$

implying that for incompressible, multiphase flow the total flux is independent of depth. Equation 16 makes no statement concerning the time dependency of q_t . For the remainder of section 5, q_t is taken as a constant, while time dependent total fluxes are discussed in section 6. Normalized fractional flows, f_i , can be defined as

$$f_i = q_i/q_t$$

where the subscript refers to fluid i . Note that the fractional flow represents the fraction of the total flux which is contributed by the flux of fluid i . Obviously,

$$1 = f_a + f_o + f_w$$

A consequence of depth-independent total flux and filled pore space is that any one of the three conservation equations for the fluids may be eliminated from the system of equations. For example, the air equation (14) can be written as,

$$\eta \frac{\partial(1-S_w-S_o)}{\partial t} + q_t \frac{\partial(1-f_w-f_o)}{\partial z} = 0 \quad 17$$

which is immediately reduced to an identity by noting the phase conservation equations for water and oleic liquid. Thus the resulting model consists of a system of only two coupled mass conservation equations in two unknowns. In the following discussion, the water and oleic liquid equations are used

in developing the solution. At times, use of the water/air and oleic liquid/air formulations is convenient and is noted in the report.

Expanding the spatial derivatives in terms of the saturations, S_w and S_o , in the water and oleic liquid conservation equations (12 and 13) gives

$$\eta \frac{\partial S_w}{\partial t} + q_t \left[\frac{\partial f_w}{\partial S_w} \frac{\partial S_w}{\partial z} + \frac{\partial f_w}{\partial S_o} \frac{\partial S_o}{\partial z} \right] = 0 \quad 18$$

and

$$\eta \frac{\partial S_o}{\partial t} + q_t \left[\frac{\partial f_o}{\partial S_o} \frac{\partial S_o}{\partial z} + \frac{\partial f_o}{\partial S_w} \frac{\partial S_w}{\partial z} \right] = 0 \quad 19$$

where the fractional flow derivatives can be expressed in terms of fundamental multiphase transport parameters, as discussed below. Writing the equations in matrix form gives

$$\frac{\partial S}{\partial t} + A(S) \frac{\partial S}{\partial z} = 0 \quad 20$$

where the saturation composition vector, S , is given by

$$S = \begin{Bmatrix} S_w \\ S_o \end{Bmatrix}$$

and the matrix, $A(S)$,

$$A(S) = \frac{q_t}{\eta} \begin{bmatrix} \frac{\partial f_w}{\partial S_w} & \frac{\partial f_w}{\partial S_o} \\ \frac{\partial f_o}{\partial S_w} & \frac{\partial f_o}{\partial S_o} \end{bmatrix}$$

Specific values of S will be denoted by $S(S_w, S_o, S_a)$, where numerical values replace S_w, S_o , and S_a (S_a is included in this notation only for convenience. It is recognized that S_a is not properly a part of the vector S). The model equation 20 is a two by two system of quasi-linear partial differential equations. Semi-analytical solutions of the model equations are sought, as they are useful in revealing the behavior of the system. Consequently, attention is restricted to uniform porous media.

The fractional flows and their derivatives can be related to fundamental transport properties by the use of Darcy's law equations for the phases. Fractional flow functions in terms of water and oleic liquid parameters are presented in appendix 1. For the system of equations presented here, there are two independent expressions for the fractional flow of the oleic liquid,

$$f_{o1} = f_{o1}(k_{ro}, k_{rw}, f_w)$$

$$f_{o2} = f_{o2}(k_{ro}, k_{ra}, f_w)$$

where k_{ri} is the fraction of the saturated conductivity to fluid i . The relationships are linear and easily solved for f_o ($f_o = f_{o1} = f_{o2}$) and f_w , given S . The partial derivatives of the fractional flows are likewise given by systems of two linear equations in two unknowns (appendix 1). All coefficients appearing in equation 20 are either constants or are determined by S , which is the only unknown appearing in that equation.

As indicated in appendix 1, the model neglects the gradients of the capillary pressure by omitting them from the fractional flow functions. This assumption is critical for eliminating the parabolic character of the phase conservation equations, so that the method of characteristics can be applied to this problem. One of the main effects of the capillary gradient is to smooth sharp fronts. Figure 3

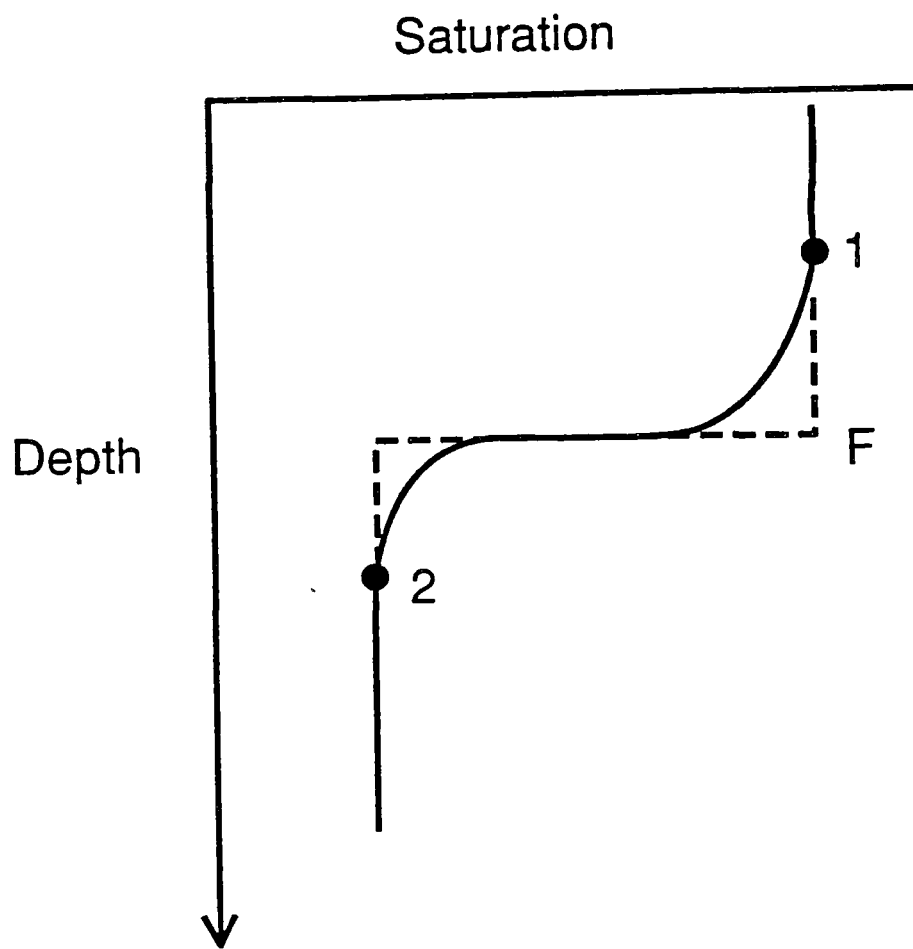


Figure 3 Sharp front approximation to a true spreading front. The sharp front is selected by mass conservation to match the speed of the true front between points 1 and 2.

shows the relationship between a true smooth front and the sharp front approximation used in this solution. Because of the way that the speed of the sharp front is determined, the mean displacement speed of the true smooth front matches that of the sharp front (Charbeneau, 1984). Flow visualization experiments conducted at the Robert S. Kerr Environmental Research Laboratory and elsewhere (Reible et al., 1990) suggest that infiltrating fronts indeed remain sharp for a variety of situations.

CLASSICAL METHOD OF CHARACTERISTICS SOLUTIONS FOR SYSTEMS OF HYPERBOLIC EQUATIONS

The following section discusses solution of systems of quasilinear equations. The primary references on this material are Jeffrey and Taniuti (1964), Lax (1957, 1973), Rozdestvenski and Janenko (1980), and Smoller (1983). For readers whose main interest is the results of the model, the next three sections may be skimmed. The definition of the Riemann problem must be noted, however, because this is the type of problem solved in this section. Application of the theory to multiphase flow problems begins to be discussed in the section entitled "On the Occurrence of Continuous and Discontinuous Waves." A summary of the equations used for each part of the solution is given in the next section ("Summary of Approximate Governing Equations").

For an arbitrary quasilinear system of equations, a characteristic form can be derived as follows.

The k^{th} left eigenvector, \mathbf{l}_k of the matrix $\mathbf{A}(\mathbf{S})$ is defined by

$$\mathbf{l}_k (\mathbf{A}(\mathbf{S}) - \lambda_k \mathbf{I}) = 0$$

where the scalar, λ_k , is by definition the k^{th} eigenvalue of $\mathbf{A}(\mathbf{S})$, and \mathbf{I} is the identity matrix. For systems of two equations in two unknowns, the eigenvalues of matrix $\mathbf{A}(\mathbf{S})$ are denoted by λ_1 and λ_2 , and defined as

$$\lambda_1 = \frac{1}{2} \left\{ a_{11} + a_{22} - \left[\left(a_{11} - a_{22} \right)^2 + 4a_{12}a_{21} \right]^{1/2} \right\} \quad 21$$

and

$$\lambda_2 = \frac{1}{2} \left\{ a_{11} + a_{22} + \left[\left(a_{11} - a_{22} \right)^2 + 4a_{12}a_{21} \right]^{1/2} \right\} \quad 22$$

Note that λ_1 , λ_2 , or λ_k refer to eigenvalues, while λ refers to Brooks and Corey's exponent (equation 8).

The components of the left eigenvectors are determined by solving

$$l_k(1) a_{11} + l_k(2) a_{21} = \lambda_k l_k(1)$$

$$l_k(1) a_{12} + l_k(2) a_{22} = \lambda_k l_k(2)$$

and arbitrarily fixing the value of $l_k(1)$ or $l_k(2)$. Multiplying equation 20 by l_k , and noting the definition of the left eigenvector, gives

$$l_k \left(\frac{\partial S}{\partial t} + \lambda_k \frac{\partial S}{\partial z} \right) = 0$$

The substantial derivative of S, DS, is the sum of the temporal and spatial derivatives,

$$DS = \frac{\partial S}{\partial t} + \frac{dz}{dt} \frac{\partial S}{\partial z}$$

Thus the classical method of characteristics form for equation 20 is simply seen to be

$$l_k DS = 0 \quad 23$$

along paths, which are called characteristics, defined by

$$\frac{dz}{dt} = \lambda_k \quad 24$$

where $k = 1, 2$ for the two by two system. There may be some systems for which equations 23 and 24 have analytical solutions, resulting in closed-form relations for the independent variables. For three-phase porous media flow, however, an analytical solution is not known and numerical solutions of these equations must be found. Application of the method of characteristics, however, reduces the system of n coupled partial differential equations to a system of $2n$ coupled ordinary differential equations. In general, the latter are easier to solve numerically than the former. The relationship between the kinematic model solution for three-phase flow presented by Charbeneau et al. (1989) and Weaver (1988) and the classical method of characteristics solution is discussed in appendix 2.

For a two by two system, equation 23 becomes

$$\frac{dS_2}{dS_1} = - \frac{f_k(1)}{f_k(2)} \quad k = 1, 2 \quad 25$$

In each k direction specified by equation 24. Since there are two eigenvalues of $A(S)$, all four ordinary differential equations represented by equations 24 and 25 must be solved simultaneously to determine $S(z,t)$. Such solutions are defined as classical solutions of equation 20 by the method of characteristics.

Two important caveats must be noted. First, a necessary condition for the existence of classical solutions determined from (equations 23 and 24) is that the system remains hyperbolic throughout the solution domain. The condition for hyperbolicity is that the eigenvalues remain real and distinct throughout the solution domain. For the multiphase flow problem considered here, this will be demonstrated below. Second, the classical solutions are guaranteed to exist only in the "small," i.e., in a small neighborhood of the initial data. Proper initial data does not prevent discontinuities from forming within the solution domain. At these discontinuities, the partial derivatives appearing in equation 20 do not exist, so neither do the classical solutions. In order to overcome this difficulty,

solutions which satisfy integral forms of the mass conservation equations are used. In the present work, these are used where the sharp fronts replace the true fronts. The classical and generalized solutions are patched together to construct the complete solution, which consists of regions with smooth saturation variation separated by sharp fronts.

GENERALIZED METHOD OF CHARACTERISTICS SOLUTIONS FOR DISCONTINUITIES

When the saturation derivatives, $\partial S/\partial t$ and $\partial S/\partial z$, fail to exist within the solution domain, the classical method of characteristics solution presented in the previous section also fails to exist. The differential mass conservation equations 12 to 14 are no longer meaningful and must be supplanted with generalized (also called integral or weak) solutions. By integrating the mass conservation equations (e.g., Charbeneau, 1984) an integral solution that conserves mass is found. For example, a discontinuity in the water phase obeys

$$s = \frac{dz_f}{dt} = \frac{q_f}{\eta} \left(\frac{f_{w2} - f_{w1}}{S_{w2} - S_{w1}} \right) \quad 26$$

where s is the speed of the discontinuity, z_f is the location of the sharp front, and the subscripts 1 and 2 refer to points on either side of the discontinuity (Figure 3). Analogous equations exist for discontinuities in the oleic and air phases.

Discontinuous solutions are notorious for being non-unique and abundant examples of this behavior exist (e.g., Jeffrey and Taniuti, 1964, pp 119-121). Generalized entropy conditions (shock inequalities) are used to select physically realistic discontinuous solutions. Two types of discontinuous solutions are important for this report, k-shocks and contact discontinuities. By obeying the shock inequalities, a discontinuous solution is assured to be physically realistic and therefore the proper discontinuous solution. The shock inequalities define k-shocks, and are given by (Smoller, 1983)

$$\lambda_k(S_2) < s < \lambda_{k+1}(S_2) \quad 27$$

$$\lambda_{k-1}(S_1) < s < \lambda_k(S_1) \quad 28$$

where the subscripts 1 and 2 on S refer to points behind and ahead of the discontinuity, respectively.
For a two by two system with $\lambda_1 < \lambda_2$, either

$$\lambda_1(S_2) < s < \lambda_2(S_2) \quad 29$$

and

$$s < \lambda_1(S_1) \quad 30$$

which defines a 1-shock, or

$$\lambda_2(S_2) < s \quad 31$$

and

$$\lambda_1(S_1) < s < \lambda_2(S_1) \quad 32$$

which defines a 2-shock, must be satisfied. The shocks appearing in the solutions presented below are shown to be 2-shocks.

The second type of shock is a contact discontinuity, for which the shock speed matches the characteristic speed on one side of the shock (Smoller, 1983, pg. 334). As Smoller demonstrates, this condition results from linear degeneracy in the k^{th} characteristic field, which occurs when

$$\langle \nabla \lambda_k, r_k \rangle = 0 \quad 33$$

where the bracket, $\langle \cdot, \cdot \rangle$, is defined as the inner product of two vectors. Linear degeneracy in a characteristic field implies that the system, although nonlinear, behaves like a linear system where shock speeds always match characteristic speeds. For the multiphase problem $\nabla \lambda_k$, has not been calculated explicitly. Instead of showing that the characteristic fields are linearly degenerate by satisfying equation 33, the examples below demonstrate that the characteristic speed of the smooth wave matches, to within numerical error, the shock speed. In fact, the contact discontinuities presented below are "almost" 1-shocks, since they satisfy equation (29) and violate equation (30) only because $s = \lambda_1(S_1)$.

RIEMANN PROBLEM DEFINITION AND SOLUTION

An important class of problems is defined by equation 20 and the boundary and initial data,

$$S(0,t) = S_1$$

$$S(z,0) = S_2$$

where S_1 is the boundary saturation composition and S_2 is the initial saturation composition. These are called Riemann problems, and are the focus of this section. For the Riemann problem, the characteristic form given by equations 23 and 24 simplifies as discussed below.

Momentarily restricting the discussion to small neighborhoods of the initial data for hyperbolic systems, the following definition is made. A function w is defined as a k -Riemann invariant of the system, if it is a smooth function, $w(S_w, S_o)$, that satisfies

$$\langle r_k, \nabla w \rangle = 0$$

34

where r_k is the k^{th} right eigenvector of $A(S)$. The k^{th} right eigenvector is defined by

$$(A(S) - \lambda_k I) r_k = 0$$

35

The components of the right eigenvector r_k are determined by solving the homogeneous equations.

$$(a_{11} - \lambda_k) r_k(1) + a_{12} r_k(2) = 0$$

$$a_{21} r_k(1) + (a_{22} - \lambda_k) r_k(2) = 0$$

By assigning $r_k(1) = 1$, and using the first of the above equations, $r_k(2)$ is found to equal $-a_{12}/(a_{11} - \lambda_k)$.

Using the second equation to determine $r_k(2)$ can be shown to give the same result.

Details of the following results for hyperbolic systems are presented by Smoller, and form the basis for construction of the solutions. When S is a C^1 continuous solution of 20 in a domain D , and all k -Riemann invariants are constant, then S is defined as a λ_k -simple wave. When the λ_k -simple wave depends only on a parameter $\xi = (z - z_0)/(t - t_0)$, the wave is defined as a λ_k -centered simple wave. The wave is centered at the point (z_0, t_0) . Simple waves are important for the Riemann problem, because they are one of the main features of the solutions.

For equation 20, a Riemann invariant (equation 34) can be written as

$$r_k(1) \frac{\partial w}{\partial S_w} + r_k(2) \frac{\partial w}{\partial S_o} = 0$$

which leads to

$$\frac{\frac{\partial W}{\partial S_w}}{\frac{\partial W}{\partial S_o}} = \frac{-r_k(2)}{r_k(1)} \quad 36$$

When the Riemann invariants are constant, i.e., within a simple wave, the implicit function theorem shows that

$$\frac{\partial W}{\partial S_w} + \frac{\partial W}{\partial S_o} \frac{dS_o}{dS_w} = 0$$

Now equation 36 can be rewritten in terms of the unknown values of the variables, S_w and S_o , as

$$\frac{dS_o}{dS_w} = \frac{r_k(2)}{r_k(1)} \quad 37$$

Equation 37 applies throughout the simple wave, notably across the characteristics. For a given eigendirection, k , equation 37 is a single non-linear ordinary differential equation. The non-linearity results from the right eigenvectors being functions of the saturations. The direction in saturation composition space given by this equation varies for a given eigendirection, because the eigenvalue and eigenvector vary with the saturation composition, S .

A similarity solution of equation 20 is possible because the problem has no characteristic time (t) or depth scales (z) (Charbeneau, 1988). The two independent variables z and t collapse into a single independent variable $\xi = z/t$. Equation 20 is transformed by the relations

$$\frac{\partial S}{\partial t} = \frac{dS}{d\xi} \frac{d\xi}{dt} = S_\xi \frac{-z}{t^2}$$

$$\frac{\partial S}{\partial z} = \frac{dS}{d\xi} \frac{d\xi}{dz} = S_\xi \frac{1}{t}$$

resulting in

$$(A(S) - \xi I)S_{\xi} = 0 \quad 38$$

where the initial data is transformed as $S(0) = S_1$, and $S(\infty) = S_2$. When ξ is not an eigenvalue of $A(S)$, S_{ξ} must be equal to zero. Thus the saturation change vector equals zero and solutions are admitted which consist of regions in z - t space with no change in saturation composition. Such regions of constant state are called plateaus.

As a consequence of the definition of the right eigenvector, if ξ is an eigenvalue of $A(S)$, then S_{ξ} must be a right eigenvector of $A(S)$. This relationship is noted by comparing the definition of the right eigenvectors (equation 35) with equation 38. Further, for a given eigenvalue, λ_k , the eigenvectors satisfy a bi-orthogonality relation, (e.g., Young and Gregory, 1988)

$$\begin{aligned} l_i r_j &\neq 0 & i = j \\ l_i r_j &= 0 & i \neq j \end{aligned}$$

So, for the Riemann problem where $r_k = S_{\xi}$,

$$l_k r_k = l_k S_{\xi} \neq 0$$

The classical method of characteristics form (equation 23), which states that $l_k DS = 0$ along $dz/dt = \lambda_k$, is satisfied when $DS = 0$, since $l_k \neq 0$, and as shown in the last equation $l_k S_{\xi} \neq 0$. For the Riemann problem

$$DS = 0 \quad \text{along} \quad \frac{dz}{dt} = \lambda_k \quad 39$$

The characteristic form for the Riemann problem (equation 39) shows that the saturation change vector DS is zero along the characteristics, implying that saturation compositions remain fixed along each characteristic. Since $\lambda_k = \lambda_k(S)$, the characteristics must be straight lines. From a computational viewpoint straight characteristics are convenient features, since equation 24 has a simple analytical solution and numerical integration is not needed.

Equation 37 provides a powerful and necessary tool for characterizing the possible saturation compositions. By picking an eigendirection, k , the saturation composition across the wave is determined by solving equation 37. A map of all possible states, S , which satisfy equation 37 given a starting saturation composition can be drawn. Such S maps are discussed below in the section entitled, "Construction of the Saturation Composition Space for Three-Phase Flow." Since during the construction of the S map, all waves are assumed to be continuous, modification of the routes is required before using the map to construct solution profiles containing shocks.

The variation of saturation along a shock can be determined by equating the jump equations. For example, the shock speeds are the same for discontinuities in water and oleic liquid saturations, so

$$s = \frac{dz_f}{dt} = \frac{q_f}{\eta} \left(\frac{f_w - f_w^*}{S_w - S_w^*} \right) = \frac{q_f}{\eta} \left(\frac{f_o - f_o^*}{S_o - S_o^*} \right)$$

where (S_w^*, S_o^*) is a fixed point in the saturation space, and f_o^* and f_w^* the values of f_w and f_o evaluated at (S_w^*, S_o^*) . As a result, the water and oleic liquid saturations across the discontinuity are related by,

$$S_o = S_o^* + \frac{f_o - f_o^*}{f_w - f_w^*} (S_w - S_w^*) \quad 40$$

which is used to adjust the routes across the saturation space when the solution becomes discontinuous.

ON THE OCCURRENCE OF CONTINUOUS AND DISCONTINUOUS WAVES

Since there are two model equations, there are two eigenvalues of the matrix $A(S)$. Thus two waves are created for each change in boundary condition. Following Helfferich (1986), figure 4 shows a smooth transition from constant state 1 to constant state 2. Since each value of saturation composition on the boundary is associated with two characteristic directions, two waves are created by the boundary transition. One wave corresponds to λ_1 and the other corresponds to λ_2 . Note that this is not a Riemann problem and the general method of characteristics solution (equations 23 and 24) must be integrated throughout the triangular region ABC to find the solution shown in this figure. The waves shown are λ_k -simple waves which define a continuous solution of equation 20. When more transitions are included, more regions with overlapping characteristics appear (figure 5). In a Riemann problem the boundary transition between the states is reduced to a single point, so there is immediate resolution into two distinct waves. Since they originate from a common point, the waves are λ_k -centered simple waves. This condition is illustrated in figure 6. All of these figures assume that λ_1 and λ_2 decrease smoothly from state 1 to state 2 so that the characteristics form typical fan-shaped simple wave patterns.

Either one or both of the waves may be replaced wholly or in part by a discontinuity which corresponds to k-shocks or contact discontinuities respectively. Since the discontinuities can be created instantly, there may be no continuous portion of the wave, as in the case of the k-shock. Figures 7 to 9 illustrate, in a schematic fashion, functions which generate simple waves and discontinuities for both smooth and abrupt boundary transitions. In figure 7a a monotonically increasing $\lambda(S)$ function is shown. If there is a gradual transition from a low (S_1), to a high (S_2), saturation composition, a simple wave is generated along the boundary, as each eigenvalue increases with increasing S . Since characteristic speeds are equal to the eigenvalues, each successive characteristic has a greater slope than its predecessor, causing the characteristics to separate (figure 7b). When the transition zone shrinks to a point (i.e., an abrupt transition of a Riemann problem) the smooth wave still exists, as shown in figure 7c. Figure 7c shows a centered simple wave as the characteristics originate from a common point. Solutions for soil moisture (Charbeneau, 1984) and

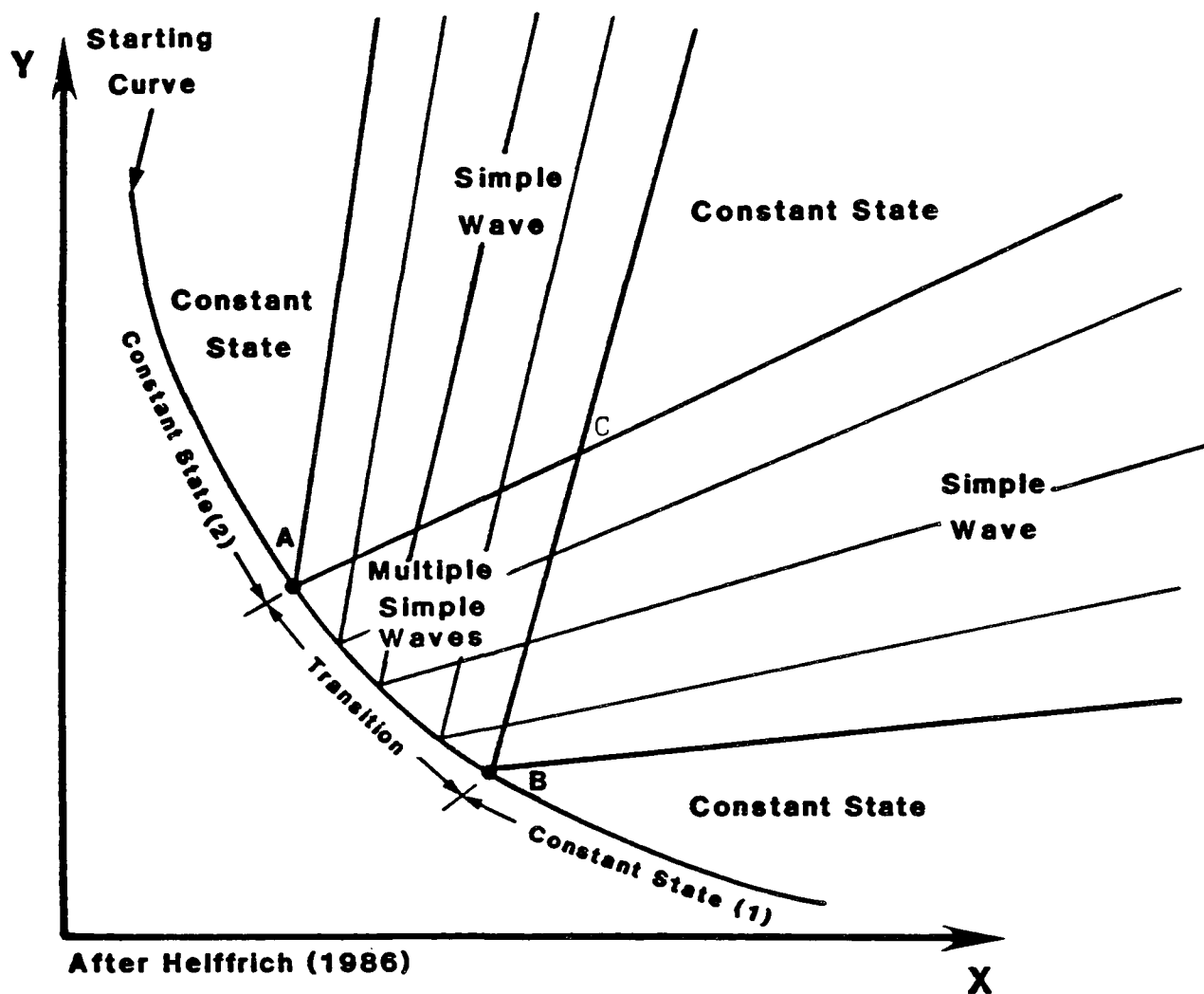


Figure 4 General boundary transition effects in two-wave systems. A gradual transition between constant state(1) and constant state(2) creates two overlapping simple waves (triangle ABC).

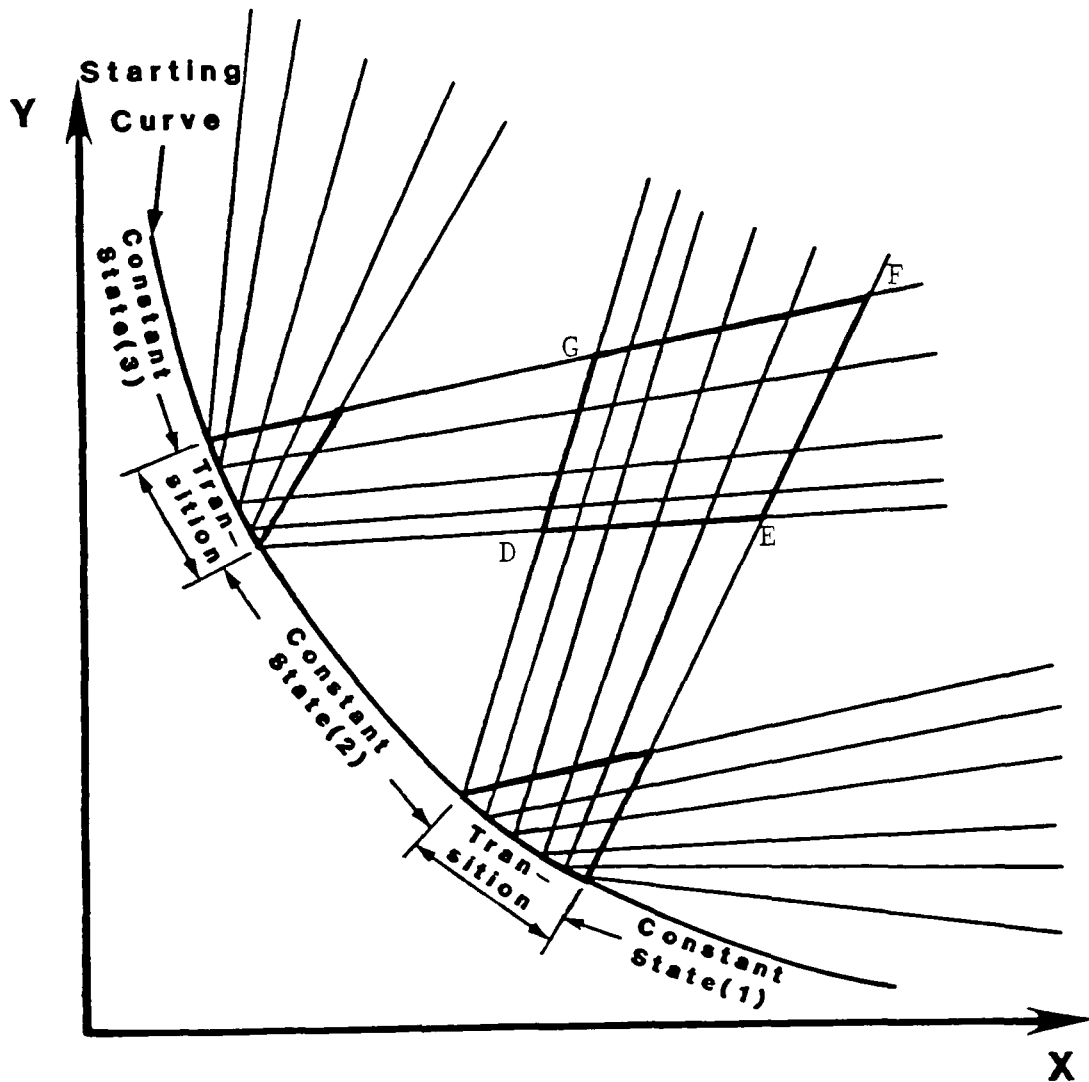


Figure 5 Multiple boundary transitions in two-wave systems. Multiple transitions create regions with overlapping simple waves which originate from different boundary transitions (DEFG).

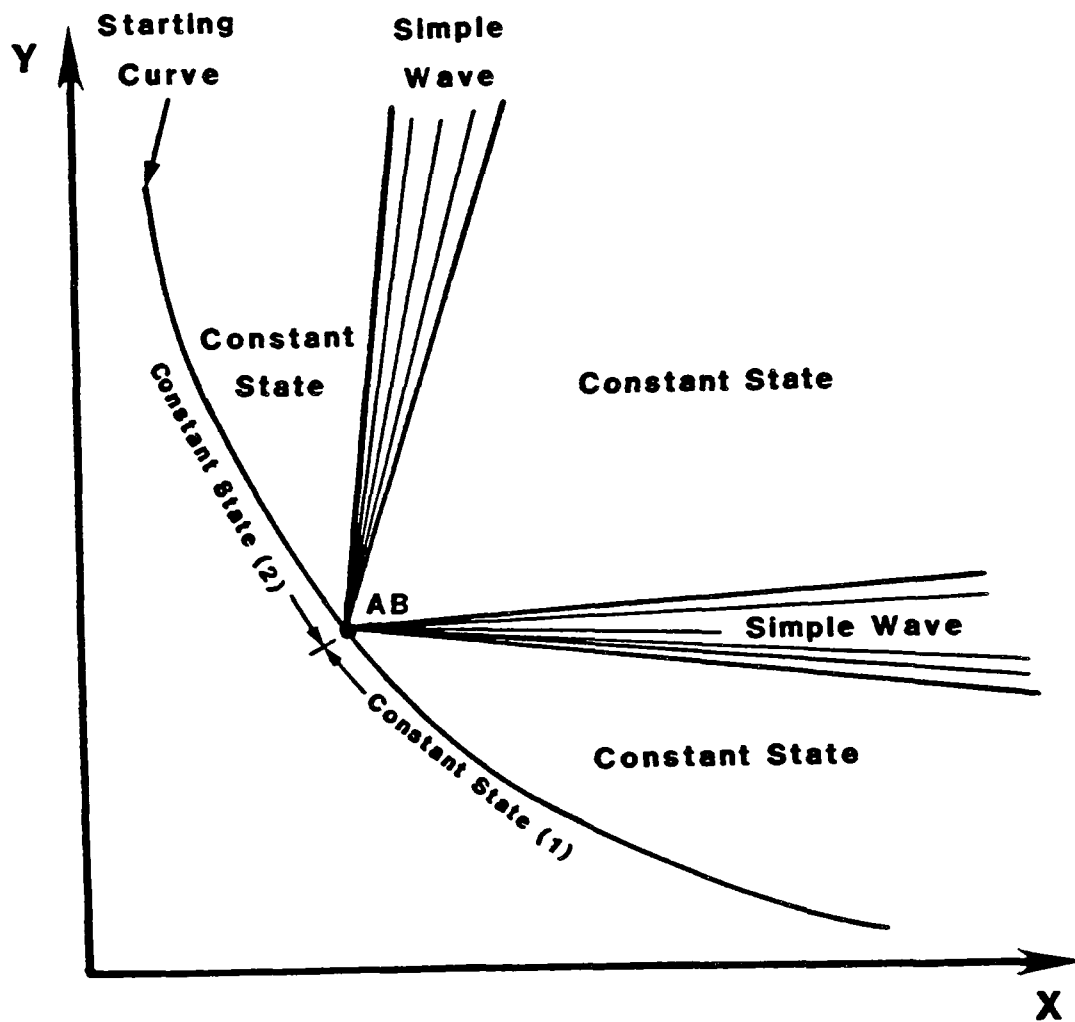


Figure 6 Abrupt transition in two-wave systems. When the boundary transitions shrink to a point there is immediate resolution into simple waves.

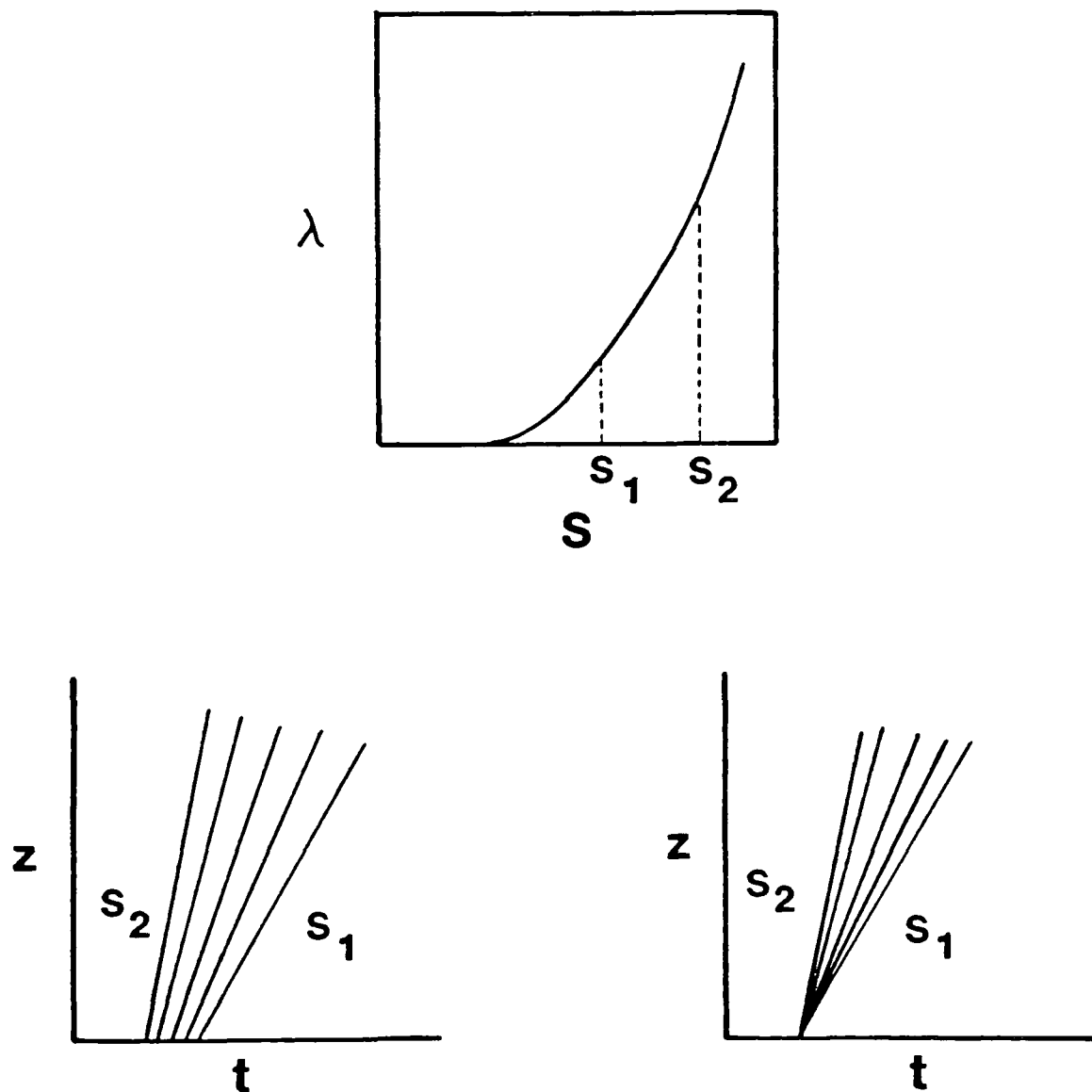


Figure 7 Monotonically increasing wave generating function. Figure 7a shows eigenvalues which are monotonically increasing with S . Figure 7b shows a gradual boundary transition (in time) from constant state, S_1 to constant state, S_2 which results in a simple wave. Figure 7c shows a similar abrupt transition.

oleic liquid transport with constant water saturation (Weaver and Charbeneau, 1989) use this type of function, and show this type of result.

In the case of monotonically decreasing $\lambda(S)$ (figure 8a), characteristics cross at some point A inside the z - t space (figure 8b). At point A, a discontinuity forms, since the characteristics each carry a distinct saturation composition value and there cannot exist any point with multiple saturation compositions. If such points existed, they would have, simultaneously, multiple water, oleic liquid and air saturations. This situation is clearly meaningless. A discontinuity replaces the multiple-valued saturation composition and is analogous to wave breaking. When the transition is abrupt (figure 8c), the variation is immediately resolved into a discontinuity. This situation corresponds to a complete displacement of one composition by another, a condition which is solely determined by the $\lambda(S)$ function. Plug flows are thus admitted as possible solutions of the hyperbolic system.

Discontinuities in the kinematic models at the leading edge of the infiltrating fluid are of the type presented in figure 8c. Note, however, that a monotonically decreasing function is followed when the transition on figure 7a is from S_2 to S_1 . Thus one $\lambda(S)$ function can generate both continuous and discontinuous waves depending on the direction of the transition.

When the $\lambda(S)$ function has the form shown in figure 9a, the resulting wave displays both continuous and discontinuous behavior. In figure 9b there is a portion of the wave which remains continuous, corresponding to the increasing portion of the $\lambda(S)$ function. When $\lambda(S)$ becomes a decreasing function, the wave breaks as in figure 9b. For the abrupt transition (figure 9c), the discontinuity originates on the boundary. Since the speed of the discontinuity equals the characteristic velocity on one side, it is a contact discontinuity by definition.

The precise saturation composition where the wave breaks is determined by the particular problem being solved. In some cases (presented below), no discontinuity forms because the initial condition is reached before the wave breaks. In other cases the initial condition helps determine the saturation composition at the edge of the breaking wave.

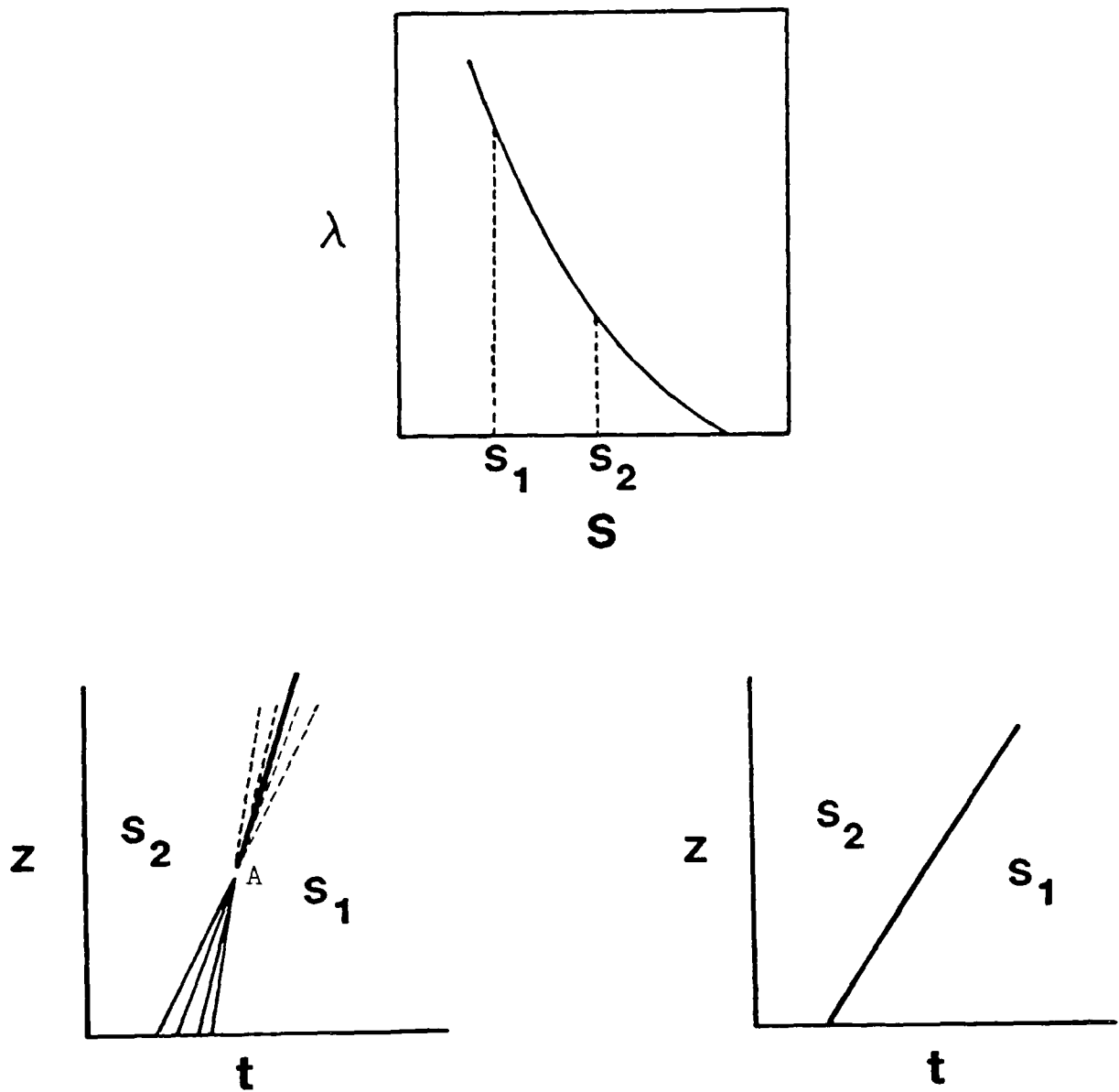


Figure 8 Monotonically decreasing wave generating function. Figure 8a shows eigenvalues which are monotonically decreasing with increasing S . Figure 8b shows a gradual boundary transition (in time) from constant state, S_1 , to constant state S_2 which results in overlapping characteristics (point A). Figure 8c shows a similar abrupt transition which immediate resolution into a discontinuity.

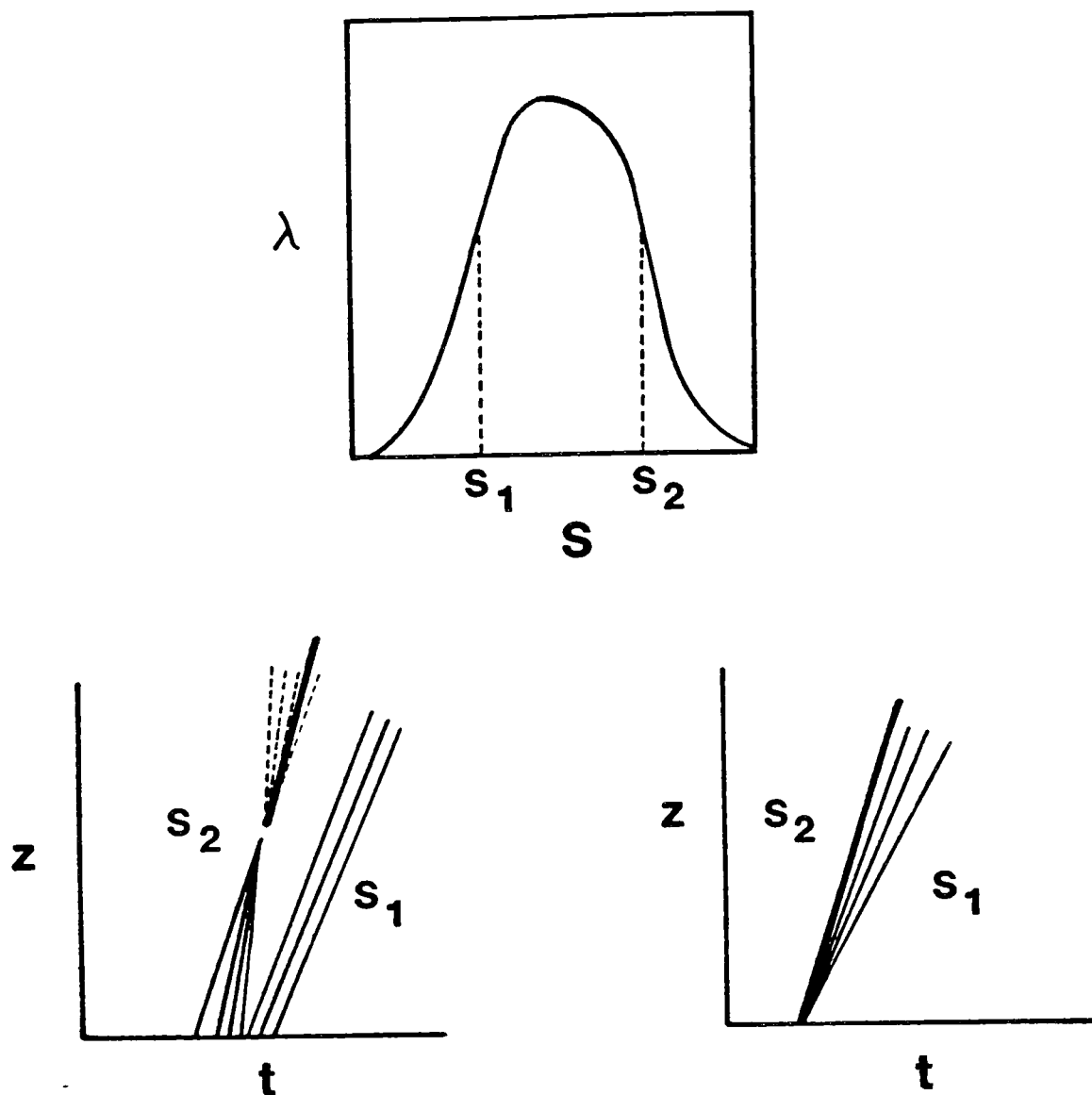


Figure 9 Composite wave generating function. Figure 9a shows eigenvalues which first increase, then decrease with S . Figure 9b shows a gradual boundary transition (in time) from constant state S_1 to constant S_2 . The wave contains both a continuous and a discontinuous portion. Figure 9c shows a similar abrupt transition.

Figure 10 shows the λ_1 eigenvalues as a function of water saturation for example 1, which is described below. Injection at high water saturation follows a path with initially increasing eigenvalues. At some point this wave breaks, causing a contact discontinuity to form. Wave breaking is associated with the decreasing eigenvalues. By comparison with figure 9a, the solutions for the multiphase Riemann problem are expected to consist of shocks and continuous waves which terminate in contact discontinuities. Figure 11 shows the λ_2 eigenvalues, which behave similarly to the λ_1 eigenvalues. The λ_2 eigenvalues, however, decrease very steeply in the vicinity of the maximum water saturation (approximately 0.85). Most injections at high water saturation experience decreasing λ_2 eigenvalues as the initial condition is approached, resulting in discontinuous paths.

SUMMARY OF APPROXIMATE GOVERNING EQUATIONS

For a Riemann problem, equation 20 along with initial data of the form

$$S(0,t) = S_1$$

$$S(z,0) = S_2$$

is reduced to the following forms. For continuous saturation composition variation, solution of equation 37

$$\frac{dS_o}{dS_w} = \frac{r_k(2)}{r_k(1)}$$

gives the saturation compositions across simple waves. The continuous wave speeds are given by equation 24

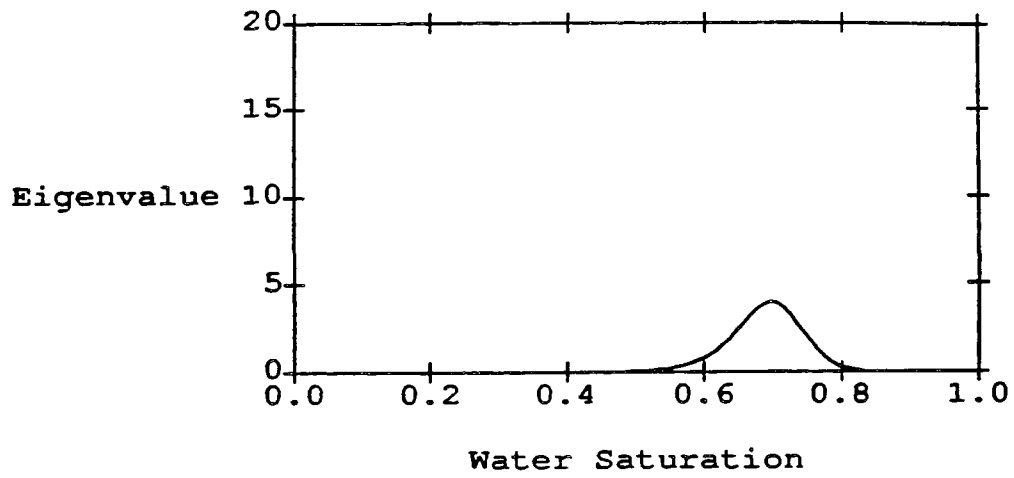


Figure 10 Example 1 λ_1 eigenvalues plotted as a function of water saturation.

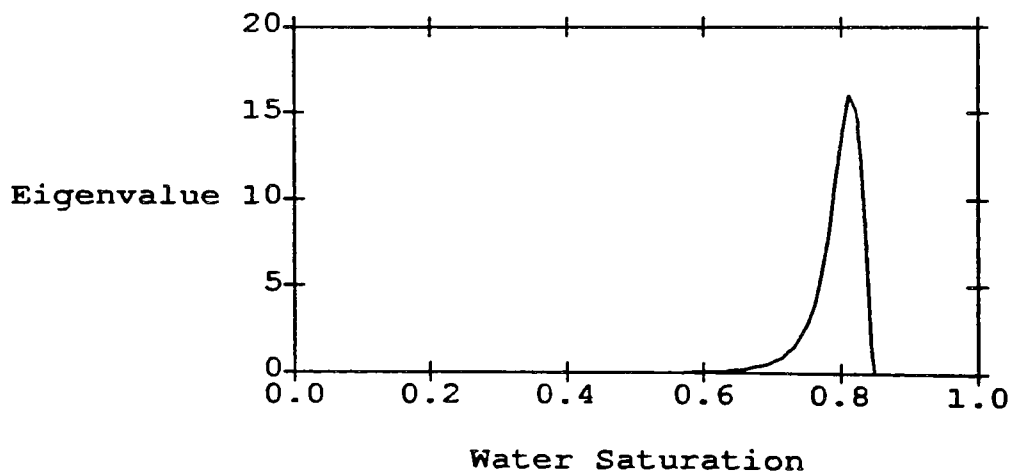


Figure 11 Example 1 λ_2 eigenvalues plotted as a function of water saturation.

$$\frac{dz}{dt} = \lambda_k$$

Since the characteristics within simple waves are straight lines, equation 24 has a simple analytical solution. When saturation composition variations are discontinuous, solution of the non-linear algebraic equation 40

$$S_o = S_o^* + \frac{f_o - f_o^*}{f_w - f_w^*} (S_w - S_w^*)$$

gives the saturation compositions across the discontinuities. The speeds of the discontinuities are given by equation 26

$$\frac{dz}{dt} = \frac{q_1}{\eta} \left(\frac{f_{w2} - f_{w1}}{S_{w2} - S_{w1}} \right)$$

NUMERICAL SOLUTION METHODS

Most of the model equations are reduced to ordinary differential equations by the application of the method of characteristics. Equations which do not have analytical solutions are solved by a Runge-Kutta-Fehlberg method (RKF, Fehlberg, 1969). Fehlberg's methods have the advantage that they contain automatic step size control based on a specified truncation error tolerance. For this work a third order method is used for the solution and an embedded fourth order method is used for the step size control (called RKF3(4)). Equation 37 is solved with the RKF3(4) solver for the saturation composition variation across the simple waves. Since the characteristic speeds are constant for simple waves and the speeds of the discontinuities are also constant, equations 24 and 26 represent straight lines and need not be solved numerically.

Discontinuous paths across the saturation space diverge from continuous paths when the latter are not straight (Helfferich 1970). Since equation 40 is a single non-linear algebraic equation, it is solved by a method which combines bisection, inverse quadratic interpolation, and the secant method (Press et al., 1986). The routine automatically chooses the most appropriate technique. The specific usage of equation 40 is discussed below. Note however, that for breaking waves, the origin (i.e., the point (S_w^*, S_o^*)), of a solution of equation (40) depends on the point at which the wave breaks. The solutions are thus problem dependent so that a general solution cannot be mapped in advance. This situation is in direct contrast to the continuous case where the saturation paths can be mapped for any initial and injection conditions.

CONSTRUCTION OF THE SATURATION COMPOSITION SPACE FOR THREE-PHASE FLOW

The input data for all the examples appears in appendix 5. In the first example, the oleic liquid's mobility is approximately one-third that of the water, since its density is less than that of water and its viscosity is higher. The media is a silt loam soil, with average parameters from Brakensiek et al. (1981). Since one potential application of the model is to the unsaturated zone, parameters representing actual soils are used. Soils, in general, are expected to have wider pore size distributions than aquifer materials, so the results presented here may differ somewhat from those determined for aquifer materials. Because of the width of the pore size distribution, the relative permeabilities drop rapidly as the saturation drops, due to the relatively high viscous dissipation in the smaller pores. Significant flow of the fluids thus occurs when saturations are high. These conditions, in fact, represent severe conditions for the mathematical model.

Figure 12 shows the solution of equation 37 for a number of initial saturation composition vectors. The results are plotted on a triangular domain where each point represents a particular value of $S = S(S_w, S_o, S_a)$. This representation of the solution is not unique to the Riemann problem, as any three-phase flow solution could be plotted this way. The saturations are read off the graph by noting

Riemann Problem Saturation Composition Space
Example 1

Residual Saturations

$S_{wr} = 0.0370$

$S_{or} = 0.0500$

$S_{ar} = 0.0518$

Matrix Properties

$\Lambda = 0.2099$

Fluid Properties

W-Density = 1.0000

O-Density = 0.7000

A-Density = 0.0012

W-Viscosity = 1.0019

O-Viscosity = 2.0039

A-Viscosity = 0.0170

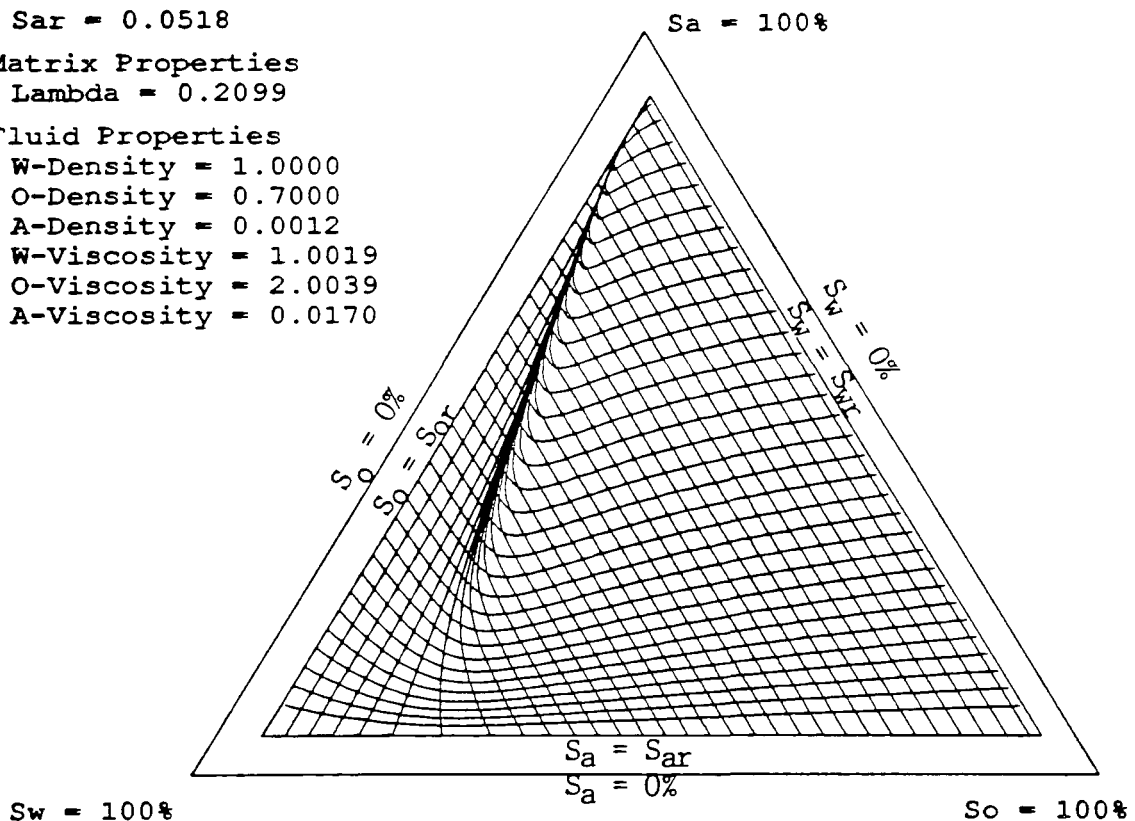


Figure 12 Example 1 saturation composition space showing all paths (variations in saturation composition) which occur as solutions of the Riemann problem. The triangle vertices are points of 100% saturation, while the edges are lines of zero saturation.

that each side represents zero saturation of a fluid and the vertex opposite that side represents full saturation. For example, the top vertex represents completely air-filled pore space, $S_a = 1$, and the bottom of the triangle represents the two-phase water/oleic liquid system where no air is present in the pore space, $S_a = 0$. The point at the middle of the triangle represents equal saturation of all fluids, $S(0.3333, 0.3333, 0.3333)$.

The inner triangle bounds the region where all three fluid saturations are above residual. Air is assumed to have a trapped (called residual) saturation during the injection processes considered here. The trapped air saturation is assumed to be the air saturation which results in water relative permeability of one-half, a value which comes from observation (Bouwer, 1966). In between the boundaries, each path drawn represents part of a classical Riemann problem solution, as they are determined from solution of equation 37. At each point within the saturation space, there are two possible directions of saturation change, one associated with each eigenvalue. So the inner triangle is filled with a grid representing all possible saturation composition variations which are solutions of equation 37.

The calculations required for developing the entire saturation composition space typically require less than 20 minutes of CPU time on a VAX 11/785 minicomputer. Solutions for specific problems like those discussed below require much less CPU time as they do not require construction of the entire saturation composition space.

The solutions for the λ_1 -waves originate at points with oleic liquid saturations just above residual. Beginning at residual saturation is not possible, because the three-phase equations are singular at $S_o = S_{or}$ and the two-phase water-air equations have no component (see equation 37) which points toward increasing oleic liquid saturation. The λ_1 -waves are determined via solution of the water/oleic liquid equation 37. This equation is used instead of oleic liquid/air or water/air formulations, because the paths end at the $S_w = S_{wr}$ edge. Thus the end point of the interval of integration is known. The solution for the λ_2 -waves uses equation 37 and its water/air analogue to complete the paths. The solutions begin at points with $S_a = 0.15$ and solved toward $S_a = S_{ar}$ with the water/air equations, then

solved toward $S_o = S_{or}$ with the water/oleic liquid equation. The partial derivatives of the fractional flow for the water/air system are found in a fashion similar to that presented in appendix 1. Solving across the domain with different sets of equations (water/air, water/oleic liquid, oleic liquid/air) provides a check of the solution. Here, all three sets produced identical paths.

QUALITATIVE NATURE OF THREE-PHASE FLOW

Before discussing specific Riemann problem solutions which can be constructed from figure 12, the qualitative nature of three-phase flow in this domain will be discussed. These results are representative of results obtained with other oleic liquids, soils and total fluxes. Paths resulting from solution of equation 37 with the small eigenvalue, λ_1 , begin on the residual oleic liquid side of the triangle and end on the residual water side. These paths are all bowed toward the residual air side of the triangle, indicating that water/air and oleic liquid/air injections beginning on the left and right sides of the triangle, respectively, tend to cause displacement of air from the pore space. The eigenvalues associated with an injection at $S_w = 0.849$, $S_o = 0.0501 \equiv S_{or}$, and $S_a = 0.1009$ are shown in figure 10. Since the eigenvalues decrease in magnitude after the water saturation decreases below approximately 0.70, a λ_1 -wave with this path becomes discontinuous. Breaking of the wave results in a contact discontinuity, which determines the exact saturations at the wave front.

Paths originating along the base of the inner triangle are associated with the larger eigenvalue, λ_2 , and follow three distinct patterns. First, those originating near the left vertex ($S_w = 1$) are nearly parallel to the left edge of the triangle. In waves associated with such paths there is no appreciable change in oleic liquid saturation even though all three phases flow. Although the oleic liquid is flowing and its saturation is above residual, there is unsteady flow in only the water and air phase along these paths. Second, paths originating near the right vertex ($S_o = 1$) display similar behavior with regard to the water phase, in that only the oleic liquid and air saturations vary. The third type of path is intermediate between the extremes and shows variation in all three saturations. These latter paths

cover only a small region of the space. This behavior agrees with intuition as there is only a relatively small region where all three relative permeabilities are significant (e.g., Leverett and Lewis, 1941).

CONSTRUCTION OF SATURATION PROFILES

Solutions are constructed from figure 12 by determining an injection condition-plateau-initial condition route on the diagram. This terminology follows Helfferich (1981) as portions of paths are used to construct routes for each specific problem. Construction of the complete set of paths crossing the saturation space is not necessary for a specific problem; only the route is needed. The wave associated with λ_1 (the smaller eigenvalue) is followed from the injection condition toward the plateau. This wave is called a λ_1 -wave or slow wave, and is followed first, because with smaller eigenvalues this wave must be traversed before the faster wave (the λ_2 -wave). At the plateau, the solution switches to the λ_2 -wave to complete the route to the initial condition. The route determines the specific saturation compositions which exist in the solution. The occurrence in space and time of the saturations along the route is determined by equation 24 on the continuous portion of the wave. When discontinuities form, the route is adjusted as discussed below. The adjustment alters the saturation composition at the plateau and thus the wave speeds. The speeds of the discontinuous portion of the waves (shocks) are determined by equation 26. The continuous and discontinuous paths for this example are shown in figure 13. When the routes are straight lines, the continuous and discontinuous routes are identical, and only one λ_2 route exists. In this example the λ_1 routes are almost coincident.

Riemann Problem Saturation Composition Space
Example 1 Saturation Routes

Residual Saturations

$S_{wr} = 0.0370$

$S_{or} = 0.0500$

$S_{ar} = 0.0518$

Matrix Properties

$\Lambda = 0.2099$

Fluid Properties

W-Density = 1.0000

O-Density = 0.7000

A-Density = 0.0012

W-Viscosity = 1.0019

O-Viscosity = 2.0039

A-Viscosity = 0.0170

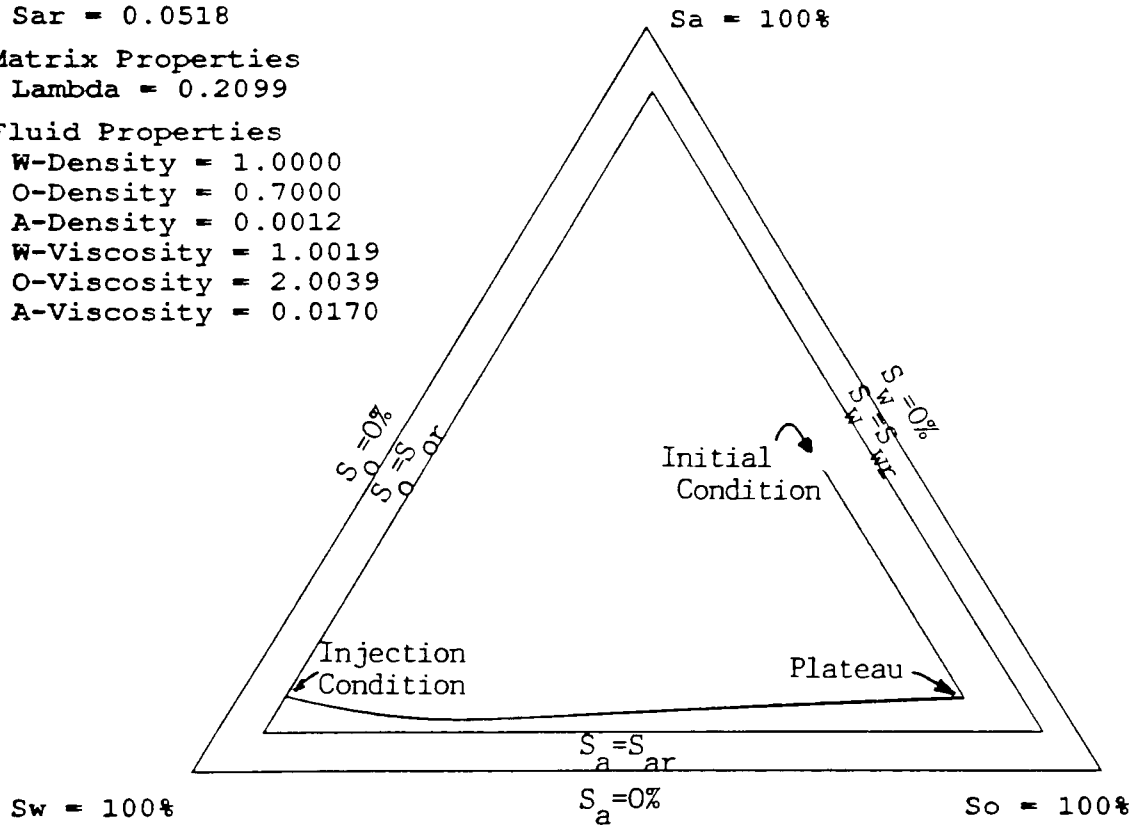


Figure 13 Example 1 saturation routes showing continuous solution of equation 37 and the correction due to equation 40, which are nearly identical.

TWO-PHASE INJECTIONS

Example 1 Oleic Liquid Bank Formation

In example 1, water and air are injected into the soil at a saturation composition of $S = S$ (0.8490, 0.0501, 0.1009). Air is injected for illustrative purposes in these examples; later, injections without air are discussed. The oleic liquid saturation at injection is slightly above residual ($S_{or} = 0.0500$), because the solution along the side of the inner triangle is degenerate. That is, the side is a two-phase region, with no path which enters the three-phase region. Also, the three-phase equations are singular along the edge (i.e. $k_{ro} = 0$ at $S_o = S_{or}$ in equation 53) and cannot be used. In this example the total flux equals 2.00 m/d. The water, oleic liquid and air fluxes are determined from the fractional flow equations (52 and 53), given the injection saturation composition. Selection of the injection saturation composition is an important aspect of the problem solution. Allowing air to be above residual serves two purposes. First, water may not fill the pore space during injection (rainfall). This is particularly the case when air actually flows out of the domain (McWhorter, 1971). The second reason for this type of injection is that it causes the λ_1 and λ_2 waves to separate from each other completely so that there is no overlap. This condition is similar to that occurring in ion-exchange chromatography solutions (Helfferich, 1970) which were studied in preparation for application to three-phase flow.

A depth-time plot of the solution, which is called the base characteristic plane, is shown in figure 14. Shown on the plot are the λ_1 - and λ_2 -waves. In this case, the λ_1 -wave has a continuous portion which is illustrated by the fan-shaped characteristic pattern. This wave is a λ_1 -centered simple wave which terminates in a contact discontinuity. The λ_2 -wave is discontinuous and is demonstrated below to be a 2-shock. The plateau emerges from the origin and expands with time because of the difference in speed between the contact discontinuity and the 2-shock. Ahead of the 2-shock is the initial condition; at any time the location of the 2-shock corresponds to the maximum influence of the injection.

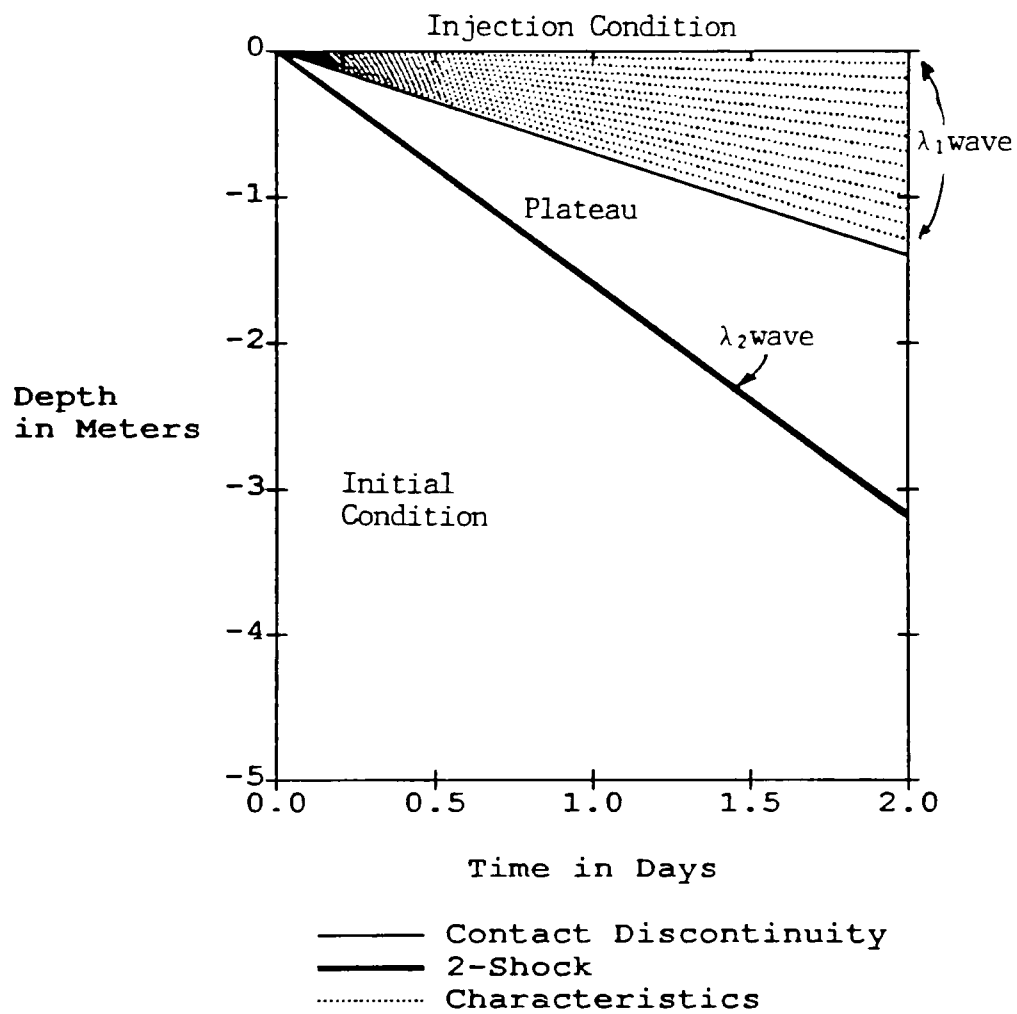


Figure 14 Example 1 base characteristic plane (depth-time plot of the solution). The solution consists of a centered simple wave, contact discontinuity and 2-shock.

Figure 15 shows a depth-saturation profile for the solution at 24 hours after the beginning of the injection. Depth-saturation profiles compliment the base characteristic plane as they show the fluid saturations at a given time in the solution. The water and total liquid saturation are plotted directly against the depth. The oleic liquid saturation is the difference between the total liquid and water saturations. Likewise, the air saturation is determined by subtracting the total liquid saturation from one. Recall that at the boundary (depth = 0) the oleic liquid is very near its residual saturation, and water and a small amount of air are injected. The general nature of this solution is that the injection at the surface causes the oleic liquid to be displaced into a bank moving ahead of the water front (CEFG on figure 15). At this time, the water front is located at a depth of 0.73 meters (CD). The water saturation at the front remains constant at 0.7821. The oleic liquid displacement is not complete, as some of it is left behind the water front at saturations above residual (ABDE, the distance between A and B is the oleic liquid injection condition which is close to residual). The water saturation decreases from the injection (A) to the water front due to the oleic liquid that is bypassed (AD). The smooth variation in saturation above the water front corresponds to the λ_1 -centered simple wave on figure 14.

Most of the oleic liquid is displaced, however, into a bank moving ahead of the water front. In this example the oleic liquid bank is bounded above by the contact discontinuity and below by the 2-shock (figure 14). The bank corresponds to the plateau in the saturation space where $S = S(0.1000, 0.8034, 0.0966)$. The water saturation at the plateau equals the initial water saturation ($S_w = 0.1000$), because the λ_2 -wave portion of the route is a straight line parallel to the water axis. The bank front (FG) moves faster than the water front (CD), and so the bank expands with time. (Compare the solution at 24 hours with that for 48 hours, as shown on figures 15 and 16.) The bank forms because the flux of the oleic liquid is high enough so that it can move ahead of the incoming water. The leading edge of the oleic liquid bank (FG) is discontinuous, because the λ_2 eigenvalues decrease from the plateau to the initial condition. The details of how the discontinuous route is established follow.

When the λ_1 - wave breaks, equation 40 is used to determine the route from the water front to the plateau. The saturation at the wave front, where the wave breaks, is the known (starred) saturation composition in equation 40, and the discontinuous plateau saturation is unknown. The saturation composition at the front is determined in the following way. By iteration, a characteristic

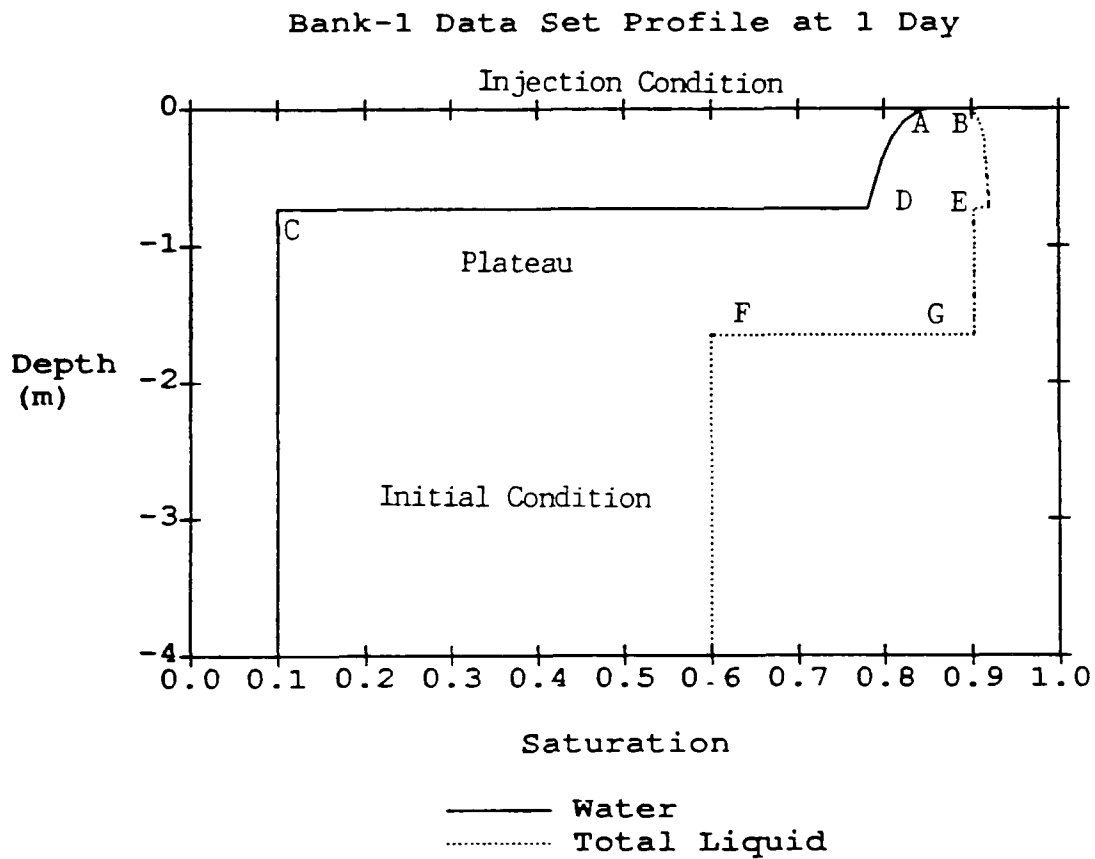


Figure 15 Example 1 saturation profile at 24 hours showing fluid saturations versus depth of penetration. The oleic liquid is being displaced into a bank (CEFG) by the incoming water and air.

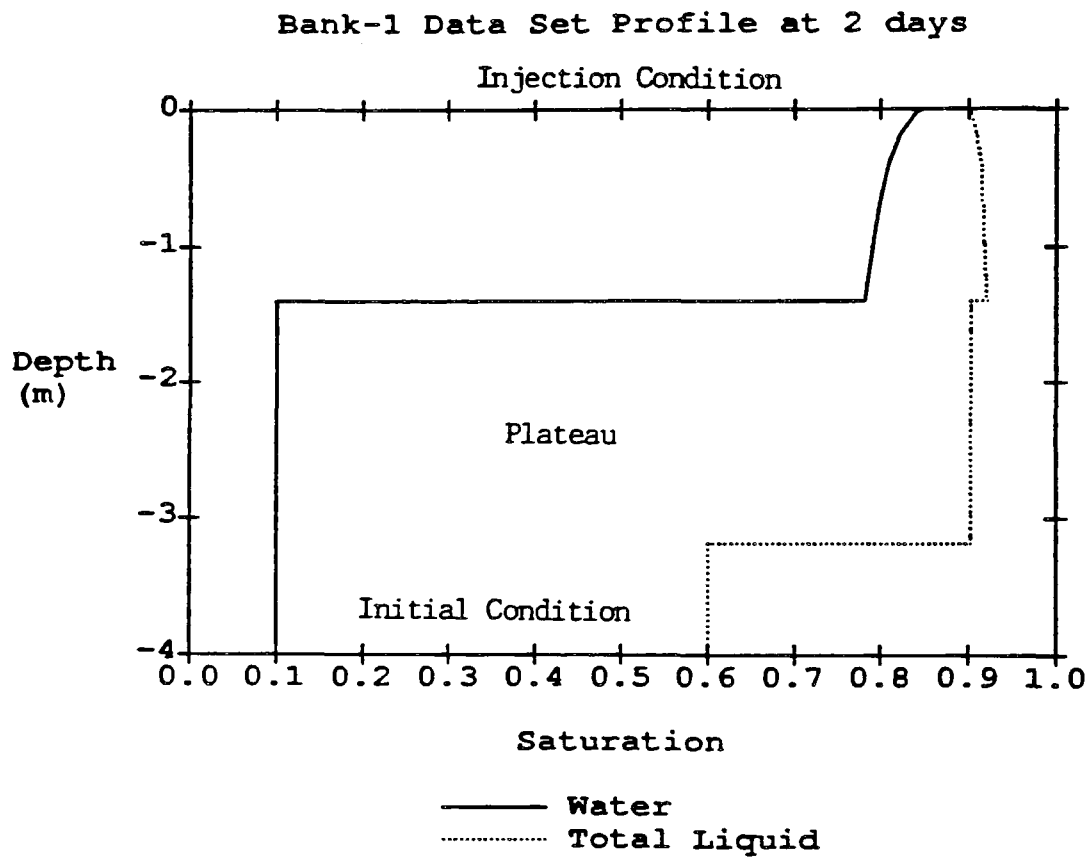


Figure 16 Example 1 saturation profile at 48 hours showing migration of the fronts at fixed saturations (compare with figure 15).

speed is found that matches the speed of the discontinuity (jump condition, equation 26) from the front composition to the plateau (initially estimated by the intersection of the continuous waves). The discontinuous route is found by solving equation 40 with the trial frontal saturations. An outer iteration is used to determine the value of the frontal saturations and plateau saturations which satisfy both the jump condition (equation 26) and equation 40 simultaneously. Typically two or three iterations are required to find the correct compositions.

For most of the saturation space, the paths from a plateau to an initial condition experience decreasing eigenvalues. So the route from plateau to the initial condition is discontinuous and must also be determined by solution of equation 40. In this case the starred saturation composition is the initial composition, and once again the plateau saturation is unknown. Solution of equation 40 for both front to plateau and plateau to initial condition gives a new composition route across the saturation space. The point where the two lines meet is the new plateau, and both equations are satisfied simultaneously. In practice the plateaus diverge slightly from the continuous wave plateaus. The slight divergence is enough to significantly affect the mass balance of the solution. Figure 13 shows the continuous and the discontinuous routes, which are almost identical for this example.

The location in S-space of the intersection between the two waves is critical in determining the character of the solution. If the intersection occurs after the λ_1 -wave breaks, a discontinuity forms in the λ_1 -wave before the plateau is reached. The λ_2 -wave from the plateau to the initial condition is a breaking wave because the eigenvalues decrease in the direction of the initial condition. This sequence describes the bank profile discussed above. When the plateau is reached before the λ_2 -wave breaks, however, a second type of profile is produced. Here there is a continuous wave solution from the injection condition all the way to the plateau, and again a discontinuity from the plateau to the initial condition. The discontinuity in the oleic phase saturation is very slight in this case, and the solution is characterized by bypassing of the oleic liquid by the water.

Example 2 Oleic Liquid Bypassing

Figure 17 shows the bypassing profile that is produced when the initial condition is $S(0.5000, 0.1000, 0.4000)$, and the injection condition is the same as for example 1. In essence, the effective conductivity of oleic liquid present initially is insufficient to match the speed of the incoming water. All of the oleic liquid is bypassed by the water. The base characteristic plane for example 2 is shown in figure 18. The λ_1 -centered simple wave merges with the plateau before a discontinuity can form, so there is no contact discontinuity and no oleic liquid bank in this example. As in example 1, the λ_2 -wave is a 2-shock, the position of which determines the maximal influence of the injection. There is a slight discontinuity in oleic liquid saturation (0.1019 above vs. 0.1000 below) at this front (A). This small jump moves at the same speed as the water front.

Example 3 Oleic Liquid Bank Formation, Second Type

When the initial condition is nearer the center of the saturation space, the λ_2 path is curved, thus all three fluid saturations in the bank differ from the initial condition. Figure 19 shows a resulting profile with this initial condition. For such a displacement process the difference between the continuous and discontinuous routes through the saturation space is significant (figure 20, contrast to figure 13).

The three types of solutions discussed above (bypassing, bank forming with the plateau water saturation equal to the initial water saturation, and bank forming with different plateau and initial water saturations) are related to each other by the locations of the λ_2 routes in the saturation composition space (figure 21). At low initial air saturation, as used in the above examples, the character of the solution changes gradually from bypassing to bank forming as the initial oleic liquid saturation increases along the line labeled A-A' on figure 21. When the air saturation is higher, as the oleic liquid saturation increases along line B-B', the zone where the λ_2 paths merge is relatively abrupt, and so is the transition between the types of solutions. Initial conditions lying near this zone represent problems

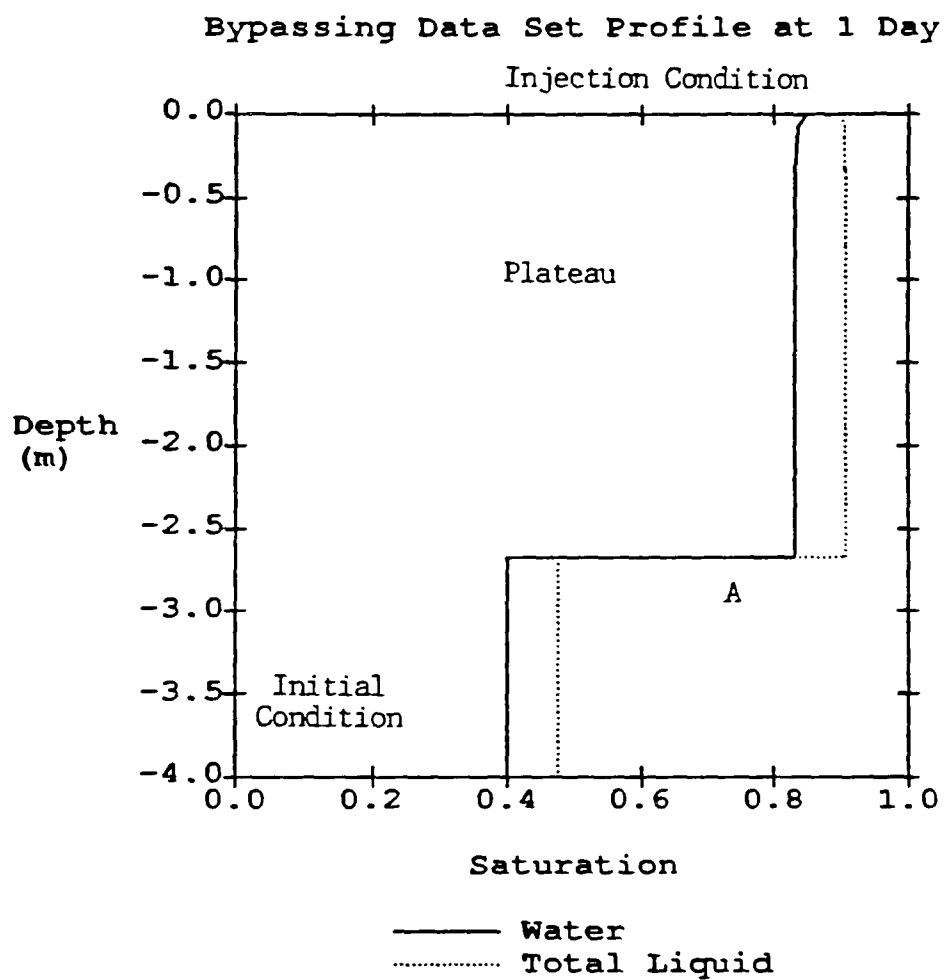


Figure 17 Example 2 bypassing profile showing fluid saturation versus depth. The incoming water and air bypasses the oleic liquid.

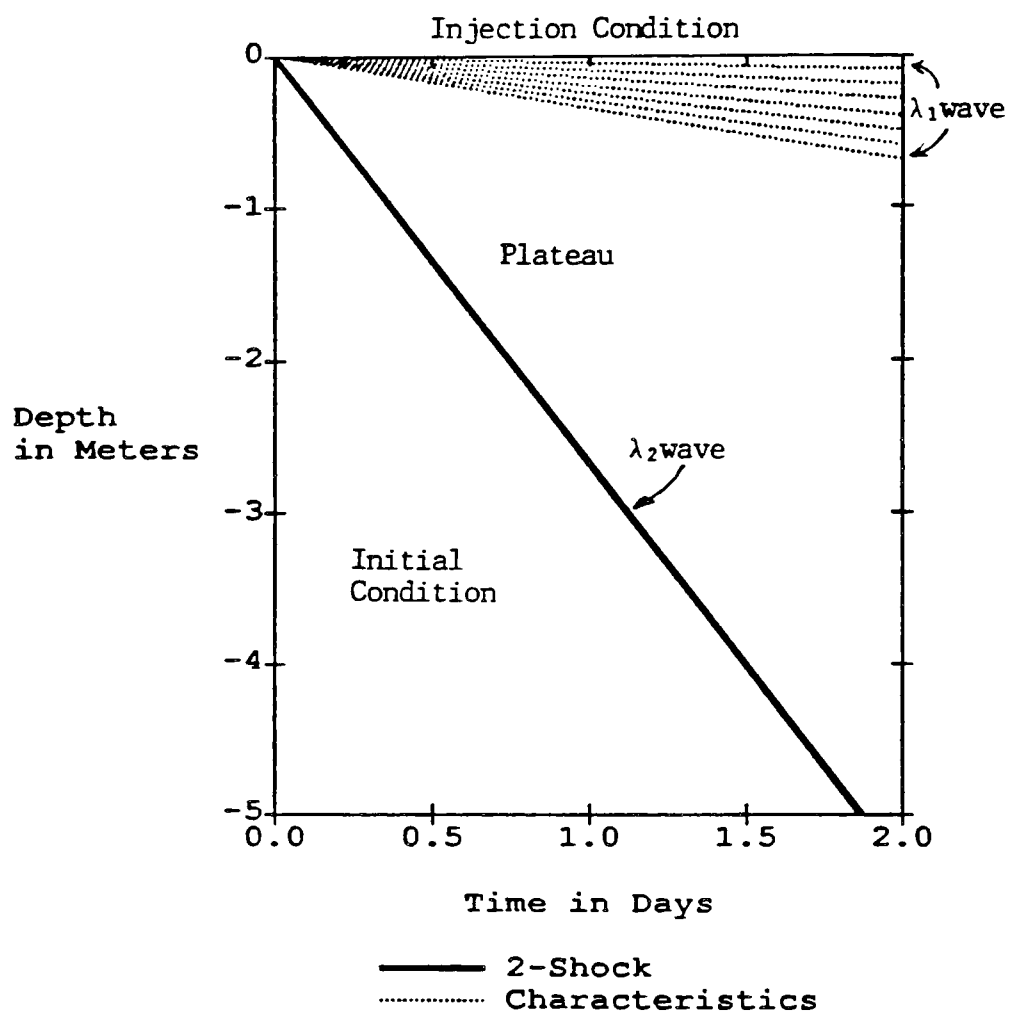


Figure 18 Example 2 base characteristic plane (depth-time plot of the solution). The solution consists of a centered simple wave, and 2-shock.

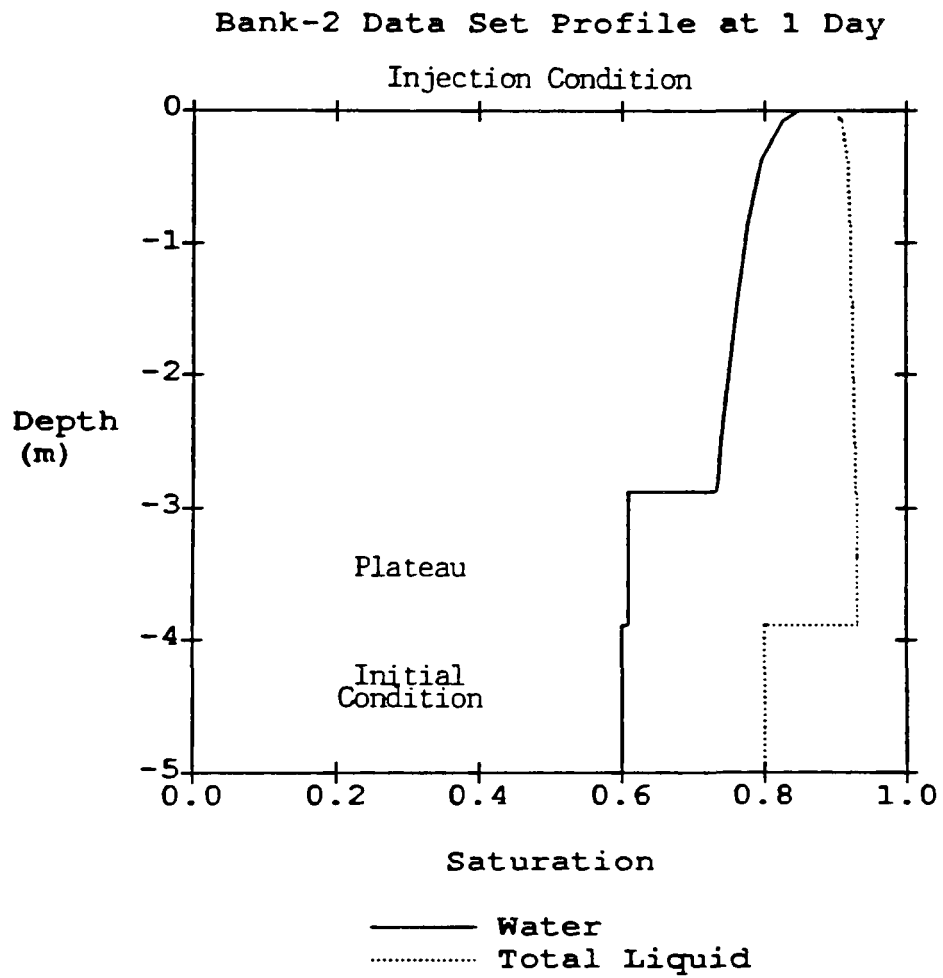


Figure 19 Example 3 bank profile with differing initial and plateau water saturations.

Riemann Problem Saturation Composition Space
 Example 3 Saturation Routes

Residual Saturations

$S_{wr} = 0.0370$
 $S_{or} = 0.0500$
 $S_{ar} = 0.0518$

Matrix Properties

$\Lambda = 0.2099$

Fluid Properties

W-Density = 1.0000
 O-Density = 0.7000
 A-Density = 0.0012
 W-Viscosity = 1.0019
 O-Viscosity = 2.0000
 A-Viscosity = 0.0170

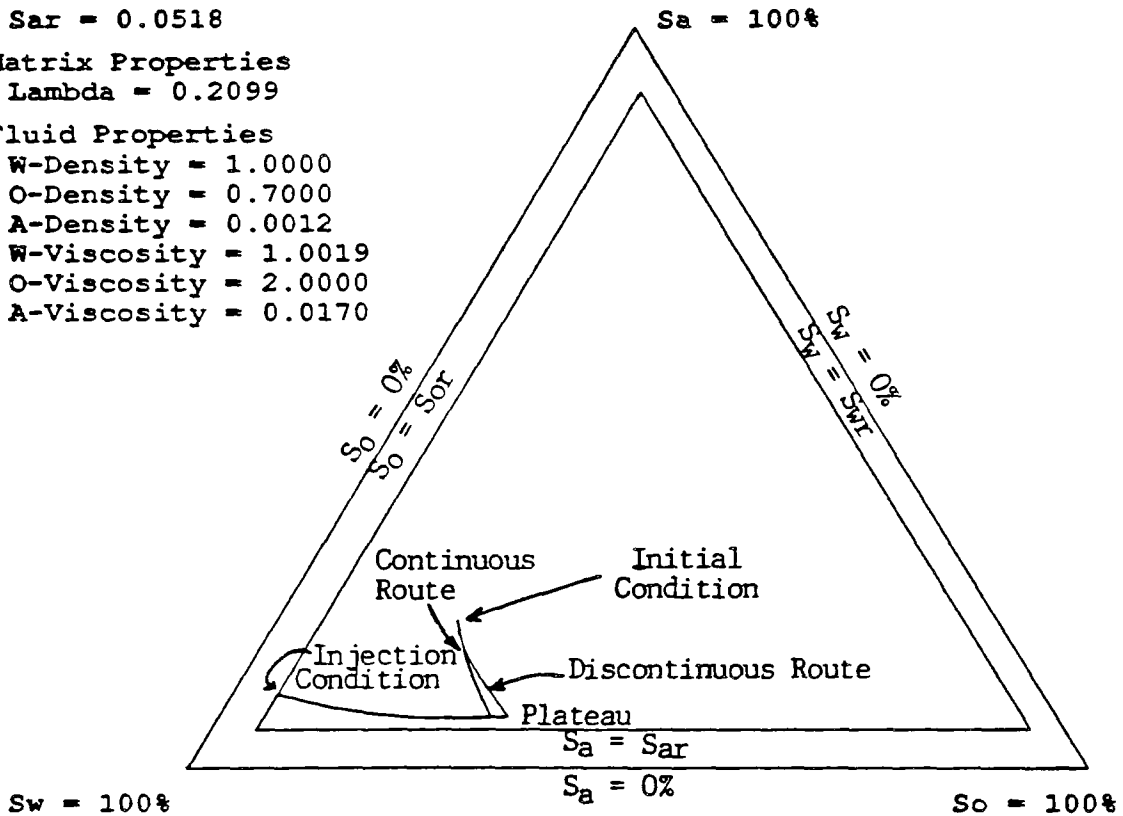


Figure 20 Example 3 saturation routes showing the continuous solution of equation 37 and its discontinuous correction with equation 40.

Riemann Problem Saturation Composition Space
Example 1

Residual Saturations

$S_{wr} = 0.0370$

$S_{or} = 0.0500$

$S_{ar} = 0.0518$

Matrix Properties

$\Lambda = 0.2099$

Fluid Properties

W-Density = 1.0000

O-Density = 0.7000

A-Density = 0.0012

W-Viscosity = 1.0019

O-Viscosity = 2.0039

A-Viscosity = 0.0170

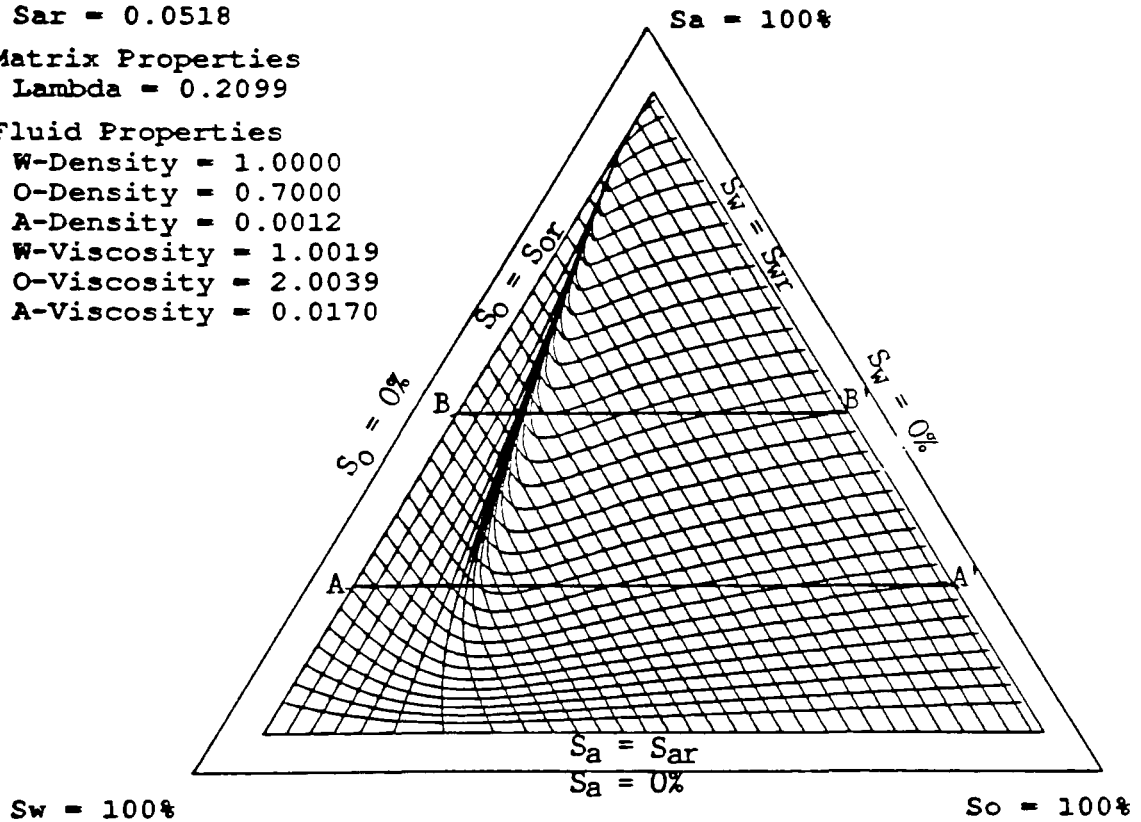


Figure 21 Profile transition from bypassing to bank forming. Line AA' crosses a region with a smooth variation from bank to bypassing profiles. Line BB' crosses a region with an abrupt variation from bank to bypassing profiles.

where the method is essentially unstable, because the paths heading down toward the bottom of the triangle diverge in many directions. A small change in the initial data causes a large change in the solution.

Low mass conservation error in the examples demonstrates the existence of the solution to the model equation 20. Since the governing equations are derived from mass conservation equations, mass conservation is required in the solution. In other numerical methods, higher mass balance errors are sometimes tolerated. Here, however, correct mass balance provides some assurance that the solution has the correct plateaus, λ_k -simple waves, shocks and contact discontinuities. These features must be programmed into the model, instead of arising purely from the solution. This difficulty is the reason why so much emphasis is placed on the qualitative nature of the solutions in the previous sections. Incorrect choices of solution features always lead to "solutions" which do not conserve mass. So very low mass balance errors are required for these Riemann problem solutions. Table 1 shows the mass balance errors for examples 1 to 3. All of the errors are less than 0.2% and most are one or two orders of magnitude lower. The highest mass balance error occurs for example 3, where the plateau water saturation is different from the initial water saturation. In some regard this case is the most difficult computationally.

Table 1 Mass Balance Errors for Examples 1 to 3

<u>Example</u>	<u>Water Phase % error</u>	<u>Oleic Liquid % error</u>
1	-0.0019	-0.0358
2	-0.0056	0.0652
3	-0.0700	-0.1570

Table 2 shows the eigenvalues and shock speeds for the major examples (1 to 3) presented in this report. Examples 1 and 3 each have two shocks in their solutions: a contact discontinuity, and a 2-shock. The contact discontinuity is "almost" a 1-shock. Example 2 has only one shock, which is a 2-shock. The results presented in this table demonstrate that the discontinuities in the solutions obey the appropriate shock inequalities (equations 28 to 32).

Table 2 Shock Inequalities Satisfied by Examples 1 to 3

Example 1

a. Incoming water front

Shock speed, $s = 0.7014$ m/d

$$\lambda_1(S_1) = 0.7013$$

$$\lambda_1(S_2) = 0.1453e-11$$

$$\lambda_2(S_1) = 21.94$$

$$\lambda_2(S_2) = 14.24$$

Shock inequalities satisfied: $\lambda_1(S_2) < s < \lambda_2(S_2)$

$$s = \lambda_1(S_1)$$

Shock type: "almost" 1-shock, contact discontinuity

b. Oleic liquid bank front

Shock speed, $s = 1.5921$ m/d

$$\lambda_1(S_1) = 0.1453e-11$$

$$\lambda_1(S_2) = 0.2770e-12$$

$$\lambda_2(S_1) = 14.24$$

$$\lambda_2(S_2) = 0.6706e-2$$

Shock inequalities satisfied: $\lambda_2(S_2) < s$

$$\lambda_1(S_1) < s < \lambda_2(S_1)$$

Shock type: 2-shock

Table 2 (Continued)

Example 2

Oleic liquid bypassing

Shock speed, $s = 2.6684 \text{ m/d}$

$$\lambda_1(S_1) = 0.9648e-1$$

$$\lambda_1(S_2) = 0.6072e-5$$

$$\lambda_2(S_1) = 38.31$$

$$\lambda_2(S_2) = 0.1727e-3$$

Shock inequalities satisfied: $\lambda_2(S_2) < s$
 $\lambda_1(S_1) < s < \lambda_2(S_1)$

Shock type: 2-shock

Example 3

a. Incoming water front

Shock speed, $s = 2.8900 \text{ m/d}$

$$\lambda_1(S_1) = 2.890$$

$$\lambda_1(S_2) = 1.021$$

$$\lambda_2(S_1) = 29.58$$

$$\lambda_2(S_2) = 32.32$$

Shock inequalities satisfied: $\lambda_1(S_2) < s < \lambda_2(S_2)$

$$s = \lambda_1(S_1)$$

Shock type: "almost" 1-shock, contact discontinuity

Table 2 (Continued)

Example 3 (continued)

b. Oleic liquid bank front

Shock speed, $s = 3.8951 \text{ m/d}$

$$\lambda_1(S_1) = 1.021$$

$$\lambda_1(S_2) = 0.3161\text{e-}1$$

$$\lambda_2(S_1) = 32.32$$

$$\lambda_2(S_2) = 0.6853\text{e-}1$$

Shock Inequalities satisfied: $\lambda_2(S_2) < s$
 $\lambda_1(S_1) < s < \lambda_2(S_1)$

Shock type: 2-shock

Example 4 Flow of TCE

When the mobility of the oleic liquid is greater than water, the character of the results changes slightly. For the same soil as examples 1 to 3, but with TCE as the oleic liquid, figure 22 shows the saturation composition space. Here the mobility of the TCE is almost three times that of the water. With higher oleic phase mobility, there is a greater tendency for oleic liquid banks to form as the diagram has fewer bypassing paths (paths parallel to the $S_o = S_{or}$ edge). More initial conditions result in banks than previously (examples 1 to 3), and only the lowest oleic liquid initial conditions result in bypassing profiles. The oleic liquid, although now more mobile than water, still occupies the middle range of the pore size distribution. Much of the qualitative character of the oleic liquid flow is due to this fact, largely independent of the oleic liquid properties.

Example 5 Horizontal Flow

When the flow is horizontal, some terms drop out of the fractional flow equations (appendix 3). Given the same soil type, oleic liquid, and total flux as example 1, the loss of the gravity terms causes a slight change in the saturation composition space, resulting in slightly changed saturation profiles. (Compare figures 12 and 23). Comparison of the gravity and non-gravity forms of the fractional flow equations (52 and 53 vs. 60 and 61) shows that the effect of gravity depends on the density differences, oleic liquid relative permeability, and air relative permeability. For example, the saturation composition space (figure 23) for horizontal flow is almost identical to that for vertical flow at low air saturation. Profiles for both vertical flow (example 1) and horizontal flow are shown in figures 24 and 25. The only difference in the scenarios is the absence of gravity in the horizontal flow case. At one day after the beginning of the injection, the water and oleic liquid fronts are deeper when gravity is included. Obviously, gravity adds a driving force to the vertical system that is absent from the horizontal. Figure 25 shows the profiles at the end of 2 days. Only very slight differences in saturation are seen in the continuous portions of the profiles as the air saturations are low.

Riemann Problem Saturation Composition Space
TCE Saturation Composition Space

Residual Saturations

$S_{wr} = 0.0370$

$S_{or} = 0.0500$

$S_{ar} = 0.0518$

Matrix Properties

$\Lambda = 0.2099$

Fluid Properties

W-Density = 1.0000

O-Density = 1.4600

A-Density = 0.0012

W-Viscosity = 1.0019

O-Viscosity = 0.5699

A-Viscosity = 0.0170

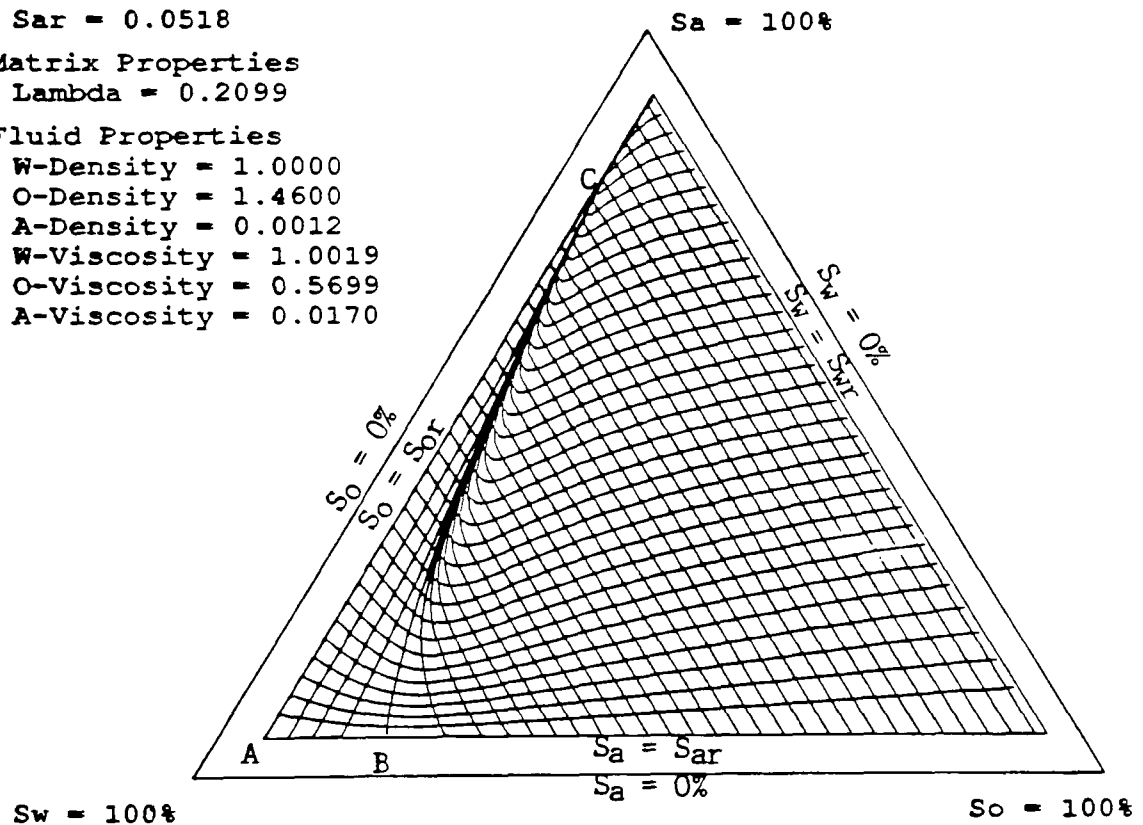


Figure 22 Example 4 TCE saturation composition space showing, by comparison to figure 12, a compressed zone of bypassing profiles (ABC).

Riemann Problem Saturation Composition Space
 Example 5 Horizontal Flow

Residual Saturations

$S_{wr} = 0.0370$

$S_{or} = 0.0500$

$S_{ar} = 0.0518$

Matrix Properties

$\Lambda = 0.2099$

Fluid Properties

W-Density = 1.0000

O-Density = 0.7000

A-Density = 0.0012

W-Viscosity = 1.0019

O-Viscosity = 2.0039

A-Viscosity = 0.0170

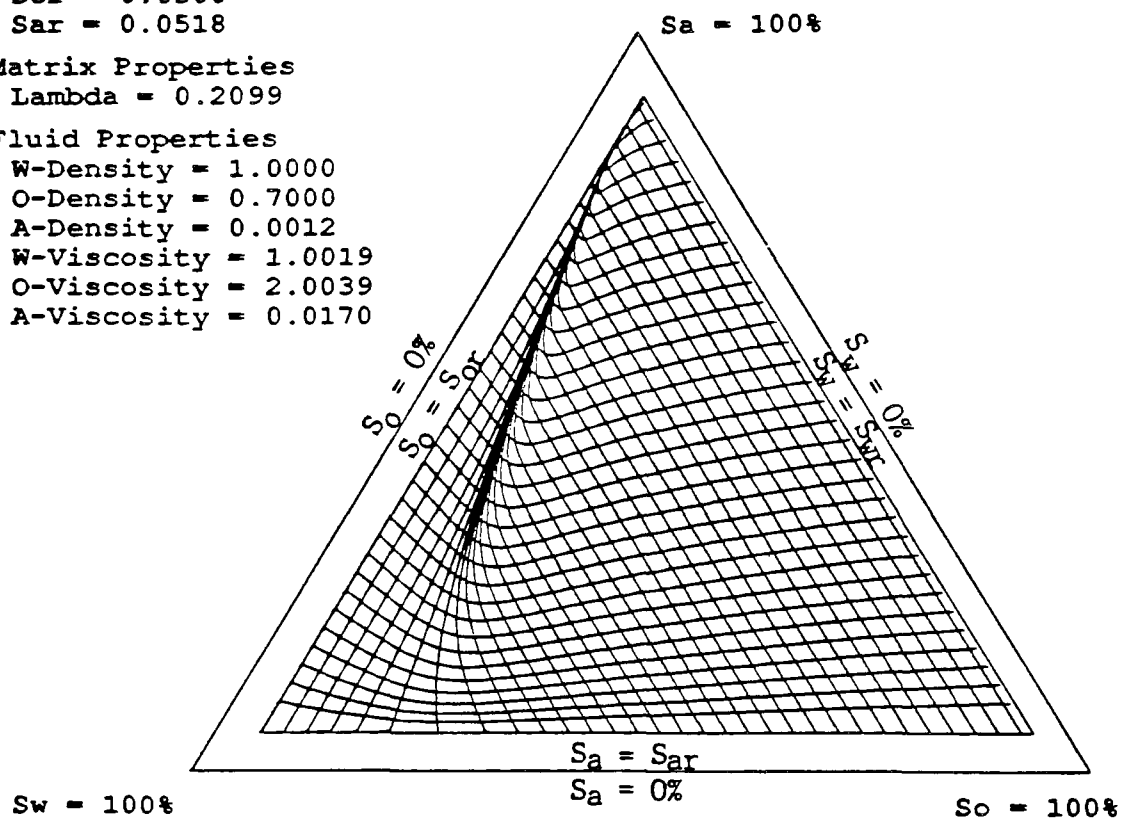


Figure 23 Example 5 horizontal flow saturation composition space.

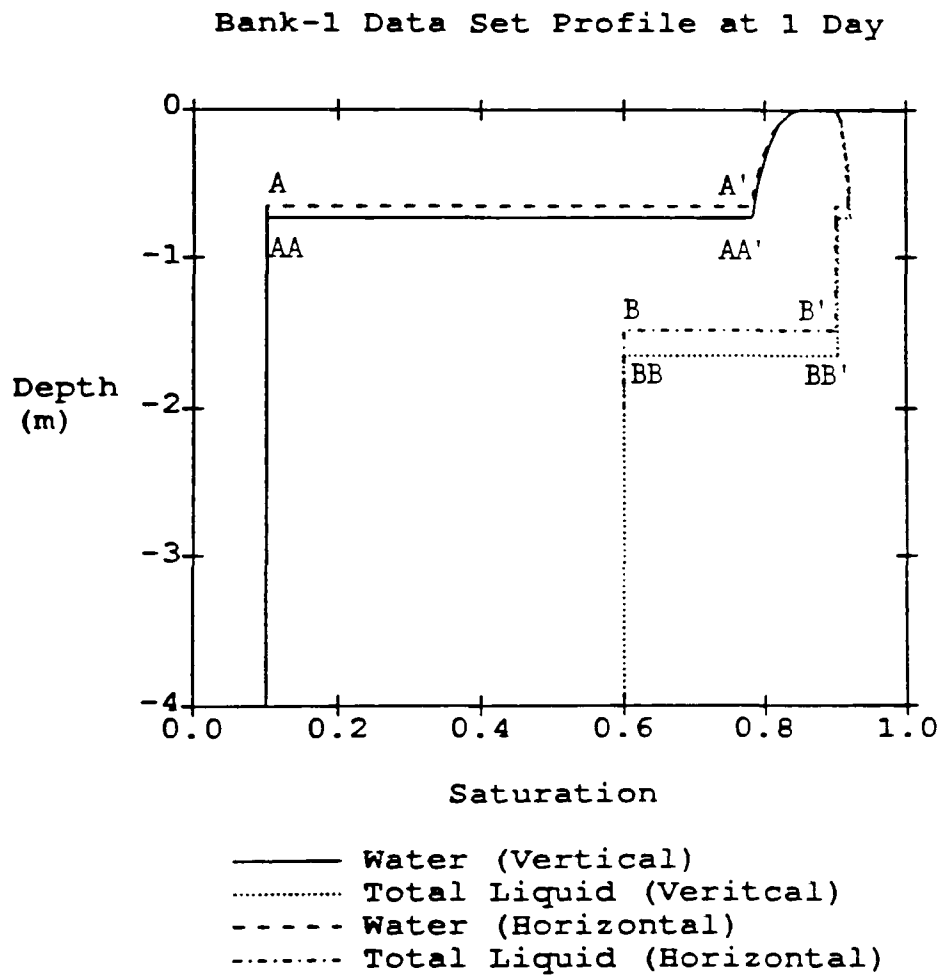


Figure 24 Example 5 comparison of horizontal (A-A' and B-B') and vertical (AA-AA' and BB-BB') bank profiles at 1 day.

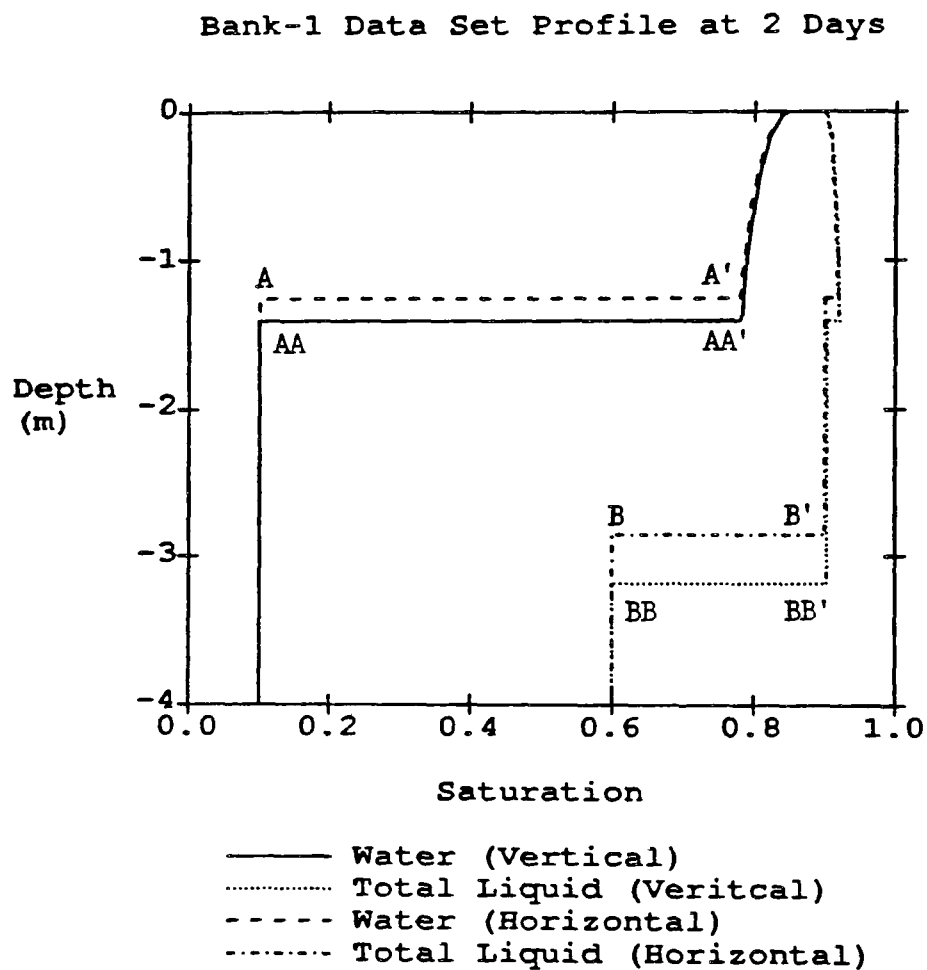


Figure 25 Example 5 comparison of horizontal (A-A' and B-B') and vertical (AA-AA' and BB-BB') bank profiles at 2 days.

Example 6 Oleic Liquid/Air Injection

The previous examples have focused on injections with the oleic liquid at residual. When the injection consists of oleic liquid and air, with water at residual, the solution is constructed exactly as described above, only with different initial and injection conditions. Returning to figure 12, injections from the right edge ($S_w = S_{wr}$) can be seen to favor bypassing of the water by the oleic liquid over water bank formation. The explanation for these phenomena follows. The eigenvalues (figure 10) increase slowly as the water saturation increases, reaching a maximum at $S_w = 0.85$. Thus the contact discontinuity occurs only after the oleic liquid saturation decreases to a low value. As before, if the initial condition lies on a λ_2 path which intersects the λ_1 path before the discontinuity occurs, then the solution is characterized by bypassing. In this case, it is water that is bypassed, and the large number of paths parallel to the $S_w = S_{wr}$ edge results in mostly bypassing profiles. The water bank profiles result mostly from λ_2 paths which are parallel to the $S_o = S_{or}$ edge. Only a relatively few λ_2 paths of this type exist. The latter paths are associated with very low initial oleic fluid saturations.

Injection at $S(0.10, 0.80, 0.10)$ with an initial condition of $S(0.700, 0.075, 0.225)$ results in displacement of the water into a water bank (figure 26). The oleic liquid saturation drops very rapidly in the upper part of the slow wave (EH). The oleic liquid saturation at the front is lower than the water saturation for a corresponding water injection. This behavior indicates the tendency for the water to remain in place in the small pores. Only when water is in the large pores does the oleic liquid succeed in displacing it.

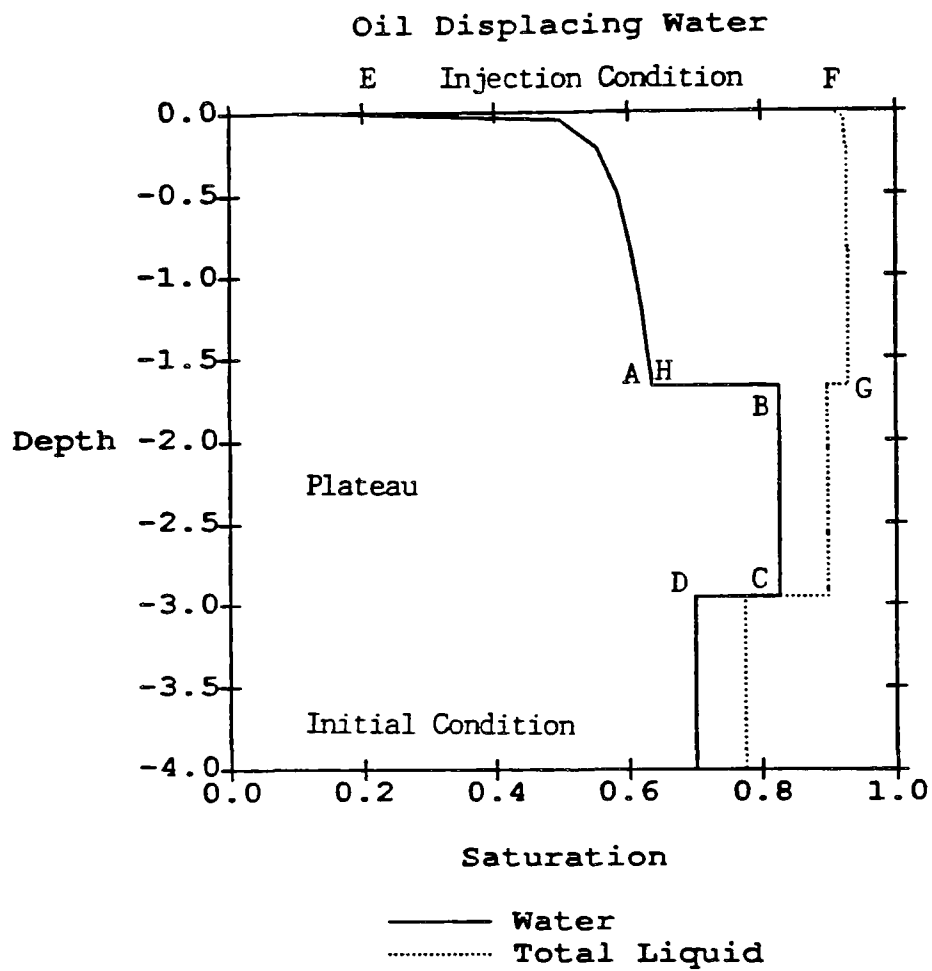


Figure 26 Example 6 oleic fluid injection showing displacement of water into a bank (ABCD) by the incoming oleic liquid (EFGH) and air.

PARAMETER VARIABILITY

Subsurface modeling is subject to uncertainty, as parameters may vary or be difficult to measure precisely. In this section the effects of variation of saturated hydraulic conductivity and Brooks and Corey's λ are discussed.

By increasing the saturated hydraulic conductivity by one standard deviation for the average silt loam soil (Brakensiek et al., 1981), the saturation composition space is seen to shift (compare figures 27 and 12). The λ_1 paths show less of a dip toward the $S_a = S_{ar}$ edge than figure 12. The previous solution of example 1 at two days is compared to the solution with higher hydraulic conductivity in figure 28. As expected, the water and oleic liquid fronts are deeper with increased hydraulic conductivity. The continuous saturation profiles reflect the variation in the saturation composition space. Slightly higher water and oleic liquid saturations are encountered above the water front, since less mobile air is apparently retained in the profile as the hydraulic conductivity increases. In figure 29, the bypassing profile of example 2 is compared with its counterpart with higher hydraulic conductivity. Very slight increases in water saturation occur which result in a significantly higher front speed. This phenomena implies a certain instability in the result as slight perturbations in saturation lead to large changes in front position.

Increasing Brooks and Corey's λ by one standard deviation for this soil type gives the saturation composition space shown in figure 30. (Recall that a " λ " with no subscript refers to a parameter of the Brooks and Corey Model (equation), while a " λ " with a subscript refers to an eigenvalue.) With a higher λ the pore size distribution is more uniform, although in this case the distribution is still relatively wide. The apparent effect of the increase is to increase the number of λ_2 paths with constant oleic liquid saturation. More initial conditions lead to bypassing conditions than with lower λ s. Figure 31 shows the effect of the change in λ on the bank profile result from example 1. With higher λ the water and oleic liquid fronts are deeper into the profile, and the continuous water saturation profile shows a greater drop in saturation from the surface to the water front, for example. The generally increased speeds are due to the fact that given a saturation above residual, the relative permeability increases with λ (equations 9 to 11). This

Riemann Problem Saturation Composition Space
 Hydraulic Conductivity = $3.35e-3$

Residual Saturations

$S_{wr} = 0.0370$

$S_{or} = 0.0500$

$S_{ar} = 0.0518$

Matrix Properties

$\Lambda = 0.2099$

Fluid Properties

W-Density = 1.0000

O-Density = 0.7000

A-Density = 0.0012

W-Viscosity = 1.0019

O-Viscosity = 2.0039

A-Viscosity = 0.0170

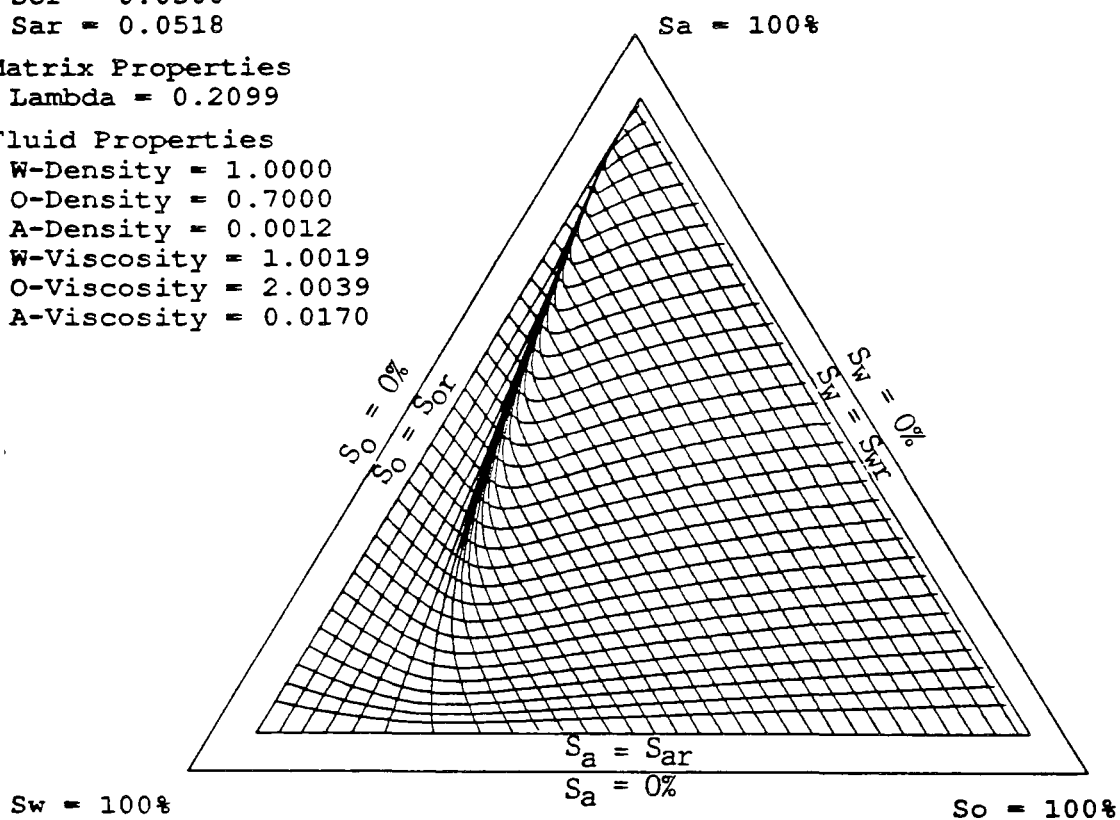


Figure 27 Saturation composition space for hydraulic conductivity of $3.35e-3$ cm/s

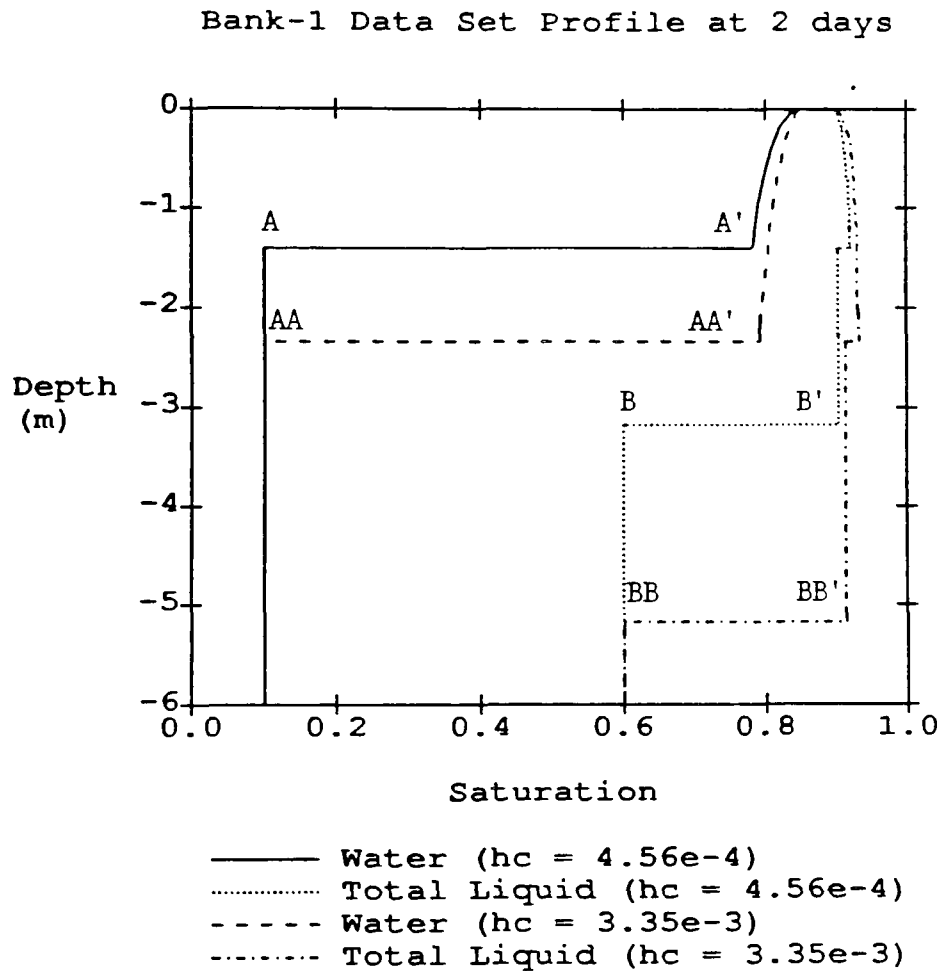


Figure 28 Effect of saturated hydraulic conductivity on bank profiles, showing increase in depth of water and oleic liquid fronts with increase in hydraulic conductivity (AA-AA' vs. A-A' and BB-BB' vs. B-B').

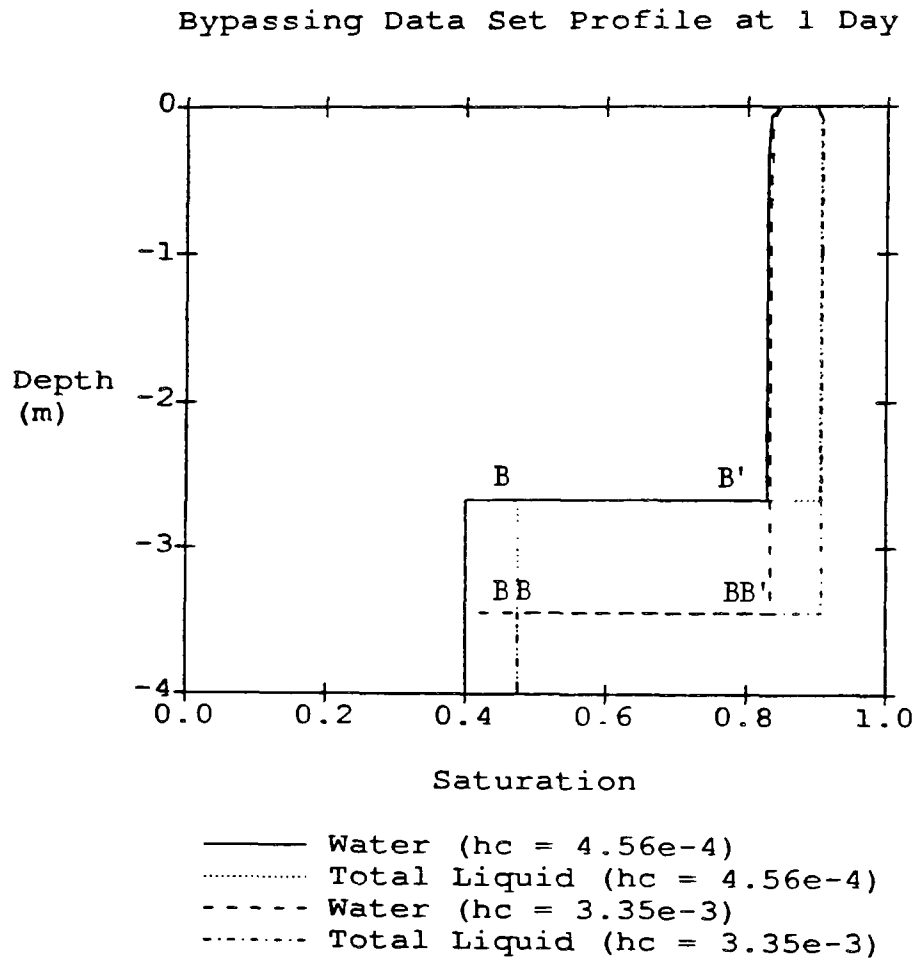


Figure 29 Effect of saturated hydraulic conductivity on bypassing profiles showing greater front depth (BB-BB' vs. B-B') with higher hydraulic conductivity.

Riemann Problem Saturation Composition Space
 $\Lambda = 0.30$

Residual Saturations
 $S_{wr} = 0.0370$
 $S_{or} = 0.0500$
 $S_{ar} = 0.0666$

Matrix Properties
 $\Lambda = 0.3000$

Fluid Properties
W-Density = 1.0000
O-Density = 0.7000
A-Density = 0.0012
W-Viscosity = 1.0019
O-Viscosity = 2.0039
A-Viscosity = 0.0170

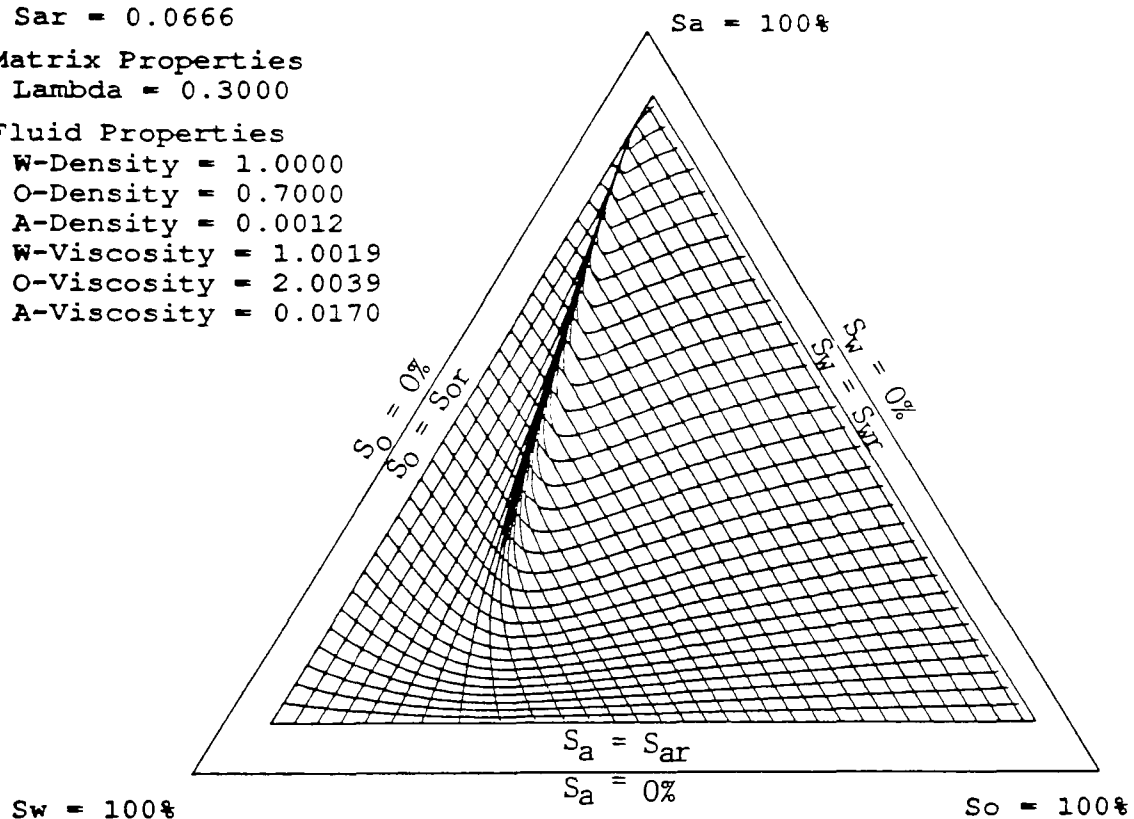


Figure 30 Saturation composition space for Brooks and Corey's $\lambda = 0.30$ showing a shift away from the $S_o = S_{or}$ axis (compare with figure 12).

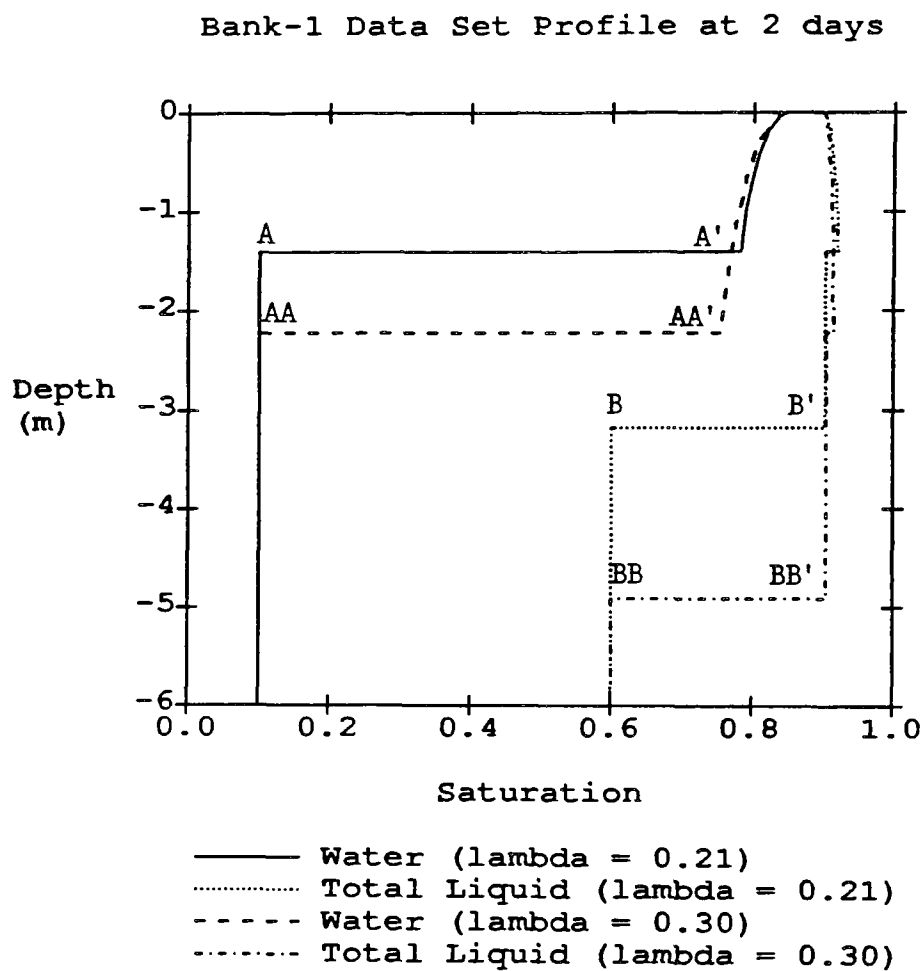


Figure 31 Effect of Brooks and Corey's λ on bank profiles showing that increased λ leads to deeper water (AA-AA' vs. A-A') and oleic liquid fronts (BB-BB' vs. B-B').

effect is evident on the bypassing profiles shown in figure 32. The profiles show only a very slight change in saturation as λ increases, but with higher λ much higher front speeds result.

SINGLE-PHASE WATER INJECTION

Injections at $S = S(1 - S_{or} - S_{ar}, S_{or}, S_{ar})$ correspond to injections of water only into systems containing oleic liquid and air. This S corresponds to a single-phase flow condition. Thus relative to the three-phase flow problem, this injection is doubly degenerate. The slow (λ_1) route leaving this point lies along the bottom side of the inner triangle. This route must be followed before a fast (λ_2) route is followed. The implication of this fact is that until the plateau is reached the solution follows a degenerate (two-phase) route. Any injection of water with both air and oleic liquid at residual results in saturation profiles with no mobile air from the injection point to the water front.

The routes from the plateau to the initial condition take the solution into three-phase saturation space. The λ_2 eigenvalues, however, are identically zero at $S_a = S_{ar}$. Thus both the λ_1 -waves and λ_2 -waves begin with characteristic speeds identical to zero, and the waves must overlap. (In the previous examples, $\lambda_1 < \lambda_2$ at the plateau, so the waves separate).

Two additional problems are encountered in this transition to three-phase flow. First the λ_2 paths have a minute bend toward the $S_w = S_{wr}$ axis, which not visible on any of the saturation composition triangles shown. The shape of this bend is similar to the visible bend in all the λ_1 paths. Numerical integration of equation 37 is very difficult across the bend.

The second problem may be related to either finite precision arithmetic or the loss of hyperbolicity of the governing equations in part of the region of the $S_a = S_{ar}$ side of the triangle. Holden (1990) discusses the possible loss of hyperbolicity for multiphase flow systems. The existence of real and

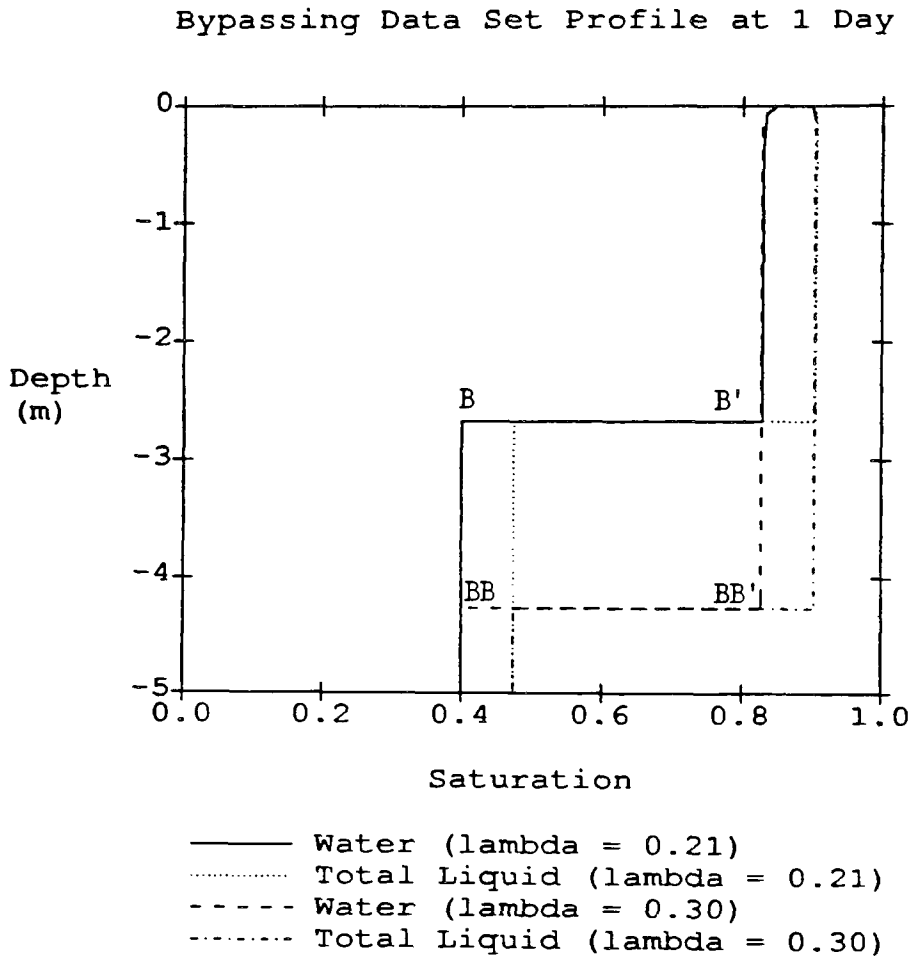


Figure 32 Effect of Brooks and Corey's λ on bypassing profiles showing a deeper front (BB-BB') than with smaller λ (B-B').

distinct λ_1 and λ_2 eigenvalues, and thus hyperbolic character of the governing equations throughout the rest of the domain is demonstrated by the solution of equation 37. If the real eigenvalues did not exist, the paths could not be drawn as shown in figures 12, 22, 27, and 30. Extension of the paths to the triangle sides revealed truncation errors in a double precision version of the code. Calculation using 128 bit arithmetic (VAX FORTRAN quad precision) allows the paths to be determined as shown. Further increases in precision are not possible with RSKERL computing resources. Thus failure of the equations to remain hyperbolic within the solution domain cannot be ruled out.

Since no assumptions are made about the type of the partial differential equations when deriving the jump equation (Charbeneau, 1984), it holds regardless of the hyperbolicity of equation (20). The λ_2 portion of the route is discontinuous, despite the initial increase of eigenvalues from $\lambda_2 = 0$ along the route (figure 11), which otherwise would lead to a continuous wave solution. The continuous λ_2 -wave does not exist because the λ_1 - and λ_2 -waves overlap. The λ_1 -wave must have a continuous portion, since the displacement of the oleic liquid by water cannot be complete. The solution for injection at $S(1-S_{or} - S_{ar}, S_{or}, S_{ar})$ must be analogous to the two-phase Buckley-Leverett solution which requires oleic liquid bypassing.

The only difficulty remaining in profile construction relates to the location in S of the plateau. Since discontinuities exist in the solution, the discontinuous route differs from the continuous route when the continuous route is curved. Where the λ_2 routes are straight at their intersection with the $S_a = S_{ar}$ side, solutions can be reliably obtained by the methodology discussed above.

SECTION 6

GENERALIZATION OF RIEMANN PROBLEM SOLUTIONS

Although solutions of Riemann problems provide much insight into fundamental fluid flow phenomena, the restrictive nature of their boundary and initial conditions limits their usefulness. In this section, the limitations on the boundary conditions are removed for the two-phase flow of air and water during infiltration. All of the principles involved also apply to three-phase flow problems. After presenting the model equations, two major issues are discussed: first is the determination of the total flux and second is the interaction of overlapping characteristic patterns.

MODEL EQUATIONS FOR THE INFILTRATION OF WATER SUBJECT TO AIR PHASE RESISTANCE

The problem considered is the infiltration of water, subject to resistance due to the air phase flow. The air is assumed to be displaced downward by the infiltrating water. Mass conservation for water,

$$\eta \frac{\partial S_w}{\partial t} + \frac{\partial q_w}{\partial z} = 0 \quad 41$$

the incompressible flow condition,

$$q_a + q_w = q_t \quad 42$$

and the saturation condition,

$$S_a + S_w = 1 \quad 43$$

give a single first-order hyperbolic equation to describe the system. The same procedure is followed as was applied to the three-phase flow problem presented previously in section 5. The fractional flow equation and its first derivatives are given in appendix 4. After substituting in the fractional flow function, the approximate governing equation is

$$\frac{\partial S_w}{\partial t} + \frac{q_t}{\eta} \frac{\partial f_w}{\partial S_w} \frac{\partial S_w}{\partial z} = 0 \quad 44$$

The continuous wave solution of the single hyperbolic equation 44 is

$$\frac{\partial S_w}{\partial t} + \frac{dz}{dt} \frac{\partial S_w}{\partial z} = 0 \quad 45$$

along paths defined by

$$\frac{dz}{dt} = \frac{q_t}{\eta} \frac{\partial f_w}{\partial S_w} \quad 46$$

The characteristic lines defined by equation 46 are straight lines only if the total flux, q_t , does not vary with time. For this problem q_t is allowed to vary with time, so curved characteristics must be tracked.

GENERALIZED TOTAL FLUX

One reason why Riemann problem solutions become attractive is that there often can be found a single point in time and space where the total flux is known. Usually this is an injection condition, as was the case in the previous section and in the classic Buckley-Leverett solution, where

constant flux boundary conditions are applied. When the injection is not constant, then difficulty is encountered in determining the total flux. One time when the total flux cannot be considered constant is when a constant flux condition abruptly ends. After this occurs there is zero flux of the injected fluid at the boundary, but the total flux clearly is not zero throughout the domain. A second case occurs when there is a constant rate rainfall at the boundary. The amount of water that can enter the profile is limited by the infiltration capacity of the soil, which is a function of the saturated hydraulic conductivity, relative permeability, antecedent water saturation, cumulative infiltration, and other factors (Bear, 1972). Thus the water flux entering the profile varies with time, even when the precipitation rate is constant. An expression for the water flux can be used to determine the total flux, assuming that at the surface the water flux equals the total flux. Although this is recognized as being only an assumption, it is expected that in most cases little error is introduced into the water flow.

The total flux is determined by summing and then integrating Darcy's law equations for water and air. This procedure is taken from Morel-Seytoux (1973). Summing the Darcy's law equations gives the total flux, for downward flow

$$q_a + q_w = q_t = \frac{k k_{rw}}{\mu_w} \left(\frac{-\partial P_w}{\partial z} + \rho_w g \right) + \frac{k k_{ra}}{\mu_a} \left(\frac{-\partial P_a}{\partial z} + \rho_a g \right) \quad 47$$

By adding an identity and rearranging, the following is obtained

$$q_t = k \left(\frac{k_{rw}}{\mu_w} + \frac{k_{ra}}{\mu_a} \right) \left(\frac{-\partial P_w}{\partial z} + \rho_w g \right) - \frac{k k_{ra}}{\mu_a} \left(\frac{\partial P_c}{\partial z} + (\rho_w - \rho_a) g \right) \quad 48$$

which is further manipulated to give

$$\frac{q_t}{k \left(\frac{k_{rw}}{\mu_w} + \frac{k_{ra}}{\mu_a} \right)} = - \frac{\partial P_w}{\partial z} + \rho_w g - \frac{\mu_w k_{ra}}{\mu_a k_{rw} + \mu_w k_{ra}} \left(\frac{\partial P_c}{\partial z} + (\rho_w - \rho_a) g \right) \quad 49$$

This results in an expression which can be integrated for the total flux, q_t .

$$\begin{aligned}
q_1 \int_{z_1}^{z_2} f_1(k_{ra}, k_{rw}) dz &= p_{w_1} - p_{w_2} + p_w g (z_2 - z_1) - \int_{z_1}^{z_2} f_2(k_{ra}, k_{rw}) \frac{\partial p_c}{\partial z} dz \\
&- (p_w - p_a) g \int_{z_1}^{z_2} f_2(k_{ra}, k_{rw}) dz
\end{aligned} \tag{50}$$

where

$$f_1(k_{ra}, k_{rw}) = \frac{\mu_a \mu_w}{k(\mu_a k_{rw} + \mu_w k_{ra})}$$

$$f_2(k_{ra}, k_{rw}) = \frac{\mu_w k_{ra}}{\mu_w k_{ra} + \mu_a k_{rw}}$$

Each integral appearing in equation 50 can be evaluated numerically at any time necessary in the solution, since they depend only on the saturation profile. The total flux so found applies instantaneously to the whole profile, because of equation 16. The integrals are evaluated numerically by a seven-point Gaussian quadrature routine (Abramowitz and Stegun, 1965).

OVERLAPPING CHARACTERISTIC PATTERNS

Each change in boundary condition of a quasi-linear system generates a set of waves. Since there is one equation solved for this problem, each boundary condition change creates one wave. The derivative of the fractional flow function determines the smoothness of the solution, as in a sense, this derivative is the eigenvalue of the system. For this problem the fractional flow derivative has a shape similar to that shown on figure 10. Recalling the discussion in section 5, each wave consists of a continuous portion which terminates in a contact discontinuity.

Figure 33 shows the base characteristic plane for a problem which consists of a finite duration rainfall of constant precipitation rate which both begins and ends with abrupt boundary transitions. The beginning of the rainfall creates the first wave. This wave is centered at the beginning of the rainfall. There is a transition from the high boundary saturation to the relatively low initial saturation. Characteristics originate from this point. The characteristic associated with the highest possible water saturation has zero velocity, and thus remains at the ground surface. Each successive characteristic associated with lower saturations has a faster velocity than the previous characteristic. At some point, however, the wave "breaks" as the characteristics cross. After that point, decreasing the saturation decreases the speed of the characteristic. As before, without a discontinuity, the solution would suggest that one point (z,t) is associated with two values of water saturation. Clearly this is not physically realistic and the classical method of characteristics is supplemented by a generalized solution for the contact discontinuity.

Figure 34 shows the saturation profile at 0.2 days after the beginning of the rainfall. Initially, the profile contained a uniform water saturation of 0.51. By 0.2 days, the water front has progressed 60 cm into the soil. The water saturation decreases slightly from its maximum of 0.9328 at the surface to 0.9208 at the contact discontinuity (front). Physically, the immobility of the maximum water saturation suggests that water cannot completely displace the mobile air. If the water entered the profile at its maximum saturation, all mobile air would be displaced. As it is, some of the mobile air above residual remains behind the water front. Flow into the profile can only take place when a small amount of mobile air remains behind the water front. The speed of the characteristics is directly proportional to the magnitude of the total flux (equation 46), so when the total flux is constant, as during the initial portion of the rainfall, the characteristics are straight lines. When the total flux is decreased, due to decreasing infiltration capacity, the characteristics begin to curve toward the time axis. After this time, equation (34) must be solved numerically for the position of each characteristic. The additional numerical integration adds significantly to the computational burden of the solution.

If the water is supplied at such a rate that the water saturation at the surface is less than the maximum ($S_w \leq 1. - S_{ar}$), then the characteristic associated with the boundary has a nonzero speed. Thus the characteristic moves into the subsurface. A plateau region emerges behind this

Base Characteristic Plane
Silt Loam Soil
6 Hour Duration Rainfall

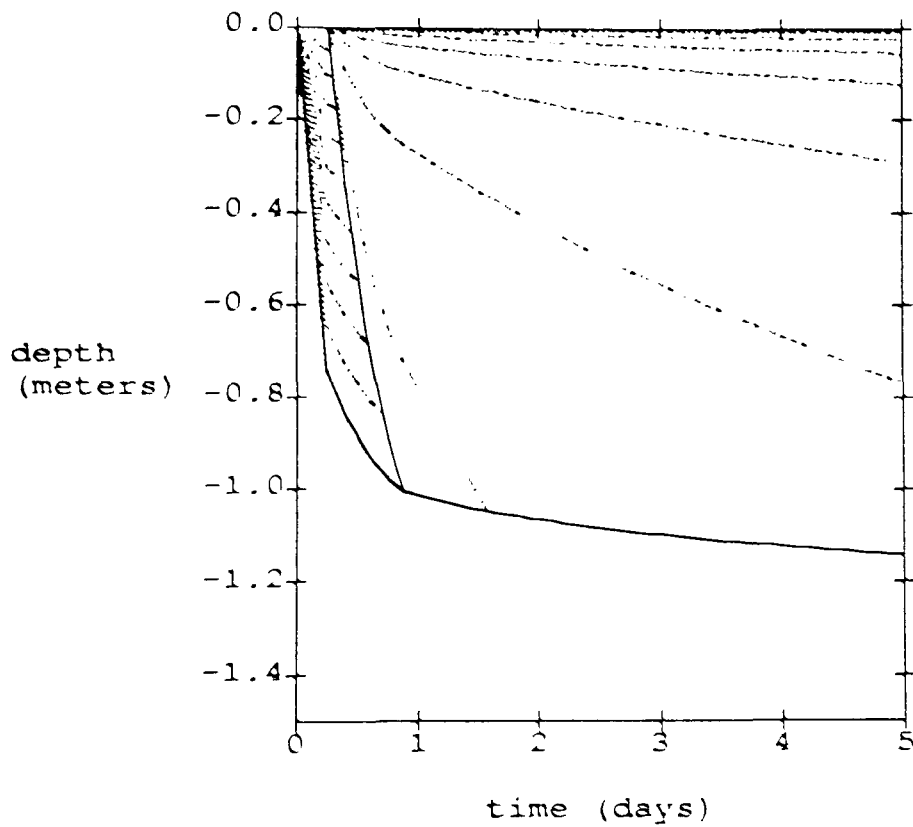


Figure 33 Water-air infiltration base characteristic plane showing depth of fronts and characters with time. Fronts are created when the rainfall begins at 0.0 days and when it ends at 0.25 days.

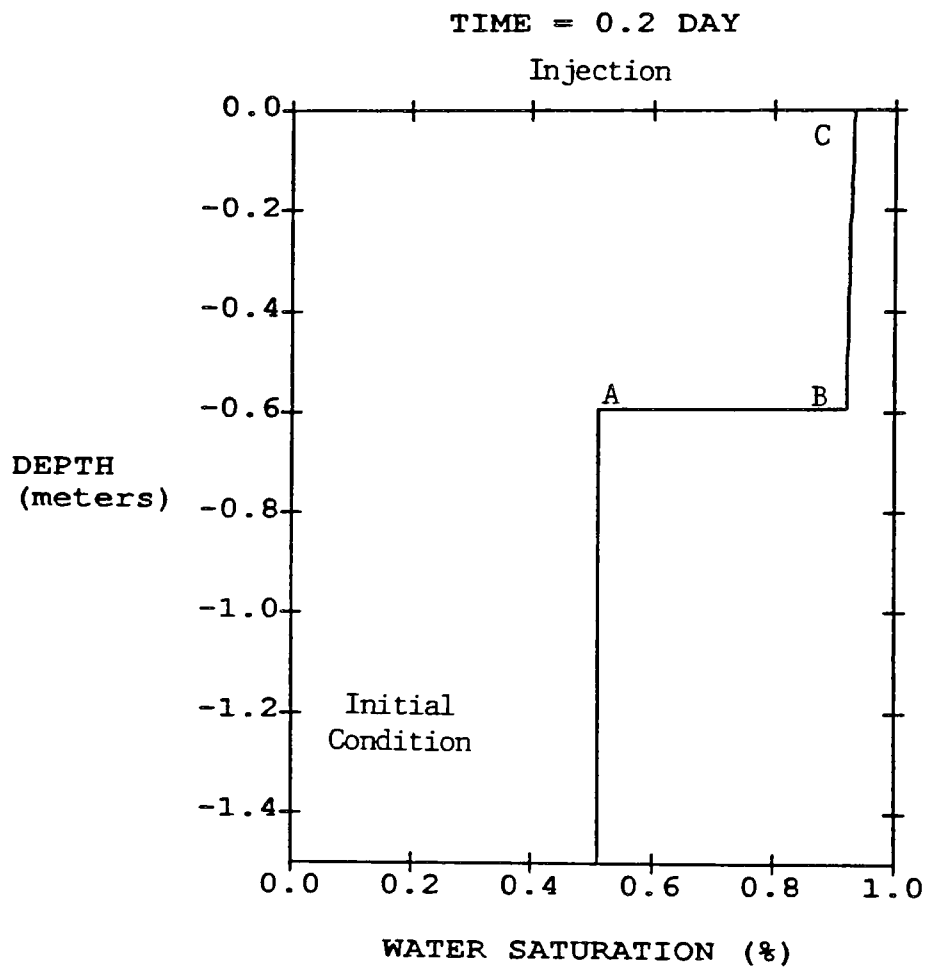


Figure 34 Water-air infiltration profile at 0.2 Days showing rainwater (ABC) and slight decrease in water saturation from the injection condition to the front (CB).

characteristic. The water saturation in the plateau must remain constant at the boundary value, because there is only enough water supplied to sustain this value.

When the rainfall ends, there is a second abrupt change in the boundary condition. The change results in the formation of a second wave. This wave is governed by the same fractional flow derivative as the first wave. Note that the transition from low saturation to high saturation follows the same general shape of the function as did the transition from high to low saturation. Thus the boundary saturation, which in this case is taken as residual, is again associated with an immobile characteristic. Increasing the water saturation gradually increases the speed of each successive characteristic, so that the smooth, fan-shaped characteristic pattern begins to emerge. Once again a saturation is reached where the characteristic speed begins to decrease. Since the saturation cannot be multiple valued, a discontinuity must also appear in the second wave. Note that a discontinuity must also appear between the first and second waves, because characteristics from the second wave would touch characteristics from the first wave which are associated with different water saturations.

The profile at 0.3 days (figure 35) shows the second wave originating at the ground surface and terminating in a shock which separates the two waves at 12 cm into the profile. The water saturation at the surface is residual and the saturation increases rapidly to 0.8520 just behind the front. The front is a contact discontinuity since its speed matches the characteristic speed just above the front. Ahead of the second wave lies the first which shows the same slight decrease in saturation as it did before the rainfall ended.

As indicated by figure 36, the second wave's discontinuity rapidly overtakes the original (first wave) front. In reality, the second wave's front will be strongly smoothed by both gravity and capillary phenomena. The sharpness of the front should be viewed as an artifact of the model, but is essential for the conservation of mass in the solution.

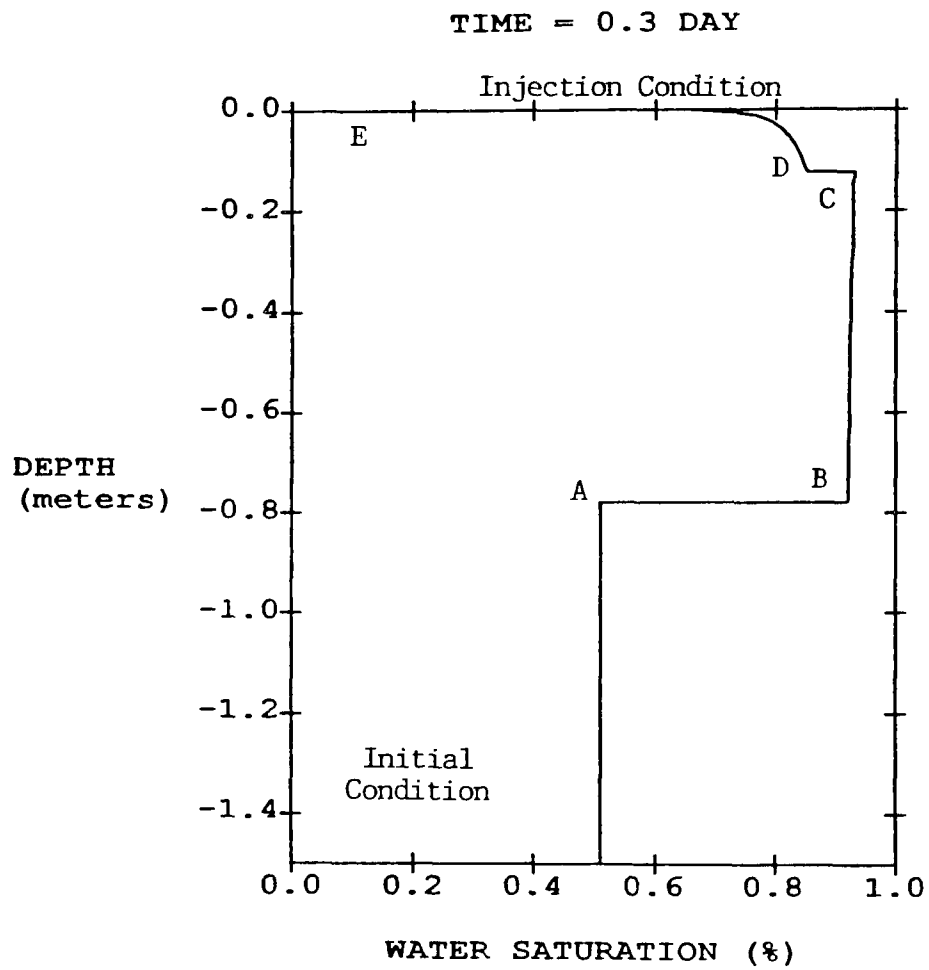


Figure 35 Water-air infiltration profile at 0.3 Days showing the second shock (DC) created when the injection drops to zero (E).

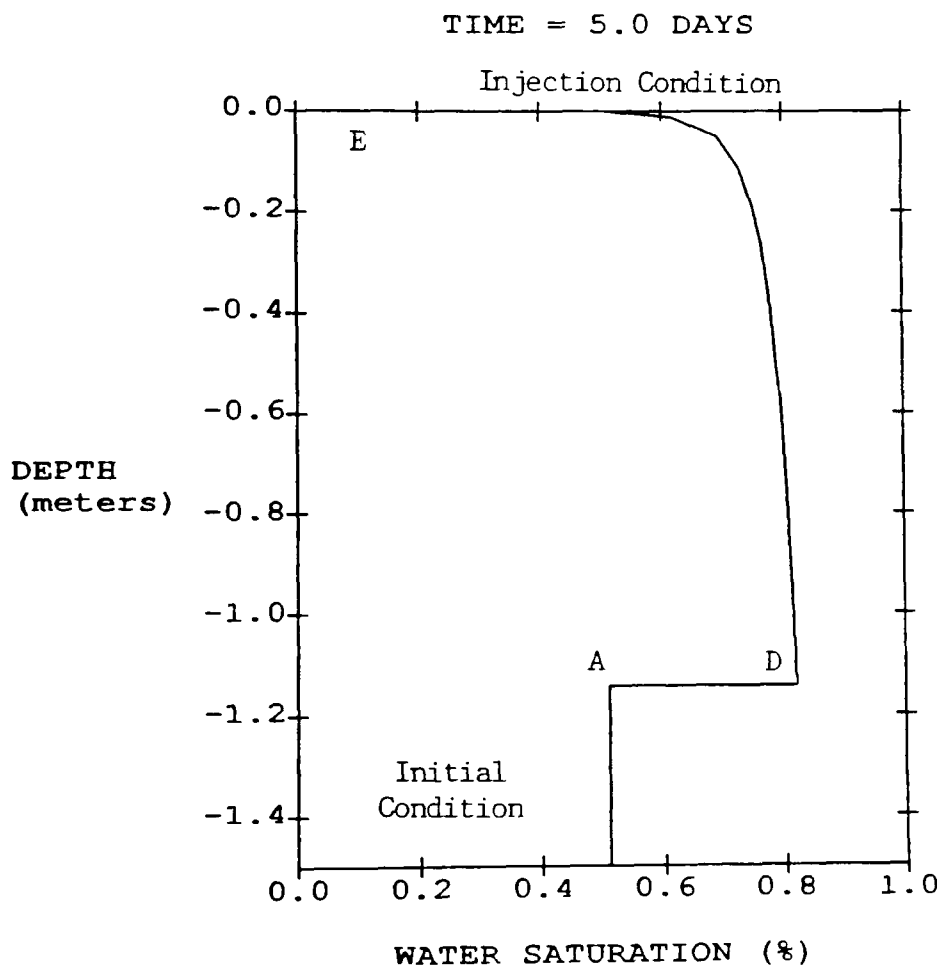


Figure 36 Water-air infiltration after the original front has been overtaken by the second (AD).

SECTION 7

DISCUSSION OF RESULTS

The application of characteristic methods to one-dimensional flow problems reveals the fundamental behavior of three-phase systems. Although the full governing equations are parabolic, the approximate hyperbolic equations which are solved in this report describe a fundamental portion of the flow phenomena. The efficiency that is achieved by simplifying the governing equations allows results to be developed which apply to any pair of injection and initial conditions for a given oleic phase and soil type (e.g., figure 12). The semi-analytic nature of the solution is primarily responsible for the generation of these "universal" results. The following conclusions are drawn from the work:

For systems with constant injection conditions and uniform initial conditions (Riemann problems), flow occurs in two regimes. When the injection consists mostly of water, mobile oleic liquids (organic liquids or so-called NAPLs) are displaced into "banks" or are bypassed. The banks move ahead of, and are driven by, the incoming water. The bypassing profile is characterized by the water moving past the oleic liquid, without causing it to be displaced into the profile. The occurrence of the regimes is determined by the oleic liquid properties, media properties, and the initial amount of all fluids present.

Although the type of boundary condition used in these solutions is not what is expected in the field, mathematically, it causes the hyperbolic problem to be a Riemann problem, for which there exists a large body of precise mathematical results. The flow regimes which exist in these solutions are believed to be fundamental for those expected from the solution of the hyperbolic system with general initial and boundary conditions.

The dependency of the results on the initial condition suggests that for cases where the oleic liquid has drained to a low saturation in the upper part of the soil profile, incoming rainfall will likely bypass the oleic liquid. Near the surface, this condition is likely to occur when a rainfall follows the end of an oleic liquid release by some hours. The oleic liquid has enough time to begin draining from the surface, so the incoming water experiences oleic liquid saturations which are low. Thus the bypassing regime is likely to be favored. Conversely, water injections at relatively high oleic liquid saturations are dominated by the

bank formation regime. Following the previous discussion, when the rainfall begins infiltrating there is likely to be bypassing near the surface. As the water front moves deeper into the profile, however, a saturation composition may be reached where the oleic liquid forms a bank. Thus the event may be characterized by both regimes. Verification of this behavior awaits the development of the general model. These composite flow regimes point out the necessity of full understanding of the three-phase Riemann problem before attempting to solve general problems.

For systems with injections of mostly oleic liquid, the dominant flow regime is water bypassing. This conclusion confirms the intuition that the oleic liquid, which occupies a mid-range of the pore space due to its wetting behavior, does not displace water from the small pores. Preferential wetting causes the water to be too tightly held to the media to be easily displaced by a non-wetting liquid. Thus spills of oleic liquid to soil profiles, which contain water at the so-called field capacity, are likely to bypass the pre-existing water.

In all cases, the behavior of the oleic liquid is dependent on its properties (density and viscosity) relative to those of water. As the oleic liquid becomes more mobile, water injections favor the bank formation regime somewhat, because the oleic liquid is of high enough mobility to match the speed of the incoming water. The character of the results, however, always reflects preferential wetting as indicated in the conclusion stated above. Thus in the example presented, the bypassing regime was only slightly larger for the higher mobility TCE case than the lower mobility oil, because of preferential wetting.

The conclusions stated lead to the following recommendations:

The three-phase solutions should be extended to simulate conditions with more general boundary and initial conditions. The methodology presented for two-phase flow simulation appears to be adaptable for this purpose. Models could then be created for discrete pulses of water which represent rainfalls preceding and following oleic liquid releases. For each liquid entering the profile, air phase resistance could be included by following the procedures developed in section 6. Alternatively, the kinematic formulation could be used when the flow is gravity driven. The next step is to develop useful models for field problems which include interphase partitioning phenomena. Previous work on kinematic models demonstrates that such phenomena are amenable for inclusion into this type of model. Multi-dimensional extension of the models should be considered, since one-dimensional flow is a restrictive condition, which

doesn't apply to heterogeneous field sites. The one-dimensional models can be useful, however, for spills occurring over large areas or for screening applications.

Laboratory validation of the existence of sharp fronts would be valuable for demonstrating the usefulness of the model. However, absolutely sharp fronts are not necessary for the model, because the sharp fronts can be shown theoretically to move at the same speed as the true fronts. The relative permeability equations used in the models were derived for drainage conditions. Experimental work would indicate the importance of hysteresis in the constitutive relations governing the flow and the necessity of including imbibition relative permeabilities.

The laboratory work should include investigation of the saturation conditions at the ground surface. Somewhat arbitrary conditions are used in the work discussed in this report. A related issue is that the injections used here force flow to be unidirectional. Experimental work indicates countercurrent flow is common, so the model should also be adapted for this condition.

REFERENCES

- Abramowitz, M., and I. A. Stegun, Handbook of Mathematical Functions, Dover, New York, 1965.
- Bear, J., Dynamics of Fluids in Porous Media, American Elsevier, New York, 1972.
- Bouwer, H., Rapid field measurements of air entry value and hydraulic conductivity of soil as significant parameter in flow system analysis, Water Resources Research, 2, 729-738, 1966.
- Brakensiek, D. L., R. L. Engleman, and W. J. Rawls, Variation within texture classes of soil water parameters, Transactions of the American Society of Agricultural Engineers, 335-339, 1981.
- Brooks, R. H. and A. T. Corey, Hydraulic Properties of Porous Media, Colorado State University Hydrology Paper No. 3, Ft. Collins, Colorado, 1964.
- Buckley, S. E. and M. C. Leverett, Mechanism of fluid displacement in sands, Transactions American Institute of Mining Engineers, 146, 107-116, 1942.
- Burdine, N. T., Relative permeability calculations from pore size distribution data, Transactions American Institute of Mining Engineers, 198, 71-78, 1953.
- Charbeneau, R. J., Multicomponent exchange and subsurface solute transport: Characteristics, coherence, and the Riemann problem, Water Resources Research, 24(1), 57-64, 1988.
- Charbeneau, R. J., Kinematic models for soil moisture and solute transport, Water Resources Research, 20, 699-706, 1984.
- Charbeneau, R. J., J. W. Weaver, and V. J. Smith, Kinematic Modeling of Multiphase Solute Transport in the Vadose Zone, United States Environmental Protection Agency, Report, EPA/600/2-89/035, June 1989.
- Dougherty, E. L. and J. W. Sheldon, The use of fluid interfaces to predict the behavior of oil recovery process, Society of Petroleum Engineers Journal, 4(2), 171-182, 1964.
- Fehlberg, E., Low-order Classical Runge-Kutta Formulas With Stepsize Control and Their Application to Some Heat Transfer Problems, NASA TR R-315, 1969.
- Glimm, J., B. Lindquist, O. McBryan, and L. Padmanabhan, A front tracking reservoir simulator, five-spot validation studies and the water coning problem, in The Mathematics of Reservoir Simulation, R.E. Ewing, editor, Society of Industrial and Applied Mathematics, Philadelphia, Pennsylvania, 107-136, 1983.
- Green, W. H. and G. A. Ampt, Studies on soil physics, Journal of Agricultural Science, 4, 1-24, 1911.
- Helfferich, F. G., Theory of multicomponent, multiphase displacement in porous media, Society of Petroleum Engineers Journal, 21, 51-62, 1981.

Helfferich, F. G., Multicomponent wave propagation: Attainment of coherence from arbitrary starting conditions, Chemical Engineering Communications, 44, 275-285, 1986.

Helfferich, F. G., and G. Klein, Multicomponent Chromatography. Theory of Interference, Marcel Dekker, New York, 1970.

Holden, L., On the strict hyperbolicity of the Buckley-Leverett equations for three-phase flow in a porous medium, SIAM Journal of Applied Mathematics, 50(3), 667-682, 1990.

Jeffrey, A., and T. Taniuti, Non-Linear Wave Propagation, Academic Press, New York, 1964.

Lax, P. D., Hyperbolic systems of conservation laws II, in Communications on Pure and Applied Mathematics, Interscience Publishers, New York, Vol. 10, 1957.

Lax, P. D., Hyperbolic Systems of Conservation Laws and the Mathematical Theory of Shock Waves, Society for Industrial and Applied Mathematics, Philadelphia, Pennsylvania, 1973.

Leverett, M. C., and W. B. Lewis, Steady flow of gas-oil-water mixtures through unconsolidated sands, Transactions. American Institute of Mining Engineers, 142, 107-152, 1941.

Kreyszig, E., Advanced Engineering Mathematics, 3rd edition, Wiley, New York, 1972.

McWhorter, D. B., Infiltration Affected by Flow of Air, Colorado State Hydrology Paper No. 49, Ft. Collins, Colorado, 1971.

Morel-Seytoux, H. J., Two-Phase Flows in Porous Media, in Advances In Water Resources, Vol. 9, V. T. Chow, editor, Academic Press, New York, 119-202, 1973.

Mull, R., The migration of oil-products in the subsoil with regard to ground-water pollution by oil, Proceedings of the Fifth International Conference on Advances in Water Pollution Research, San Francisco and Hawaii, S. A. Jenkins, editor, Pergamon, Oxford, Vol. 2, HA 7(A)/1-8, 1970.

Peaceman, D. W., Fundamentals of Numerical Reservoir Simulation, Elsevier Scientific, Amsterdam, 1977.

Pope, G. A., L. W. Lake, and F. G. Helfferich, Cation exchange in chemical flooding: Part 1 - Basic theory without dispersion, Society of Petroleum Engineers Journal, 18(6), 418-434, 1978.

Press, W. H., B. P. Flannery, S. A. Teukolsky, and W. T. Vetterling, Numerical Recipes The Art of Scientific Computing, Cambridge University Press, 1986.

Rawls, W. J., D. L. Brakensiek, and N. Miller, Green-Ampt infiltration parameters from soils data, ASCE Journal of Hydraulic Engineering, 109, 62-70, 1983.

Richards, L. A., Capillary conduction of liquids through porous mediums, Physics, 1, 318-333, 1931.

Rieble, D. D., T. H. Illangasekare, D. V. Doshi, and M. E. Malhiet, Infiltration of immiscible contaminants in the unsaturated zone, Ground Water, 28(5), 685-692, 1990.

- Rozdestvenskii, B. L. and N. N. Janenko, Systems of Quasilinear Equations and Their Applications to Gas Dynamics, American Mathematical Society, Providence, Rhode Island, 1980.
- Schwille, F., Dense Chlorinated Solvents in Porous and Fractured Media, Lewis, Chelsea, Michigan, 1988.
- Smith, R. E., Approximate soil water movement by kinematic characteristics, Soil Science Society of America Journal, 47, 3-8, 1983.
- Smoller, J., Shock Waves and Reaction-Diffusion Equations, Springer-Verlag, New York, 1983.
- Stone, H. L., Probability model for estimating three-phase relative permeability and residual oil data, Journal of petroleum Technology, 20(2), 214-218, 1970.
- Weaver, J. W., A Critical Review of Immiscible Groundwater Pollutant Transport, Masters Thesis, The University of Texas at Austin, 1984.
- Weaver, J. W., Kinematic Modeling of Multiphase Subsurface Transport, Doctoral Dissertation, The University of Texas at Austin, August, 1988.
- Weaver, J. W., and R. J. Charbeneau, A kinematic model of oil drainage in soils, submitted for publication in Water Resources Research, 1989.
- Wyllie, M. R. J. and G. H. F. Gardner, The generalized Kozeny-Carman equation: Its application to problems of multiphase flow in porous media, World Oil, 146, 210-227, 1958.
- Young, D. M., and R. T. Gregory, A Survey of Numerical Mathematics, Volume II, Dover, New York, 1988.

APPENDIX 1

DERIVATION OF THE THREE-PHASE FRACTIONAL FLOW EQUATIONS

The three-phase fractional flow functions are derived as follows for the water-oleic liquid system. Two independent expressions for the fractional flow exist and are derived as follows. Beginning with the flux equation for the oleic liquid,

$$q_o = \frac{-k k_{ro}}{\mu_o} \left(\frac{\partial P_o}{\partial z} + \rho_o g \sin \alpha \right) \quad 51$$

where α is the angle between the flow direction and the horizontal. When flow is downward $\sin \alpha$ is equal to -1, and equation 51 is the same as equation 4. Using equation 51 and noting the capillary pressure relationships

$$P_o - P_w = P_{cwo}$$

$$\frac{\partial P_o}{\partial z} = \frac{\partial P_{cwo}}{\partial z} + \frac{\partial P_w}{\partial z}$$

the flux equation for water can be used to eliminate the derivative of the oleic liquid pressure in equation 51

$$q_o = \frac{-k k_{ro}}{\mu_o} \left(\frac{\partial P_{cwo}}{\partial z} - \frac{q_w \mu_w}{k k_{rw}} - (\rho_o - \rho_w) g \sin \alpha \right)$$

Since this model neglects the contribution of the capillary pressure gradient to the flux, the first relationship for the oleic liquid fractional flow is

$$f_{o1} = f_o \approx \frac{-k_{ro} k_{ra}}{q_t \mu_o} \left(p_o - p_w \right) g \sin \alpha + \frac{k_{ro} \mu_w}{k_{rw} \mu_o} f_w$$

52

The second of the relationships is derived from the air phase flux equation

$$q_a = \frac{-k_{ra}}{\mu_a} \left(\frac{\partial P_a}{\partial z} + \rho_a g \sin \alpha \right)$$

and capillary pressure relationships,

$$P_a - P_o = P_{coa}$$

$$\frac{\partial P_a}{\partial z} - \frac{\partial P_o}{\partial z} = \frac{\partial P_{coa}}{\partial z}$$

Using the oleic liquid flux equation to eliminate the air phase pressure derivative yields,

$$q_a = \frac{-k_{ra}}{\mu_a} \left(\frac{\partial P_{coa}}{\partial z} - \frac{q_o \mu_o}{k_{ro}} - (\rho_a - \rho_o) g \sin \alpha \right)$$

which, when the capillary gradient is neglected, is conveniently rewritten as

$$f_{o2} = f_o \equiv \frac{1 - f_w + \frac{k_{ra}}{\mu_a q_t} \left[(\rho_o - \rho_a) g \sin \alpha \right]}{\left(1 + \frac{k_{ra} \mu_o}{k_{ro} \mu_a} \right)}$$

53

The two functions can be written in compact notation as

$$f_{o1} = A k_{ro} + B f_w k_{ro} / k_{rw} \quad 54$$

and

$$f_{o2} = \frac{(1 - f_w + C k_{ra}) k_{ro}}{(k_{ro} + D k_{ra})} \quad 55$$

with

$$A = \left[K_{sw} \frac{\mu_w}{\mu_o} - K_{so} \right] \frac{\sin \alpha}{q_t}; \quad B = \frac{\mu_w}{\mu_o}$$

$$C = \left[K_{so} - K_{sa} \frac{\mu_o}{\mu_a} \right] \frac{\sin \alpha}{q_t}; \quad D = \frac{\mu_o}{\mu_a}$$

Equations 52 and 53 comprise a system of two linear equations for the two unknowns, f_o ($f_o = f_{o1} = f_{o2}$) and f_w .

The partial derivatives of the fractional flows, which are required for the mass conservation equations 18 and 19, are likewise given by a system of two linear equations in two unknowns. The derivatives with respect to water are,

$$\frac{\partial f_{o1}}{\partial S_w} = \frac{\partial f_{o1}}{\partial k_{ro}} \frac{\partial k_{ro}}{\partial S_w} + \frac{\partial f_{o1}}{\partial k_{rw}} \frac{dk_{rw}}{dS_w} + \frac{\partial f_{o1}}{\partial f_w} \frac{\partial f_w}{\partial S_w} \quad 56$$

$$\frac{\partial f_{o2}}{\partial S_w} = \frac{\partial f_{o2}}{\partial k_{ro}} \frac{\partial k_{ro}}{\partial S_w} + \frac{\partial f_{o2}}{\partial k_{ra}} \frac{\partial k_{ra}}{\partial S_w} + \frac{\partial f_{o2}}{\partial f_w} \frac{\partial f_w}{\partial S_w} \quad 57$$

While the fractional flow derivatives with respect to the oil saturation are,

$$\frac{\partial f_{o1}}{\partial S_o} = \frac{\partial f_{o1}}{\partial k_{ro}} \frac{\partial k_{ro}}{\partial S_o} + \frac{\partial f_{o1}}{\partial f_w} \frac{\partial f_w}{\partial S_o} \quad 58$$

$$\frac{\partial f_{o2}}{\partial S_o} = \frac{\partial f_{o2}}{\partial k_{ro}} \frac{\partial k_{ro}}{\partial S_o} + \frac{\partial f_{o2}}{\partial k_{ra}} \frac{\partial k_{ra}}{\partial S_o} + \frac{\partial f_{o2}}{\partial f_w} \frac{\partial f_w}{\partial S_o} \quad 59$$

The partial derivatives of the fractional flows with respect to the independent variables appearing in equations 56 through 59 are (from equations 54 and 55)

$$\frac{\partial f_{o1}}{\partial k_{rw}} = \frac{-B f_w k_{ro}}{k_{rw}^2}$$

$$\frac{\partial f_{o1}}{\partial k_{ro}} = A + B \frac{f_w}{k_{rw}}$$

$$\frac{\partial f_{o1}}{\partial f_w} = \frac{B k_{ro}}{k_{rw}}$$

$$\frac{\partial f_{o2}}{\partial k_{ra}} = \frac{Ck_{ro}}{(k_{ro} + Dk_{ra})} - \frac{D(1 - f_w + Ck_{ra})k_{ro}}{(k_{ro} + Dk_{ra})^2}$$

$$\frac{\partial f_{o2}}{\partial k_{ro}} = \frac{(1 - f_w + Ck_{ra})}{(k_{ro} + Dk_{ra})} - \frac{(1 - f_w + Ck_{ra})k_{ro}}{(k_{ro} + Dk_{ra})^2}$$

$$\frac{\partial f_{o2}}{\partial f_w} = \frac{-k_{ro}}{(k_{ro} + Dk_{ra})}$$

To complete the evaluation of the partial derivatives, the relative permeability (fraction of saturated conductivity) functions are needed. For this report, the functions are based on a Brooks and Corey integration of the Burdine equations and have the form,

$$k_{rw} = \left(\frac{S_w - S_{wr}}{1 - S_{wr}} \right)^\epsilon$$

$$k_{ro} = \left(\frac{S_o - S_{or}}{1 - S_{or}} \right)^2 \left[\left(\frac{S_o + S_w - S_{wr}}{1 - S_{wr}} \right)^{\epsilon-2} - \left(\frac{S_w - S_{wr}}{1 - S_{wr}} \right)^{\epsilon-2} \right]$$

$$k_{ra} = \left(\frac{S_a - S_{ar}}{1 - S_{ar}} \right)^2 \left[1 - \left(\frac{S_o + S_w - S_{wr}}{1 - S_{wr}} \right)^{\epsilon-2} \right]$$

For simplicity, only drainage functions are considered here. The required partial derivatives of these functions are given by,

$$\frac{dk_{rw}}{dS_w} = \left(\frac{\epsilon}{1 - S_{wr}} \right) \left(\frac{S_w - S_{wr}}{1 - S_{wr}} \right)^{\epsilon-1}$$

$$\begin{aligned} \frac{\partial k_{ro}}{\partial S_o} = & \left(\frac{\epsilon - 2}{1 - S_{wr}} \right) \left(\frac{S_o - S_{or}}{1 - S_{or}} \right)^2 \left(\frac{S_o + S_w - S_{wr}}{1 - S_{wr}} \right)^{\epsilon-3} \\ & + \frac{2(S_o - S_{or})}{(1 - S_{or})} \left[\left(\frac{S_o + S_w - S_{wr}}{1 - S_{wr}} \right)^{\epsilon-2} - \left(\frac{S_w - S_{wr}}{1 - S_{wr}} \right)^{\epsilon-2} \right] \end{aligned}$$

$$\frac{\partial k_{ro}}{\partial S_w} = \left(\frac{\epsilon - 2}{1 - S_{wr}} \right) \left(\frac{S_o - S_{or}}{1 - S_{or}} \right) \left[\left(\frac{S_o + S_w - S_{wr}}{1 - S_{wr}} \right)^{\epsilon-3} - \left(\frac{S_w - S_{wr}}{1 - S_{wr}} \right)^{\epsilon-3} \right]$$

$$\begin{aligned} \frac{\partial k_{ra}}{\partial S_o} = & \left(\frac{1 - S_o - S_w - S_{ar}}{1 - S_{ar}} \right)^2 \left(\frac{2 - \epsilon}{1 - S_{wr}} \right) \left(\frac{S_o + S_w - S_{wr}}{1 - S_{wr}} \right)^{\epsilon-3} \\ & - \frac{2}{1 - S_{ar}} \left(\frac{1 - S_o - S_w - S_{ar}}{1 - S_{ar}} \right) \left[1 - \left(\frac{S_o + S_w - S_{wr}}{1 - S_{wr}} \right)^{\epsilon-2} \right] \end{aligned}$$

$$\frac{\partial k_{ra}}{\partial S_o} = \frac{\partial k_{ra}}{\partial S_w}$$

Given a saturation composition, the evaluation of equations 56 through 59 is straightforward, since they also comprise a two by two system. Once all of the fractional flow derivatives are known for a given saturation composition, the eigenvalues and eigenvectors of matrix $A(S)$ appearing in equation 20 can be determined and the method of characteristics solutions can be found.

At times, water/air and oleic fluid/air formulations are convenient for solving the approximate governing equations by the method of characteristics. The equations for these systems can be found by switching appropriate subscripts in equations 52 and 53. The partial derivatives of the resulting equations are found in a manner similar to that presented above.

APPENDIX 2

KINEMATIC MODEL SOLUTION

The solution of the model equation 20 for kinematic conditions has been presented by Charbeneau et al. (1989), and Weaver (1988). The solutions obtained in the previous work are developed from ad hoc considerations. In this appendix, the classical method of characteristics technique is used to derive the kinematic model solution. The two solutions are shown to be identical. If all fluids flow at fluxes less than the effective conductivities given a saturation composition, then the flow is driven by gravity only. No pressure gradient term appears in the Darcy's law equations and the approximate governing equations have the form

$$\frac{\partial S}{\partial t} + \mathbf{A}^*(S) \frac{\partial S}{\partial z} = 0$$

where the matrix, $\mathbf{A}^*(S)$, is

$$\mathbf{A}^*(S) = \frac{1}{\eta} \begin{vmatrix} a_{11} & 0 \\ a_{21} & a_{22} \end{vmatrix}$$

and the components are

$$a_{11} = \frac{dK_{rw}}{dS_w}$$

$$a_{21} = \frac{\partial K_{ro}}{\partial S_w}$$

$$a_{22} = \frac{\partial K_{ro}}{\partial S_o}$$

The zero appears in matrix A^* , because the water relative permeability in a strongly water wet system is a function of water saturation only. There is no derivative of water relative permeability with respect to oil saturation. The two eigenvalues of matrix A^* are equal to the diagonal entries (e.g., Kreyszig, 1972), so $\lambda_1 = a_{11}$ and $\lambda_2 = a_{22}$.

The left eigenvectors of the matrix are defined as

$$[l_k^{(1)}, l_k^{(2)}] \begin{bmatrix} a_{11} & 0 \\ a_{21} & a_{22} \end{bmatrix} = \lambda_k [l_k^{(1)}, l_k^{(2)}]$$

One set of vectors satisfying this relationship is

$$l_1 = [1, 0]$$

$$l_2 = \left[\frac{a_{21}}{a_{22} - a_{11}}, 1 \right]$$

Equation 23, $l_k DS = 0$, can be used to determine the classical method of characteristics solution of the kinematic model.

For the first eigenvalue, λ_1 , $l_k = l_1$ and equation 23 becomes

$$l_1^{(1)} \left(\frac{\partial S_w}{\partial t} + a_{11} \frac{\partial S_w}{\partial z} \right) + l_1^{(2)} \left(\frac{\partial S_o}{\partial t} + a_{11} \frac{\partial S_o}{\partial z} \right) = 0$$

which reduces to

$$\left(\frac{\partial S_w}{\partial t} + a_{11} \frac{\partial S_w}{\partial z} \right) = 0$$

The last result can be rewritten in terms of the total derivative,

$$\frac{DS_w}{Dt} = 0$$

68

along characteristics defined by $dz/dt = \lambda_1 = (1/\eta) dK_{rw}/dS_w$. Note that the solution for λ_1 is the same as the solution for the water phase when no oleic fluid is present.

For the second eigenvalue, λ_2 , $I_k = I_2$ and equation 23 becomes

$$I_2^{(1)} \left(\frac{\partial S_w}{\partial t} + a_{22} \frac{\partial S_w}{\partial z} \right) + I_2^{(2)} \left(\frac{\partial S_o}{\partial t} + a_{22} \frac{\partial S_o}{\partial z} \right) = 0$$

$$\left(\frac{a_{21}}{a_{22} - a_{11}} \right) \left(\frac{\partial S_w}{\partial t} + a_{22} \frac{\partial S_w}{\partial z} \right) + 1 \left(\frac{\partial S_o}{\partial t} + a_{22} \frac{\partial S_o}{\partial z} \right) = 0$$

which is equal to

$$\frac{DS_o}{Dt} = \frac{-a_{21}}{a_{22} - a_{11}} \left(\frac{\partial S_w}{\partial t} + a_{22} \frac{\partial S_w}{\partial z} \right)$$

along characteristics defined by $dz/dt = \lambda_2 = (1/\eta) \partial K_{ro} / \partial S_o$. The last equation is simplified by adding an identity which, upon rearrangement, gives

$$\frac{DS_o}{Dt} = \frac{-a_{21}}{a_{22} - a_{11}} \left(\frac{\partial S_w}{\partial t} + a_{11} \frac{\partial S_w}{\partial z} + (a_{22} - a_{11}) \frac{\partial S_w}{\partial z} \right)$$

The sum of the first two terms inside the parentheses is Identically zero, since these terms are the mass conservation equation for water,

$$\frac{DS}{Dt} = -a_{21} \frac{\partial S}{\partial z} \quad 69$$

The solution given by equations 68 and 69 is the same as the solution reported previously by Charbeneau et al. (1989).

APPENDIX 3

HORIZONTAL FLOW

When the flow system is horizontal, the coefficients A and C appearing in equations 54 and 55 are equal to zero. The fractional flows become

$$f_{o1} = B f_w k_{ro} / k_{rw} \quad 60$$

and

$$f_{o2} = \frac{(1 - f_w) k_{ro}}{(k_{ro} + Dk_{ra})} \quad 61$$

The required partial derivatives of the horizontal fractional flow equations are, (from equations 60 and 61)

$$\frac{\partial f_{o1}}{\partial k_{rw}} = \frac{-B f_w k_{ro}}{k_{rw}^2} \quad 62$$

$$\frac{\partial f_{o1}}{\partial k_{ro}} = B \frac{f_w}{k_{rw}} \quad 63$$

$$\frac{\partial f_{o1}}{\partial f_w} = \frac{B k_{ro}}{k_{rw}} \quad 64$$

$$\frac{\partial f_{o2}}{\partial k_{ra}} = - \frac{D(1 - f_w)k_{ro}}{(k_{ro} + Dk_{ra})^2} \quad 65$$

$$\frac{\partial f_{o2}}{\partial k_{ro}} = \frac{(1 - f_w)}{(k_{ro} + Dk_{ra})} - \frac{(1 - f_w)k_{ro}}{(k_{ro} + Dk_{ra})^2} \quad 66$$

$$\frac{\partial f_{o2}}{\partial f_w} = \frac{-k_{ro}}{(k_{ro} + Dk_{ra})} \quad 67$$

The effect of gravity depends on the magnitude of coefficients A and C, which in turn depend on the density difference between the fluids and on the oleic fluid and/or air relative permeability. The latter dependency indicates that the soil properties play a significant role in determining the importance of the gravity term. When the oleic fluid and air relative permeabilities are low, the effect of gravity is minimized. Both expressions for the fractional flow, equations 60 and 61, depend on the gravity effect, as do some of the partial derivatives (equations 63, 65, and 66).

APPENDIX 4

DERIVATION OF THE TWO-PHASE FRACTIONAL FLOW EQUATIONS

The two-phase fractional flow functions are derived as follows for the water-air system. Beginning with the flux equation for water,

$$q_w = \frac{-k k_{rw}}{\mu_w} \left(\frac{\partial P_w}{\partial z} + \rho_w g \sin \alpha \right) \quad 70$$

and noting the capillary pressure relationships

$$P_a - P_w = P_{cwa}$$

and

$$\frac{\partial P_a}{\partial z} = \frac{\partial P_{cwa}}{\partial z} + \frac{\partial P_w}{\partial z}$$

the flux equation for air can be used to eliminate the derivative of the water liquid pressure in equation 70

$$q_w = \frac{-k k_{rw}}{\mu_w} \left(\frac{\partial P_{cwa}}{\partial z} - \frac{q_a \mu_a}{k k_{ra}} - (\rho_w + \rho_a) g \sin \alpha \right)$$

Since this model neglects the contribution of the capillary pressure gradient to the flux, the relationship for the water fractional flow is

$$f_w = \frac{\frac{k_{rw}}{k_{ra}} \frac{k_a}{\mu_w} - \frac{k_{rw}}{q_t \mu_w} (\rho_a - \rho_w) g \sin \alpha}{1 + \frac{k_{rw}}{k_{ra}} \frac{\mu_a}{\mu_w}}$$

which can be written as

$$f_w = \frac{Ak_{rw}k_{ra} + Bk_{rw}}{k_{ra} + Bk_{rw}}$$

where $A = (K_{sw} - K_{sa} \mu_a / \mu_w) / q_t$, and $B = \mu_a / \mu_w$. The partial derivative of fractional flow with respect to the water saturation is needed for equation 46, and is given by

$$\frac{\partial f_w}{\partial S_w} = \frac{\partial f_w}{\partial k_{rw}} \frac{dk_{rw}}{dS_w} + \frac{\partial f_w}{\partial k_{ra}} \frac{dk_{ra}}{dS_w}$$

The necessary partial derivatives are

$$\frac{\partial f_w}{\partial k_{rw}} = \frac{Ak_{ra} + B}{k_{ra} + Bk_{rw}} - \frac{B(Ak_{rw}k_{ra} + Bk_{rw})}{(k_{ra} + Bk_{rw})^2}$$

$$\frac{\partial f_w}{\partial k_{ra}} = \frac{Ak_{ra}}{k_{ra} + Bk_{rw}} - \frac{(Ak_{rw}k_{ra} + Bk_{rw})}{(k_{ra} + Bk_{rw})^2}$$

The relative permeabilities for the two-phase system are

$$k_{rw} = \left[\frac{S_w - S_{wr}}{1 - S_{wr}} \right]^e$$

$$k_{ra} = \left(1 - \frac{S_w - S_{wr}}{1 - S_{wr}} \right)^2 \left[1 - \left(\frac{S_w - S_{wr}}{1 - S_{wr}} \right)^{\epsilon-2} \right]$$

The required partial derivatives of these functions are given by

$$\frac{dk_{rw}}{dS_w} = \left(\frac{\epsilon}{1 - S_{wr}} \right) \left(\frac{S_w - S_{wr}}{1 - S_{wr}} \right)^{\epsilon-1}$$

$$\begin{aligned} \frac{dk_{ra}}{dS_w} = & \left(\frac{2}{S_{wr} - 1} \right) \left(1 - \frac{S_w - S_{wr}}{1 - S_{wr}} \right) \left[1 - \left(\frac{S_w - S_{wr}}{1 - S_{wr}} \right)^{\epsilon-2} \right] \\ & + \left(1 - \frac{S_w - S_{wr}}{1 - S_{wr}} \right)^2 \left(\frac{2 - \epsilon}{1 - S_{wr}} \right) \left[1 - \left(\frac{S_w - S_{wr}}{1 - S_{wr}} \right)^{\epsilon-2} \right] \end{aligned}$$

APPENDIX 5 INPUT DATA SETS

Units for the following input data sets are as follows:

Saturated hydraulic conductivity	centimeters/second
Viscosity	centipoise
Density	grams/cubic centimeter
Total Flux	meters/day
Beginning and ending time	days
Angle with the horizontal	degrees

The remaining input parameters are dimensionless:

Brooks and Corey's lambda (λ)
Porosity
Residual saturations (all fluids)
Saturations (all fluids)

The "calculated parameters" have the following dimensions:

Brooks and Corey's epsilon (ϵ)	dimensionless
Residual air saturation	dimensionless
Saturated Conductivities (all fluids)	meters/day

Example 1 Oleic Liquid Bank Formation

MULTIPHASE COHERENCE CALCULATIONS

RIEMANN PROBLEM DATA SET SILT LOAM FROM BRAKENSIEK

BROOKS AND COREYS LAMBDA	0.2100
SATURATED HYDRAULIC CONDUCTIVITY	0.4560E-03
POROSITY	0.4840
RESIDUAL WATER SATURATION	0.3700E-01
RESIDUAL OIL SATURATION	0.5000E-01
WATER VISCOSITY	1.002
OIL VISCOSITY	2.004
AIR VISCOSITY	0.1800E-01
WATER DENSITY	1.000
OIL DENSITY	0.7000
AIR DENSITY	0.1205E-02
TOTAL FLUX	2.000
ANGLE WITH HORIZONTAL	-90.00
BEGINNING TIME	0.0000E+00
ENDING TIME	24.00
INITIAL CONDITION	
WATER SATURATION	0.1000
OIL SATURATION	0.5000
AIR SATURATION	0.4000
INJECTION CONDITION	
WATER SATURATION	0.8490
OIL SATURATION	0.5010E-01
AIR SATURATION	0.1009
CALCULATED PARAMETERS	
BROOKS AND COREYS EPSILON	12.52
RESIDUAL AIR SATURATION	0.5185E-01
SATURATED WATER CONDUCTIVITY	0.3940
SATURATED OIL CONDUCTIVITY	0.1379
SATURATED AIR CONDUCTIVITY	0.2643E-01

Example 2 Oleic Liquid Bypassing

MULTIPHASE COHERENCE CALCULATIONS

RIEMANN PROBLEM DATA SET SILT LOAM FROM BRAKENSIEK

BROOKS AND COREYS LAMBDA	0.2100
SATURATED HYDRAULIC CONDUCTIVITY	0.4560E-03
POROSITY	0.4840
RESIDUAL WATER SATURATION	0.3700E-01
RESIDUAL OIL SATURATION	0.5000E-01

WATER VISCOSITY	1.002
OIL VISCOSITY	2.000
AIR VISCOSITY	0.1800E-01

WATER DENSITY	1.000
OIL DENSITY	0.7000
AIR DENSITY	0.1205E-02

TOTAL FLUX	5.000
ANGLE WITH HORIZONTAL	-90.00
BEGINNING TIME	0.0000E+00
ENDING TIME	24.00

INITIAL CONDITION	
WATER SATURATION	0.4000
OIL SATURATION	0.7500E-01
AIR SATURATION	0.5250

INJECTION CONDITION	
WATER SATURATION	0.8490
OIL SATURATION	0.5010E-01
AIR SATURATION	0.1009

CALCULATED PARAMETERS	
BROOKS AND COREYS EPSILON	12.52
RESIDUAL AIR SATURATION	0.5185E-01
SATURATED WATER CONDUCTIVITY	0.3940
SATURATED OIL CONDUCTIVITY	0.1382
SATURATED AIR CONDUCTIVITY	0.2643E-01

Example 3 Oleic Liquid Bank Formation, Second Type

MULTIPHASE COHERENCE CALCULATIONS

RIEMANN PROBLEM DATA SET SILT LOAM FROM BRAKENSIEK

BROOKS AND COREYS LAMBDA	0.2100
SATURATED HYDRAULIC CONDUCTIVITY	0.4560E-03
POROSITY	0.4840
RESIDUAL WATER SATURATION	0.3700E-01
RESIDUAL OIL SATURATION	0.5000E-01
WATER VISCOSITY	1.002
OIL VISCOSITY	2.004
AIR VISCOSITY	0.1800E-01
WATER DENSITY	1.000
OIL DENSITY	0.7000
AIR DENSITY	0.1205E-02
TOTAL FLUX	2.000
ANGLE WITH HORIZONTAL	-90.00
BEGINNING TIME	0.0000E+00
ENDING TIME	24.00
INITIAL CONDITION	
WATER SATURATION	0.6000
OIL SATURATION	0.2000
AIR SATURATION	0.2000
INJECTION CONDITION	
WATER SATURATION	0.8490
OIL SATURATION	0.5010E-01
AIR SATURATION	0.1009
CALCULATED PARAMETERS	
BROOKS AND COREYS EPSILON	12.52
RESIDUAL AIR SATURATION	0.5185E-01
SATURATED WATER CONDUCTIVITY	0.3940
SATURATED OIL CONDUCTIVITY	0.1379
SATURATED AIR CONDUCTIVITY	0.2643E-01

Example 4 Flow of TCE

```
MULTIPHASE COHERENCE CALCULATIONS
*****
RIEMANN PROBLEM DATA SET SILT LOAM FROM BRAKENSIEK

BROOKS AND COREYS LAMBDA          0.2100
SATURATED HYDRAULIC CONDUCTIVITY  0.4560E-03
POROSITY                           0.4840
RESIDUAL WATER SATURATION          0.3700E-01
RESIDUAL OIL SATURATION            0.5000E-01

WATER VISCOSITY                    1.002
OIL VISCOSITY                      0.5700
AIR VISCOSITY                      0.1800E-01

WATER DENSITY                      1.000
OIL DENSITY                        1.460
AIR DENSITY                        0.1205E-02

TOTAL FLUX                         2.000
BEGINNING TIME                     0.0000E+00
ENDING TIME                         24.00

INITIAL CONDITION
WATER SATURATION                   0.1000
OIL SATURATION                     0.5000
AIR SATURATION                     0.4000

INJECTION CONDITION
WATER SATURATION                   0.8490
OIL SATURATION                     0.5010E-01
AIR SATURATION                     0.1009

CALCULATED PARAMETERS
BROOKS AND COREYS EPSILON          12.52
RESIDUAL AIR SATURATION             0.5185E-01
SATURATED WATER CONDUCTIVITY       0.3940
SATURATED OIL CONDUCTIVITY         1.011
SATURATED AIR CONDUCTIVITY         0.2643E-01
```

Example 5 Horizontal Flow

```
MULTIPHASE COHERENCE CALCULATIONS
*****
RIEMANN PROBLEM DATA SET SILT LOAM FROM BRAKENSIEK

BROOKS AND COREYS LAMBDA          0.2100
SATURATED HYDRAULIC CONDUCTIVITY  0.4560E-03
POROSITY                           0.4840
RESIDUAL WATER SATURATION          0.3700E-01
RESIDUAL OIL SATURATION            0.5000E-01

WATER VISCOSITY                    1.002
OIL VISCOSITY                      2.004
AIR VISCOSITY                      0.1800E-01

WATER DENSITY                      1.000
OIL DENSITY                        0.7000
AIR DENSITY                        0.1205E-02

TOTAL FLUX                         2.000
ANGLE WITH HORIZONTAL              0.0000E+00
BEGINNING TIME                     0.0000E+00
ENDING TIME                         24.00

INITIAL CONDITION
WATER SATURATION                   0.1000
OIL SATURATION                     0.5000
AIR SATURATION                     0.4000

INJECTION CONDITION
WATER SATURATION                   0.8490
OIL SATURATION                     0.5010E-01
AIR SATURATION                     0.1009

CALCULATED PARAMETERS
BROOKS AND COREYS EPSILON          12.52
RESIDUAL AIR SATURATION             0.5185E-01
SATURATED WATER CONDUCTIVITY       0.3940
SATURATED OIL CONDUCTIVITY         0.1379
SATURATED AIR CONDUCTIVITY         0.2643E-01
```

Example 6 Oleic Liquid/Air Injection

MULTIPHASE COHERENCE CALCULATIONS

RIEMANN PROBLEM DATA SET SILT LOAM FROM BRAKENSIEK

BROOKS AND COREYS LAMBDA	0.2100
SATURATED HYDRAULIC CONDUCTIVITY	0.4560E-03
POROSITY	0.4840
RESIDUAL WATER SATURATION	0.3700E-01
RESIDUAL OIL SATURATION	0.5000E-01
WATER VISCOSITY	1.002
OIL VISCOSITY	2.004
AIR VISCOSITY	0.1800E-01
WATER DENSITY	1.000
OIL DENSITY	0.7000
AIR DENSITY	0.1205E-02
TOTAL FLUX	2.000
ANGLE WITH HORIZONTAL	-90.00
BEGINNING TIME	0.0000E+00
ENDING TIME	24.00
INITIAL CONDITION	
WATER SATURATION	0.7000
OIL SATURATION	0.7500E-01
AIR SATURATION	0.2250
INJECTION CONDITION	
WATER SATURATION	0.1000
OIL SATURATION	0.8000
AIR SATURATION	0.1000
CALCULATED PARAMETERS	
BROOKS AND COREYS EPSILON	12.52
RESIDUAL AIR SATURATION	0.5185E-01
SATURATED WATER CONDUCTIVITY	0.3940
SATURATED OIL CONDUCTIVITY	0.1379
SATURATED AIR CONDUCTIVITY	0.2643E-01